UNIVERSITÀ DEGLI STUDI DI VERONA

Department of Neuroscience, Psychological and Psychiatric Sciences,
and Movement Sciences

Graduate school of Applied Life and Health Sciences

PhD in Neuroscience, Psychological and Psychiatric Sciences, and Movement Sciences

XXXIII cycle A.A. 2017/2018

Advanced analyses for the identification of prognostic markers in Multiple Sclerosis

SETTORE SCIENTIFICO DISCIPLINARE MED-26

Coordinator: Prof. Gianluigi Zanusso

Firma _____

Tutor: Prof. Massimiliano Calabrese

Firma _____

PhD student: Dott.ssa Anna Isabella Pisani

Firma _____

Advanced analyses for the identification of prognostic markers in Multiple Sclerosis
Anna Isabella Pisani
Tesi di Dottorato
Verona, 8 Marzo 2021
ISBN

Summary

Multiple Sclerosis (MS) is an auto-immune demyelinating and neurodegenerative disease of the central nervous system (CNS) characterized by a wide range of neurological symptoms and accumulating disability during the disease course.

High inter-individual variability, related to the severity and duration of symptoms, mainly characterizes the prognosis of MS. At individual patient-level, it is important to identify demographic, clinical, neuroimaging and biological markers associated with the risk of experiencing the progressive phase of MS, which eventually leads to the irreversible accumulation of disability. Therefore, the estimation of risk factors most involved in disease progression over time, especially if prompted identified, provide support to the medical decision making.

The proposed aim of this thesis was to understand better the underlying mechanism of disease progression as well as disease activity providing reliable and accurate tools that may assist the clinician in the optimization of treatment choice. Firstly, by exploiting the flexibility of machine learning approach, the Secondary Progressive-Risk Score (SP-RiSc) was developed. This integrated demographic, clinical and imaging data collected during the first 2-years after the disease diagnosis, discriminating those patients with a higher probability of progression over time. The proposed tool highlighted the early accumulation of focal and diffuse grey matter (GM) damage as the most important determinants of conversion to the progressive phase, supporting the pivotal role of the cortical pathology in the occurrence of the late severe disability. Secondly, a specific Cerebral Spinal Fluid (CSF) inflammatory profile at diagnosis was identified to be associated with cortical damage (focal and global) over time and poor clinical outcome. The analysis revealed that high CSF levels of the B-cell related cytokines and pro-inflammatory and monocyte activity molecules represent a potential tool to select patients at high risk of experiencing more severe disease activity, increased GM damage, and disability progression in the early phase of the disease.

Finally, an explorative preliminary analysis was performed on an extensive CSF protein assessment to investigate the potential predictive value of inflammatory cytokine and chemokine mediators in MS.

In line with recent findings, these results, even if preliminary, underlined that the mechanism of disease and disability progression is characterized mainly by a focal and diffuse cortical pathology predominant since the early stage of the disease and that the CSF cytokine and chemokine mediators may reflect the intrathecal inflammation and have a potential predictive role in MS. Moreover, by the use of advanced methods, such as machine and statistical learning models, which overcome the limitations of conventional statistical analysis more accurate results were obtained.

In conclusion, a step forward has done to provide reliable prognostic tools, based on as detailed as possible patients' profile at diagnosis, including clinical, neuroradiological and CSF characteristics, which may assist the clinician in optimizing the therapeutic approach moving closer to personalized medicine.

1. A basic overview of Multiple Sclerosis

1.1 Definition

Multiple Sclerosis (MS) is an immune-mediated inflammatory and neurodegenerative disease affecting the central nervous system (CNS) leading to chronic long-term disability. Historically, it was considered as a demyelinating condition with predominant involvement of the white matter (WM)[1]. However, several neuropathological[2,3] and neuroimaging studies[4] have also demonstrated pathological damage of the cortical and deep grey matter (GM), occurring since the early disease stages and accumulating mainly in the progressive phase.

1.2 Epidemiology

MS is one of the world's most common neurologic disorders among young adults. The current estimates suggest that about 2.5 million individuals are affected by MS all over the world. On average, the mean age of MS diagnosis is approximately 30 years with high disease prevalence in women with respect to men (overall female:male prevalence ratio is 2.8). MS is prevalent where white people of Nordic origin live and its prevalence generally increases with increasing latitude[5]. In Italy, the estimated incidence is 3.400 new cases per year, with a prevalence of 198 per 100.00 inhabitants.

1.3 Causes and etiopathogenesis

The causes of MS are still unknown, but it is believed that a combination of immunological, genetic and environmental factors contribute to its pathogenesis. Some hypotheses on the mechanisms of MS have been proposed studying the experimental autoimmune encephalomyelitis (EAE) model which is a murine model of some of the MS clinical, histopathological, and immunological characteristics. CNS proteins, such as myelin oligodendrocyte glycoprotein (MOG), myelin proteolipid protein (PLP) and myelin basic protein (MBP), are inoculated in the animal inducing the EAE model and activating the immune response observed within two weeks after immunization. Although the cause of

activation remains unknown, the common idea is based on the aberrant T-helper lymphocytes CD4+ which promote the cascade of pathological events. Once that CD4+ lymphocytes enter in the CNS, they recognize their specific target structure and initiate an autoimmune inflammatory process which allows recruiting cytotoxic lymphocytes CD8+, B-cell, myeloid cells in the periphery and resident cells of the CNS, such as microglia and astrocytes, causing demyelination lesions. EAE studies[6] demonstrated that Th17-cells are the most implicated pro-inflammatory effectors of CD4+ T-cells entering in the CNS by the choroid plexus and this was confirmed in MS patients who are found increased of Th17-cells in blood and cerebrospinal fluid (CSF)[7]. IL-17 protein is expressed by the Th17 cells while IFN-gamma is secreted by the Th1 cells which are also implicated in MS. In EAE the myelin damage is caused mainly by the CD8+ T-cells which, under inflammatory conditions, recognize the oligodendrocyte and/or myelin antigens. In fact, CD8+ T-cells are abundant in MS lesions showing over time the phenotype of tissue-resident memory cells and the CSF analysis shows a more restricted expression of T-cell receptors than the CD4+T-cells. However, it is well documented that MS is not only a T-lymphocyte mediated disease, but it also characterized by the dysfunctions of B-cells and plasma cells with their antigen presentation and inflammatory cytokines and antibody release.

Environmental, genetic, and epigenetic factors have a causal role in MS and potentially interact with modifiable risk factors[8]. Risk factors, such as vitamin D deficiency (related to reduced exposure to sunlight and decreased natural production from sun exposure in ethnic groups with dark skin), diet, obesity in early life, and cigarette smoking are known to play a part in MS development[9,10,11].

2. Disease Phenotypes and clinical course

MS can be defined by very different patterns of evolution (**Fig.1**) and mainly characterized by two different clinical phenomena: the relapse and the progression which reflect focal inflammatory activity and degenerative process, respectively[12,13].

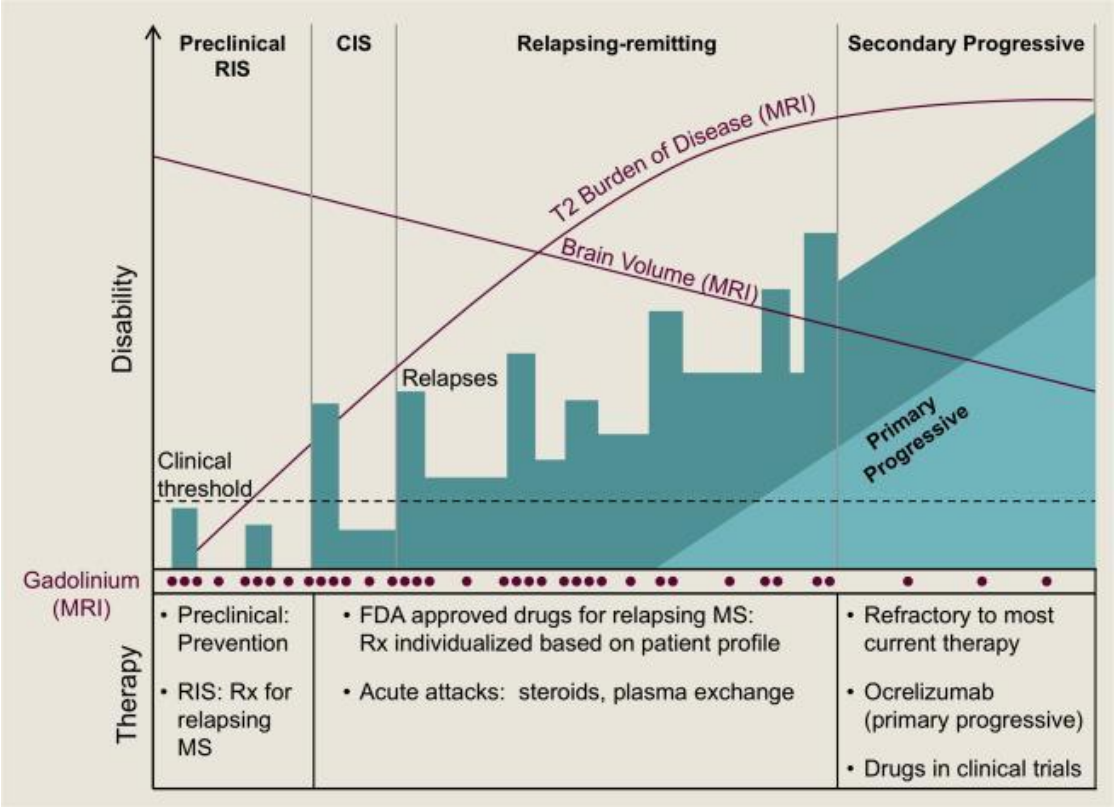

Figure 1 Multiple sclerosis is thought to begin before clinical symptoms are evident, and it can be discovered incidentally on MRI as a radiologically isolated syndrome (RIS). It then usually manifests as a clinically isolated syndrome (CIS), which is followed by a relapsing-remitting stage, characterized by discrete episodes of neurologic dysfunction with remission. The progressive stage involves steadily worsening disability and usually evolves from the relapsing- remitting stage, although some patients may have progressive disease from onset (primary progressive MS). MRI correlates of disease include accumulation of T2 burden of disease, and a decrease in brain volume as measured by atrophy[13]

The relapses are the expression of acute, focal and recurrent inflammation occurring in the CNS while the progression is related to diffuse and progressive axonal loss which is the main feature of the neurodegenerative process in MS. Acute relapses can be followed by partial or total recovery, are underpinned by magnetic resonance imaging (MRI) signs of focal inflammatory activity (appearance of new/enlargement of T2-weighted (T2w) and gadolinium-enhancing(Gad+) lesions) and are the main clinical features of relapsing-remitting MS (RRMS), representing the most common presenting form (85% of cases). In most cases, this is followed

by the secondary progressive phase (SPMS), characterized by steady disability accumulation, which occurs independently of clinical relapse/inflammatory activity. The neurodegenerative process underlying the progressive phase starts much earlier than the clinical onset of progression[14] and eventually becomes the prominent pathological features during the late stage.

In this spectrum, others two types of evolution exist: the preclinical radiologically isolated syndrome (RIS), which is a pre-clinical stage characterized by demyelinating lesions typical for MS evident only by MRI and the clinically isolated syndrome (CIS) with the occurrence of "first/isolated" clinical event suggestive for CNS demyelination. Finally, in about 15% of individuals, a progressive phase is present since the onset of disease and therefore named primary progressive phase (PPMS).

Progressive MS (primary and secondary) can be further defined as either active (with occasional relapse and/or evidence of new MRI activity) or not active, as well as with progression (evidence of disease worsening on an objective measure of change over one year, with or without relapse or new MRI activity) or without progression[15].

In MS patients, disability is assessed by the Expanded Disability Scale (EDSS)[16]. The EDSS is based on symptoms and signs in eight functional systems, walking ability and daily activities living. The EDSS is an ordinal scale ranging from 0 (no neurological abnormality) to 10 (death due to MS) steps by 0.5 increments (**Fig.2**) which must be confirmed after 3 or 6 months to discriminate true progression from disability related to the relapse, or assessment error. The assignment of EDSS is limited by the frequency of examination and the variability of inter-rater scoring.

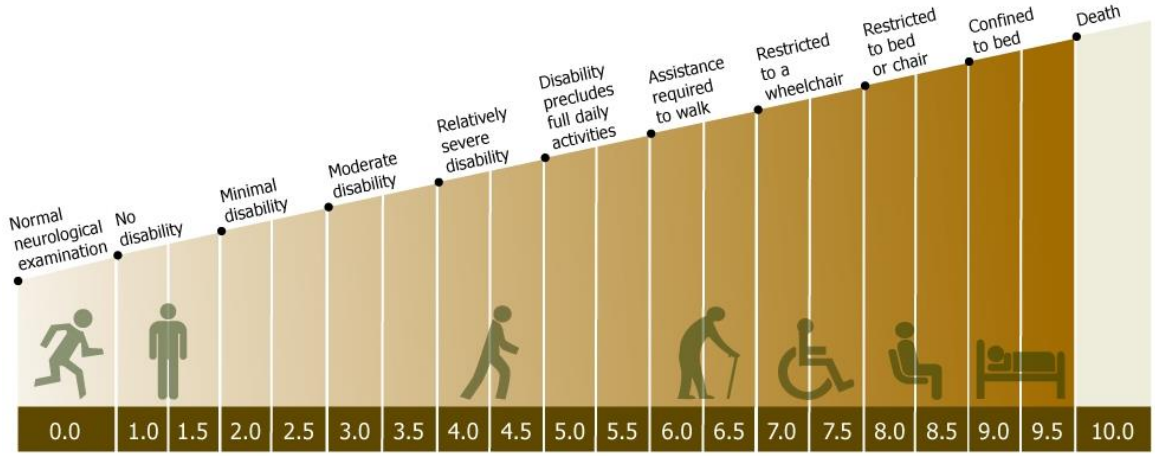

Figure 2 Schematic representation of Expanded disability status scale (EDSS)

2.1 Diagnosis

The diagnosis criteria of MS have been continuously evolved and have acquired specificity along with the development of detailed laboratory methods over time. Mainly, the MS diagnosis is based on clinical criteria: the occurrence of two or more clinically distinct episodes of CNS dysfunction is enough to diagnose multiple sclerosis[17]. MRI can support or replace some clinical criteria demonstrating demyelinating lesions, as well as dissemination in space (DIS) and dissemination in time (DIT)[18]. In fact, since 2001 MRI was formally incorporated into the diagnostic criteria suspected MS. In support of MS diagnosis there is also Cerebrospinal fluid (CSF) examinations including a normal o mildly raised white cell count and protein levels, increased immunoglobulin G (IgG) index and the presence of CSF- specific IgG oligoclonal bands (OCBs)[19]. CSF-specific IgG OCBs were included in the 2017 revision of the McDonald criteria as paraclinical demonstration of dissemination in time[19]. Inappropriate application of diagnostic criteria to patients with symptoms atypical for demyelination is the main contributor to misdiagnosis[20]. A combination of MRI and serological testing, in association with clinical features and history, should be used to navigate through the differential diagnosis of multifocal demyelinating inflammatory disorders, including neuromyelitis optical spectrum disorder (NMOSD) and acute disseminated encephalomyelitis (ADEM) and other disorders that can mimic MS. The differential diagnosis should also include immune-mediated disorders (CNS vasculitis,

encephalitis, sarcoidosis), infective diseases (neuroborreliosis, neurosyphilis, HIV encephalopathy), neoplastic, cerebrovascular, dysmetabolic and mitochondrial disorders, genetic leukoencephalopathies[21 22].

2.2 Pathology

The classic MS pathological hallmarks are focal areas (lesions/plaques) of inflammation, demyelination, neurodegeneration and, more rarely, remyelination[1,23].

2.2.1 White matter

White matter (WM) lesions are classically represented by sharply demarcated plaques with perivascular lymphocytic inflammation, variable axonal loss, and reactive gliosis. A recent study[24] suggested a unifying histologically classification of MS lesions depending on the composition of myelin degradation products, the presence, number and distribution of macrophages and microglia. Therefore, MS lesions are discriminated as active, chronic active and inactive. Active lesions are more predominant in MS patients with relatively short disease duration and active disease, chronic active lesions" or "slow expanding lesions" are classically abundant in the progressive stage of MS or in patients with long disease duration (>10 years) or in patients with shorter time to reach a significant physical disability[25]. In contrast, the inactive lesions are more frequent in MS patients with longer disease duration (>15 years) and progressive patients with few acute inflammatory attacks.

2.2.2 Grey matter

Lesions are also present in the grey matter, including the cortex (cortical lesions), the basal ganglia, brain stem, and the grey matter of the spinal cord[26,27]. These occur since the earliest phase of the disease and have a key role in MS especially during the chronic phase[28]. Perivenous and confluent demyelinated lesions can be found in the cerebral[29] and cerebellar cortex[28], the deep brainstem nuclei[30,31] , and the grey matter of the spinal cord[32]. As in WM lesions, oligodendrocyte destruction and primary demyelination is the pathological hallmark that distinguishes them from

brain damage in other diseases of the CNS. However, the degree of inflammation, edema, microglia activation, and macrophage recruitment is much less in comparison to the WM[33] lesions and is mainly associated with elevated inflammation in the leptomeninges[34]. In fact, MS patients are characterized by leptomeninges infiltrated by mainly T and B- lymphocytes and plasma cells which are retained in the meninges and only rarely infiltrate the cortical parenchyma[35] the cerebral cortex[36]. Since the detection of ectopic B-cell follicles beside the subpial cortical lesions (CLs), it seems that meningeal B-cell play a central role in the subpial demyelination. However, it has to clarify the exact correlation between leptomeningeal inflammation and subpial demyelination and whether the inflammatory mediators released by meningeal infiltrates in the CSF may cause the primary inflammatory attack to the cortex.

Inflammatory cells (lymphocytes, monocytes, activated microglia) lead to oxidative injury and mitochondrial damage causing demyelination and neurodegeneration in MS patients, particularly in the progressive disease stage[37,38].

Demyelination is associated with a variable degree of loss of axons, neurons, and glial cells, and this is accompanied by an even greater loss of synapses[39,40].

3. Prognostic factors in Multiple Sclerosis

3.1 Compartmentalized inflammation and Silent Progression

Progressive multiple sclerosis is mainly defined by a combination of inflammation, demyelination, oxidative stress and neurodegeneration process leading to a gradual accumulation of severe and chronic disability.

In most of the cases an initial relapsing-remitting phase evolves to secondary progressive MS (SPMS). Although several studies have been done to

identify SPMS onset, no standardized objective definition has been identified. Generally, the conversion to SPMS is defined by an irreversible disability progression independent of relapses[15]. The definition that had the best overall performance recently identified is that with 3-strata progression paradigm, with a minimum EDSS of 4 and a confirmation time of 3 months. Disability progression consists of 1.5 EDSS step in patients with EDSS=0, 1 in patients with EDSS <= 5.5 or 0.5 step in patients with EDSS >=6 in the absence of relapse, a minimum EDSS score of 4 and pyramidal functional system score of 2 and confirmed over 3 months[41]. The neurodegenerative process is pilot in progressive stage[32,42,43], in absence of Blood Brain Barrier (BBB) damage by a CNS compartmentalized. Such compartmentalized inflammation would be responsible for chronic disability accumulation and for the progressive phase of the disease. Two main compartmentalized inflammations have been so far identified:

1. The meningeal inflammation which is associated with the formation of subpial demyelinated lesions in the cerebral and cerebellar cortex with diffuse neurodegeneration in the normal appearing grey matter. Such diffuse subpial damage may be probably responsible for the progression of general symptoms and signs such as fatigue, paraparesis, spasticity and cognitive dysfunction.
2. The “slow expansion of pre-existing lesions” in the white and grey matter, with remyelination failure and progressive and irreversible focal axonal damage[32].

The persistence of low-level chronic activity in some WM lesions seems a relevant pathogenetic mechanism of progression being responsible for the progression of focal symptoms and signs.

3.2 Clinical and demographic markers

Prognostic markers are measures used to predict an individual risk of a patient's future outcome. This plays a key role in clinical practice discriminating patients into different risk groups and thus helping to optimising treatment strategies.

Prognosis of multiple sclerosis is characterized by a patient's individual high degree of variability. Therefore, the early identification of clinical and demographic factors is reliably helpful to predict individual poor outcome. Although many efforts have been done, clinical predictors of the onset of irreversible disability are not well clear; however, some risk factors of more rapid poor clinical outcome have been identified and widely shared. In fact, there is strong evidence that male and older patients at disease onset had a higher probability of entering in a progressive phase[44–46]. Age seems to be the major determinant of clinical evolution in MS. In healthy individuals, the CNS integrity declines with aging and this mechanism is emphasized in MS patients who present both a decrement of grey and white matter reserve. In addition, a more aggressive clinical course is influenced by the early higher relapse occurrences within two years of diagnosis. Shorter inter-attack time from the first clinical event associates with a faster deterioration and increased risk of secondary progression[47]. However, recently, relapses are not associated with the confirmed disability progression in a subgroup of RRMS patients, suggesting that a silent progression, possibly independent from relapse occurrence and associated to the degree of brain atrophy, occurs since the early disease stages[48].

3.3 Magnetic Resonance Imaging biomarkers

MRI provides a suitable, non-invasive and in-vivo tool for evaluation in MS patients during disease progression and for treatment monitoring, providing insights into disease processes.

These techniques might help to understand the in-vivo heterogeneous processes causing both focal and widespread damage in the entire CNS over the disease course. Generally, in MS clinical practise the conventional MRI techniques are used on a standard clinical MRI scanner. Conventional MRI techniques include measure of new white matter inflammation (new and enlarging T2w lesions, Gad lesions), measure of acute and chronic disease (total T2w lesions volume, and measures of degeneration (T1w - black hole)). Even if conventional MRI methods can detect the WM lesions, they are largely insensitive to conspicuous and variable disease pathological mechanisms.

Advanced (non-conventional) MRI structural and functional techniques have emerged to estimate overall MS burden in patients at different stages of the disease. The extent of focal cortical and white damage was detected both at clinical onset in MS patients influencing, differentially, the probability of disability accumulation and the conversion of CIS patients to clinically definite MS. To date, the process underlying cortical and white matter injury remains still unclear tending to a view of an independent mechanism between grey and white pathology[49]. If on the one hand, some neuropathology studies showed an intrinsic relation between cerebral white and grey matter damage[34,50,51] on the other hand it has been showed that white matter inflammatory activity is dissociated, at least partially, from the cortical pathology, both at onset relapse and during the disease course[34,52–55]. Focal cortical lesions occur early during MS disease course and their extent predicts the MS clinical, physical and cognitive evolution[56,57,58]. However, the idea may be that MS long-term disability progression is more related to grey matter pathology than to the white matter one in RRMS patients. The latter present, in the first years of disease, a compromised clinical picture caused by the occurrence of WM lesions relapse related and not-progressive disability. This view suggests that disability progression follows a 2-stage process where the first stage is defined by a focal WM inflammation characterizing the RR phase while the second part is associated with a cortical pathology prevalent in SPMS[12]. CLs, which can be detected even in the early disease phase[29,59–63], increase in number and volume along time and affect physical disability[64,65]. The implication of grey matter pathology in long-term disability was supported by the predictive role of the GM atrophy on SP onset[66]. In fact, the extent of GM, but not WM, atrophy was found to be significantly greater in SPMS patients compared to RRMS ones. Differential tissue-specific atrophy in MS could be partially explained by the different mechanisms underlying inflammatory activity in WM and GM with relatively greater compensation of cell loss by inflammatory infiltrates in WM compared with GM[66]. Cerebellar cortical atrophy was found to play a critical role in onset of irreversible

progression and appear to be more relevant than other cortical areas volume and deep GM regions[52] suggesting that damage to critical GM structures might be clinically relevant than overall GM damage. Overall, focal lesions, demyelination and irreversible tissue loss can provide a prognosis for the long-term.

Although the relationship between spinal cord lesions and disease progression is not completely clear, the cervical cord atrophy seems to be associated with poor prognosis[67]. Spinal cord lesions can provide a prognostic information resulting for CIS patients one of the relevant risk factors of conversion to clinically definite MS and early physical disability[68].

All of these data suggest that MRI acquisition and analysis tools are determinant to better explain the MS disease course and GM and WM measures combined might be useful in monitoring the course of the disease both in the early and later stage of disease.

3.4 Immunological markers

Currently, early in vivo detection of focal and diffuse cortical damage has shown that it is important to highlight the disease progressive mechanisms before an irreversible disability appears and to identify biomarkers for the long-term disability accumulation.

Nevertheless, nonconventional MRI techniques require additional assessment in order to be standardized and reliable. It is therefore important to identify additional surrogate biomarkers of GM demyelination, neurodegeneration and compartmentalized meningeal inflammation that could be available early in the disease course to select patients with high risk of disability progression. Several studies have shown that MS patients had a distinct CSF profile with respect to controls, mainly reflecting either inflammatory or neurodegeneration CNS changes. Consequently, many efforts have been done in order to study how CSF profiles could be a biomarker which could predict MS progression and disease activity.

Immunoglobulin (Ig) bands (OCBs) in the CSF are a frequent phenomenon in MS representing a hallmark of disease. The presence of OCBs in CSF not only is used as a paraclinical tool for DIT demonstration but also as a prognostic tool. In

fact, early occurrence of OCB in CSF is associated with the onset of a more severe clinical (both physical and cognitive) outcome and with evolving of cortical pathology[51]. Moreover, OCBs phenomenon have been found related to the increased levels of Neurofilaments (Nf-L), which is a marker of neuron and axon injury, and others inflammatory mediators linked mainly with B cell activity (CXCL13, CXCL12, CXCL10, TNFSF13, TNFSF13B, IL-6, IL-10) suggesting the implication of an intrathecal inflammation in the production of OCB and pathogenesis of cortical damage[51]. On the other hand, higher titre of OCBs was associated with higher probability of conversion from RR to SP MS[69].

Like OCBs IgG index has been reported to have a very high negative predictive value. Among the Ig isotypes (IgG, IgM and IgA), IgG is the common isotope used since its high amount in CSF. IgG index defines a quantitative measure of intrathecal IgG level and takes in account the BBB integrity resulting from a prognostic predictor during the disease course. RRMS patients with a high IgG index at baseline had higher probability to convert to SP phase during the follow-up[70,71]. However, it seems that IgM index may be more powerful than the IgG in predicting MS severity. Indeed, the presence and the number of IgM OCBs are predictive of new relapse and more severity disease[72].

Inflammatory cytokine and chemokine mediators underlying the intrathecal inflammation have been found in MS CSF patients covering a potential predictive role. Specifically, CXCL13, which is a chemokine involved in B cell recruitment in secondary lymphoid organ organization and in lymphoid neogenesis in several chronic inflammatory diseases such MS, predicts the MS onset from CIS condition and correlates with relapse rate, EDSS and number of MRI lesions[73].

High CSF levels of CXCL13 have been found expressed in ectopic B-cell follicle like-structures in the meninges of post-mortem MS cases with higher cortical lesions load and more severe disease progression[55]. Moreover, CXCL13 with IFN-gamma, TNF, CXCL12, IL-6, IL-10 and LIGHT were demonstrated independently associated with increased cortical lesion number and volume either at disease

diagnosis or at the time of death[74]. The increased intrathecal levels of molecules associated with B-cell recruitment and activity support a strong link between the degree of the compartmentalized meningeal immune response and both the underlying cortical pathology and a more rapid disease evolution.

In addition, Nf-L components are also gaining ground in different neurodegenerative disorders as well in MS. Nf-L factors are released in the CSF at the moment of the axon damage providing the hypothesis that high levels of Nf-L trigger a neurodegenerative process. It has been shown that RRMS patients with higher CSF Nf-L levels at baseline had higher probability to enter the SP phase[75]. Moreover, strong association between Nf-L and brain parenchymal fraction loss and percentage brain volume loss were identified[68]. This suggests the application of Nf-L as a good biomarker for prediction of poor prognosis and the detection of Nf-L also in the blood (sNf-L) take it to be a promising reliable marker in MS disease. Even if, no much studies have been done on the prognostic significance of sNfL in MS disease, like NfL in CSF, sNfl has been demonstrated to be correlated with clinical factors, such as relapse[76] and to be able to predict the brain volume loss during a 2-years follow-up.

Among the potential biomarkers a significant role was covered by Chitinase 3-Like 1 (CHI3L1) which is a glycoprotein involved mainly in activated glia and expressed on activated macrophages. CHI3L1, known also as YKL-40, has been associated with more rapid accumulation of disability and to be overexpressed in the CSF of CIS patients who converted to clinically definite MS with respect to those who remained as CIS[77].

3.5 Treatment target and clinical outcome in multiple sclerosis

For the past 25 years therapeutic landscape has dramatically expanded and, currently 15 DMTs, with immunomodulatory or immunosuppressive properties, are approved for RRMS patients. Relapses occurrence, accumulation of new and enlarging brain MRI lesions and disability progression has been found to be significantly lower in RRMS patients treated with DMTs compared with those receiving placebo or an active comparator. Substantially, DMTs according to their impact on relapses activity response can be classified as first-line treatment with

moderate effect (interferon beta, glatiramer acetate, teriflunomide, dimethyl fumarate, fingolimod) and second-line one with highly effective drugs (natalizumab, ocrelizumab, cladribine), but potentially less safe and more expensive, with the aim of obtaining a persistent disease remission19.

The identification of clinical and MRI characteristics predictive of poorer outcome or meeting of criteria for "highly active" disease may justify more aggressive DMT selection at or soon after diagnosis. Several definitions of "highly active" disease have been proposed for clinical use typically using a combination of two or more clinical relapses together with one or more of relapse severity, presence of multiple gadolinium-enhancing MRI lesions, significant T2 lesion burden, or increase in EDSS score within the preceding year[78]. Because MRI is more sensitive to disease pathological change there is increasing interest in using composite clinical and MRI measure to evaluate disease activity and treatment efficacy. Therefore, based on the clinical and MRI alterations was generated the concept of "no evidence of disease activity" (NEDA). No evidence of disease activity-3 (NEDA-3) consists of the absence of relapse and MRI activity (new/enlarging T2w lesions or Gad lesions) and no EDSS worsening confirmed after 6 months[79]. Although relapses and MRI activity are sensitive for inflammatory activity detection in MS, it does not properly account for the neurodegenerative process. Consequently, NEDA-4 was recently proposed adding into definition a pathological annualized brain volume loss (a-BVL) greater than 0.4%[80]. Accelerated (>0.4%) a-BVL is predictive of disability progression and cognitive decline in long term[81]. Moreover, the increasing recognition of an ongoing inflammatory component in progressive MS led to a wave of studies examining the effect of most common RRMS disease-modifying therapies in progressive phenotype of disease[82].

4. Machine learning and statistical learning in MS disease

The inclusion of advanced technologies and omic-based approaches in the health care setting has generated an extensive collection of heterogeneous data, the so-called big data. In this light, learning and statistical machines are promising and suitable strategies to analyse such data more than the conventional models. Machine learning (ML) includes algorithms that allow the machine to learn from data

without being explicitly programmed. In the past decade, ML tools have been acquiring more relevance in clinical practice thanks to their peculiarity to make the prediction. ML and statistical learning (SL) based on different algorithms can discriminate and stratify patients as well detect novel risk factors with high accuracy potentially in each different pathologies[83–85] assisting the clinician in medical decision making.

However, in recent years very few studies on MS have been done employing ML framework's ability to investigate predictive variables of disease evolution in time or to estimate the individual risk of a patient to progress over time[86–89].

The natural course of MS disease is hugely variable and almost unpredictable, depending on several individual characteristics. Even though some clinical, demographic and radiological features have been associated with disease worsening overtime, unfortunately this information has limited prognostic use when applied to a single individual. To date, however, all these factors have been considered separately and analysed by traditional regression methods affected by poor performance and related to restrictive assumptions.

Although ML methods have been mainly used for classification, quantification and identification of diagnostic patterns in medical image in MS[90–92], few of these strategies have been applied to handle large dimensional dataset and to define a meaningful subset of features to construct an accurate model for prediction of the disability or progression in MS.

The implication of these emerging methods in MS patients care may efficiently evaluate a large number of variables collected for MS patients and identify those patients with high risk to develop aggressive MS with important implications for preventive medicine. Early identification of patients at high risk to evolve to this irreversible phase is mandatory to implement a personalized therapeutic approach and to maximize the possibility of avoiding or postponing it.

5. Aims of the thesis

In recent years a great effort has been made to identify those MS patients at higher risk of developing aggressive as well as progressive disease course[48,93,94], but

detailed studies are still needed. Since MS is characterized by high inter-individual variability in disease course and severity, it is essential to assess, at an individual level, an objective measure of the risk of a patient experiencing the worst phase of MS in which the progressive accumulation of disability is the clinical highlight. The intrinsic clinical heterogeneity, and the multiplicity of alternative therapies lead to seeking a personalized plan to adapt MS patients' care. Therefore, the estimation of risk factors most involved in disease progression and disability over time, especially if prompted identified, provide support to the medical decision making.

Among RRMS patients several clinical and radiological features are associated with an increased risk of entering the SP phase, but their prognostic value at the individual level remains limited, which hampers the possibility of optimizing the therapeutic approach. In addition, there were promising results about the implication of cerebrospinal fluid (CSF) proteins as surrogate biomarkers for early identify and monitoring disease progression as well grey matter cortical pathology since their peculiarity to reflect either inflammatory and neurodegeneration CNS alterations. Nevertheless, most of these investigations, generally cross-sectional design, did not take in account the extensive patients' CSF proteins pattern that is related to the complex neuroimmunological and neurodegenerative events occurring in MS.

In this context, my PhD research has tried to identify an individual comprehensive MS patient profile associated with higher risk of experiencing disease progression and a severe clinical course. Therefore, the first aim of my PhD thesis was implementing an accurate individual prognostic tool, called Secondary Progressive Risk Score (SP-RiSc), based on early clinical, conventional and no-conventional radiological features to identify RRMS patients at higher risk of developing SPMS in the next ten-years from diagnosis.

A novel ML approach in MS was applied to accurately estimate the risk factors of newly diagnosed RRMS patient's conversion to the secondary progressive phase. The SP-RiSc has been specifically designed to provide an individual comprehensive index describing the risk of conversion into the progressive phase assessing the extent of the cortical pathology to improve the prognostic tool's performance. For the first time, this takes into consideration

conventional and non-conventional MRI measures, assessing the extent of the cortical pathology, in order to improve the prognostic tool's predictive ability. This will put the basis to develop in future an SP-RiSc online platform with a simple interface available for the neurologist.

The second aim of my thesis was focused on the detection of a specific extensive baseline inflammatory CSF profile mainly involved into the focal and global cortical damage both at diagnosis and after 4 years of disease. In addition, a distinct CSF baseline outline, among RRMS patients, was investigated to discriminate accurately those patients destined to have higher risk of experiencing disease activity. A statistical learning approach was applied to achieve this goal.

The last PhD purpose was to investigate how the CSF profile reflects the two consecutively stages of MS, such as the Relapsing Remitting (RRMS) and the Secondary Progressive (SPMS) one. Exploratory and pathway analysis were performed to identify and compare the two different inflammatory patterns in the two patients sets. Finally, using a machine learning model a specific CSF profile at diagnosis of patients with higher risk to convert into SPMS was identified.

In conclusion, my PhD research was intended to identify potential tools able to predict MS patients who present a clinical and worst disease course including not only clinical, demographic and MRI features, already studied, but also non-conventional MRI parameters and a complete CSF protein assessment. Therefore, during the PhD period applying statistical advanced techniques, attempts have been made in order to provide preliminary simple tools which may be employed in clinical practice and be helpful for optimising the therapeutic strategies since the large number of currently available DMTs, characterized by different efficacy.

Although these results seem to be promising in MS studying, further investigation and validation are needed for the pragmatic use of these tools.

6. Study 1: A novel prognostic score to assess the risk of progression in relapsing-remitting multiple sclerosis patients

Introduction

The MS clinical course can be extremely variable and, therefore, unpredictable at the individual level. In the most cases, recurrent episodes of clinical objective neurological dysfunction with partial or total recovery and magnetic resonance imaging (MRI) signs of disease activity (appearance of new/enlargement of T2-weighted and contrast-enhancing lesions) define the initial phase of the disease known as relapsing-remitting MS (RRMS); this is followed by the secondary progressive phase (SPMS)[95] which is usually dominated by progressive disability accumulation, neurodegeneration and axonal loss[47,96]. SPMS is characterized by poor response to most of the disease-modifying drugs (DMDs) and the failure of brain compensatory mechanisms[97].

Several demographic, clinical, neuroradiological and environmental factors have been associated with a higher risk of the conversion to SPMS[17]. The number of WM lesions, their location and MRI activity at disease onset are useful prognostic factors of physical disability[98,99]. Moreover, GM damage (cortical lesions and atrophy) has been correlated with disability progression stronger than WM damage[52,100,101] . However, despite the great effort made in recent years, the identification in the clinical practice of those patients at high risk of entering the SP phase is still challenging, especially early in the disease course when the optimization of the treatment could maximize its efficacy.

In this view, applying a machine learning approach on demographic, clinical and MRI data collected during the first 2-years of disease in a cohort of RRMS patients, we have developed the Secondary Progressive-Risk Score (SP-RiSc): a tool potentially applicable at an individual level in daily clinical practice aimed for obtaining to an objective measure of the risk of conversion into SPMS.

Methods

MS patient cohort and study design

The study was designed by retrospectively collecting demographic, clinical and MRI data (including measures of both focal and diffuse GM damage) at diagnosis (T0) and after the first two years of disease course (T2), among 262 patients diagnosed with RRMS[102], who were recruited at the MS Specialist Centre of the University Hospital of Verona (Italy) between 2005 and 2010 and were followed up to 2018, for 9.55 mean years (range 6.8-13.13 years). Each patient was treated initially with one of the licensed first-line disease-modifying therapies (DMTs) (interferon-β1a and glatiramer acetate), and clinically examined by MS neurologists every 6 months or when a relapse occurred. During the follow up period, patients experiencing disease activity were switched to second line therapies (fingolimod and natalizumab). The physical disability was evaluated with the Expanded Disability Status Scale (EDSS)[16]. A relapse was defined as the acute or subacute development of new or recurrent symptoms, lasting >24 hours and not preceded by fever[15]. The progressive course was defined by the occurrence of continuous disability accumulation independently of relapses and was confirmed 12 months later. Although transitory plateaus in the progressive course were allowed, the steady progression was the rule[15]. All procedures in this study have been performed in accordance with the ethical standards of the institutional research committee and the 2013 Helsinki Declaration[103].

MRI acquisition protocol and analysis

MRI sequences have been acquired by Philips Achieva 1.5 T MRI scanner (Philips Medical Systems, Best, Netherlands), with 33 mT/m power gradient and a 16-channel head coil. During the study period, the scanner has undergone a specific functioning test every two months to guarantee parameter stability. 3D magnetization-prepared rapid gradient-echo (MP-RAGE) [TR/TE=25/4.6 ms], 3D Fluid Attenuated Inversion Recovery (FLAIR) [TR/TE=10000/120 ms] and 3D

Double Inversion Recovery (DIR) [TR/TE=6500/265 ms, TI1/TI2=500 ms/2800 ms] sequences have been acquired to brain scan. Spinal cord sequences included dual-echo proton density and T2-weighted fast spin-echo, and short-tau inversion recovery. Patients have been carefully positioned according to published guidelines for serial MRI studies in MS patients[104]. T0 and T2 refer to RRMS diagnosis time and 2 years later, respectively. All images have been analysed by a neurologist (FC) in collaboration with another with a large experience in MS (MC). The following measures were evaluated:

a) ***Global Cortical Thickness (CTh) and Cerebellar Cortical Volume (CCV) at T0, and their relative changes at T2*** have been obtained by the application of the Freesurfer (version 6.0; http://surfer.nmr.mgh.harvard.edu/) longitudinal pipeline, a semiautomatic software, based on T1-weighted structural volumetric image. Topological defects in cortical surfaces due to WM and leukocortical lesions were corrected using a semi-automated procedure, which includes WM lesion segmentation and lesion filling. The technical details of these procedures have been described previously[50]. T0 and T2 segmentation masks have been used to calculate the percentage of the global cortical thickness or cerebellar volume change as follows: [CTh or CCV at T2 - CTh or CCV at T0] / CTh or CCV at T0.

b) ***The number of cortical lesions (CLs) at T0 and at T2*** has been assessed on DIR sequences following the recommendations for CLs scoring in patients with MS[105]. Given the poor capability of DIR sequences in visualizing subpial lesions in vivo at standard field strengths, the analysis has considered mainly the intracortical and juxtacortical lesions[58,106].

c) ***White matter (WM) lesions number at T0 and T2 have been examined on T2-weighted images***.

Statistical analysis

Analyses were performed using R version 3.5.3. Data were reported using mean and standard deviation (SD) or median and range, based on their distribution. Dichotomous and categorical variables were described using proportions. Differences between groups were assessed using analysis of variance (ANOVA) or Mann-Whitney. Fisher's exact test was applied to test the contingency tables on

categorical variables. Statistical significance was considered at $P<0.05$. The Akaike Information Criterion for Cox regression (AIC-Cox) with backward phasing out and the Cox Proportional Hazard (PHM) model were performed to compare these "traditional" approaches with a "more innovative" machine learning-based one (Random Survival Forest). Moreover, before performing the Cox regression models the variables were standardized (variables will be shifted to be zero centered and scaled to have unique variance).

Random Survival Forest model

The design of the study is summarised in **Figure 1**.

The whole cohort was randomly split into a training set (80%, n=219), which was used to model both the Random Survival Forest (RSF) and the SP-RiSc, and a testing set (20%, n=43), on which the score was validated (**Fig.1A**). The populations in both sets shared similar demographic, clinical and neuroradiological characteristics, and similar proportion of patients, who converted to SPMS during the observation period (26% vs 30% in the training and in the testing set, respectively; P=.66) (**Table 1**).

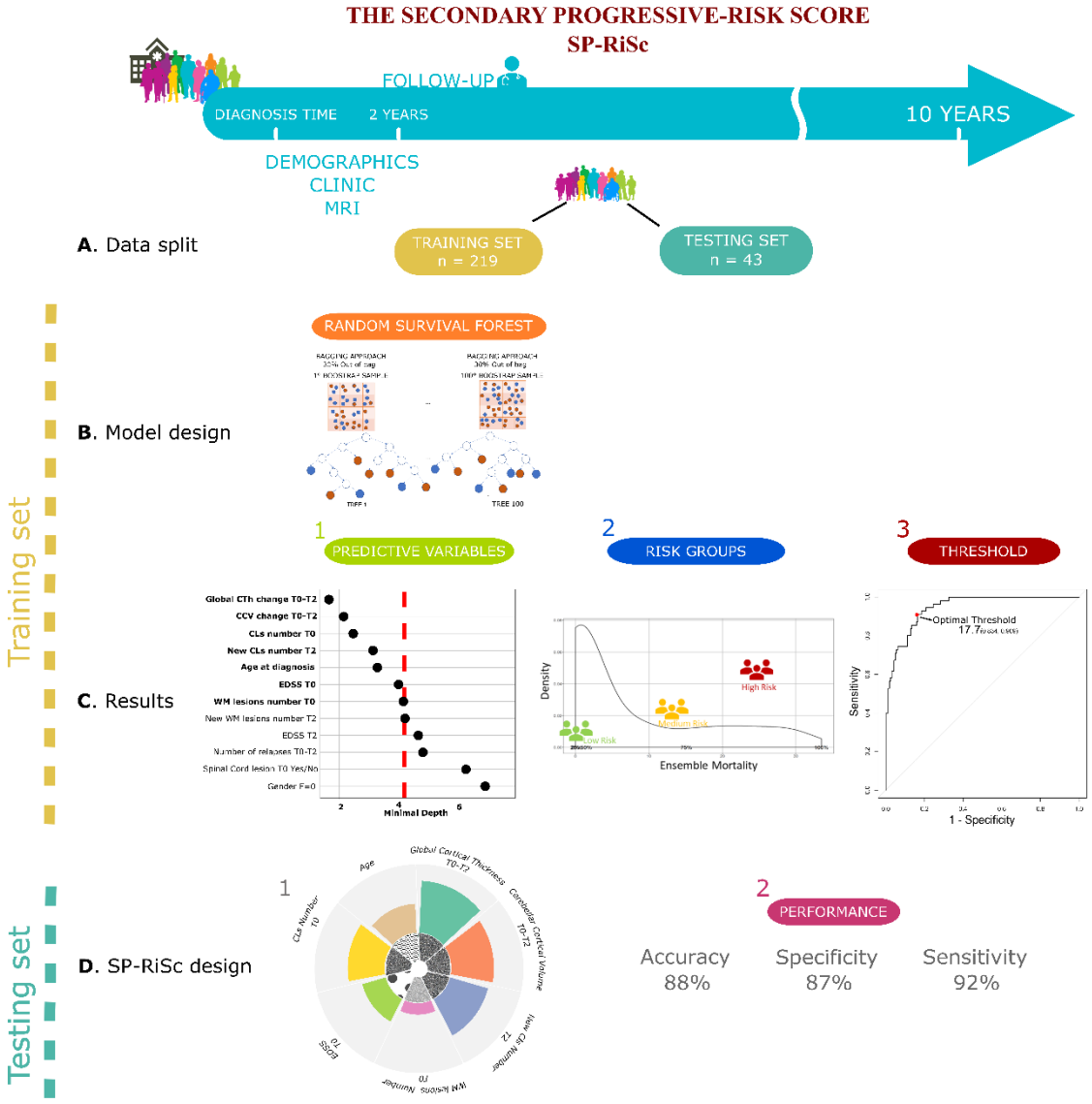

Figure 1. The overall study design: **A)** ***Data split***: The entire cohort was randomly split into training- and testing-set; **B)** ***Model design***: RSF modelling was performed on the training set. **C)** ***Results***: **1.** 7 most predictive variables were selected, based on their Minimal Depth **2.** Risk groups were identified by Ensemble Mortality. 3. The ROC analysis was used to identify the best score cut-off **D)** ***SP-RiSc design***: **1. The** Sp-RiSc tool was developed **2.** The Sp-RiSc performance specificity, sensitivity and overall accuracy were assessed on the testing-set.

Features	Training set n=219	Testing Set n=43	*P* value
Clincal phenotype No. (%) RR/SP	163(74.43)	30(70)	0.58
Age at diagnosis, mean (SD), y	33.7(9.9)	32.2(6.6)	0.40
Duration of follow-up, median (range)	9.17 (6.79-13.12)	10.80 (9.74-12.06)	<.001
Gender, Female, No. (%)	131(60)	22(51.11)	.30
Number of relapses T0-T2, median (SD)	2(0.8)	1.8(0.8)	.50
EDSS T0, median (range)	1.5(0-3.5)	1.5(0-2.5)	.40
EDSS T2, median (range)	2(0-4)	2(0-3)	.94
CLs number T0, median (range)	2(0-18)	3(4-19)	.23
New CLs T2, median (range)	1(0-8)	0(0-3)	.80
WM lesion number T0, median (range)	14(2-22)	8(4-21)	.72
New WM lesion number T2, median (range)	1(0-4)	1(0-2)	.10
CCV T0, mean (SD), cm^3	108.2(1.9)	107.8(2.1)	.50
CCV change T0-T2, mean (SD), %	2.50(2)	2.70(1.6)	0.10
Global CTh change T0-T2, mean (SD), %	1.3(0.4)	1.7(0.8)	<.001
Spinal cord lesion T0, yes, No.(%)	47(21.5)	11(25.6)	.50

Table1. Training and Testing set patient's characteristics collected during two first years of disease.

Machine learning approach

The Random Survival Forest (RSF)[107] is a machine learning-ensemble method for the analysis of right-censored survival data (**Fig.1B**), which is based on the extension of Breiman's random forest[108] and provides flexibility in highly correlated complex data.

RSF model is based on a collection of independent binary decision trees grown by bootstrapping sample which includes on average 63% of the original data excluding the remaining one, called out-of-bag (OOB). Specifically, below the description of the algorithm was reported:

1. A survival tree based on the bootstrap samples (*B*) was grown applying a random node splitting process which consists of randomly *p* candidate variable selection. The node splitting criteria is based on that candidate variable which gets a split point that maximizes the survival difference between daughter nodes.
2. The growth of a decision tree proceeds until all terminal nodes (h) contain a minimal number of unique events.
3. For each tree, the Cumulative Hazard Function (CHF) and the ensemble CHF obtained by the average over the trees were estimated.

Specifically, define $d_{l,h}$and $Y_{l,h}$ as the number of events and individuals at risk at time $t_{l,h}$ respectively, and each case l with a n-dimensional covariate x_i then the estimate of CHF for h is the Nelson- Aalen Estimator:

$$\widehat{H}_h(t|x_i) = \sum_{t_{l,h} \leq t} \frac{d_{l,h}}{Y_{l,h}}$$

The ensemble CHF is calculated by averaging B survival tree- based Nelson Aalen Estimator.

Let call $H_e^*(x_i)$ the estimate of $\widehat{H}_h(t|x_i)$ in the b-th OOB, then:

$$H_e^*(t|x_i) = \frac{1}{B}\sum_{b=1}^{B} H_b^*(t|x_i)$$

This value represents the predicted outcome $\hat{Y}_l$, called Ensemble Mortality (EM), that is the ensemble CHF summed over the observed survival times in OOB data.

The EM is calculated for each patient l. Finally, using OOB data, the prediction error was calculated for the ensemble CHF using both Brier Score (BS) and Harrel's Concordance Index (CI)[109] (See below for details).

Variables included in the model. The demographic, clinical and MRI data collected during the first two years of the disease have been included in the RSF model in order i) to identify those variables with a strong impact on the risk of developing SPMS and ii) to study the synergic cooperation of the selected risk factors. A total of 12 variables have been analysed, including: **demographic** (gender and age at T0) and **clinical** (EDSS score at T0 and T2; the number of relapses over the first two years of disease) **information**; **MRI data** (the changes over the first two years of both global CTh and CCV, CLs and WM lesions number at T0 and number of new lesions at T2; the presence of spinal cord lesion at T0). The model's results were adjusted for the treatment categorical variable, indicating whether patients have been switched to second-line DMTs during the observation period.

Quantification of the variable predictive effect. The Minimal Depth (MD) is a dimensionless measure used to quantify the predictive effect of each variable included in the model.

In RSF the measure of the predictive effect of each variable can be defined by two different and independent ways: Minimal (M) Depth (D) value and Variable Importance (VIMP). VIMP for a variable X is the difference between prediction error in OOB before and after the variable X is randomly permuted. The natural interpretation of this measure is that the higher VIMP the more predictive the variable. Although VIMP can be considered a useful measure to assess the predictive effect of the variables in the model, it has several limitations such as its dependency on the prediction error measure used. Consequently, in this study, we have decided to use MD measure that is known to be more stable than VIMP since it is based on the topology and the construction of the forest. MD is a statistical measure derived from a new tree concept, called maximal-subtree. The main idea is that in the maximal subtree the variables with higher impact on the prediction are those most frequently split nodes nearest to the root node. It is calculated for each variable and for each decision tree and finally averaged over the whole forest

distribution. The lower the MD (the shortest distance, the depth) the more predictive the variable. In general, the average MD is used as a variable selection criterion for prediction events. Moreover, even though RSF can be considered a black box, like a common machine learning method, an exact MD statistic distribution exists[110] giving us the possibility to use this measure to weigh each factor which takes part into the Secondary Progressive Risk Score design. So, the mean of the MD model distribution (MD mean distribution=4.21) was used as a reference threshold (Thr) to determine the size of the predictive effect of the variables included in the model. Variables with MD lower than Thr are those with the highest predictive power (**Fig.1C1**). The Ensemble Mortality (EM), which is the individual predicted outcome of RSF, was then calculated to identify three different SP risk groups. Finally, the EM and the MD parameters were combined to develop the SP-RiSc tool (**Fig.1D1**).

Evaluation of RSF performance. In RSF, as in every survival analysis, two different measures can be used to evaluate the prediction performance: the Brier score (BS) and the Harrel's Concordance Index (C-Index)[109]. The BS expresses the mean squared difference between the actual status and the predicted survival probability, while the C-Index is a time-independent measure indicating how well the model discriminates between patients with and without the outcome. BS is a quadratic rule and consists of the distance between the actual status and the predicted survival probability. Define i a subject which does not belong to the training set, $Y_i(t)$ the true status of the subject at time t and $\hat{S}(X_i)$ the predicted survival probability at time t for subject i considering X_i independent variables:

$$BS(t, \hat{S}) = E\left(Y_i(t) - \hat{S}(X_i)\right)^2$$

BS=0 corresponds to a good prediction while BS=1 to a poor prediction, a benchmark equals 0.33 can be considered useful since BS=0.25 means predicting 50% risk for the two status[111]. Unlike BS, C-Index is a time-independent value and the interpretation is close to a misclassification probability. For each permissible pair where $T_i \neq T_j$ count 1 if the shorter survival time has worse predicted outcome or 0 if the predicted outcomes are identical. When $T_i = T_j$ and both are deaths, count 0.5 if the predicted value is different otherwise count 1. The bootstrap cross-

validation, which is based on 10 bootstrap subsamples (drawn with replacement), was applied on the training set at the follow up quartile times (7, 8.5, 9.55, 10.5, 13.5 years), to evaluate the performance of the RSF. The training set is partitioned to 10 equal-sized subsets; one is used as a testing set, while the remaining ones are used as training sets. Higher C-index and lower BS indicate better prediction performance.

Secondary Progressive-Risk Score (SP-RiSc) implementation and evaluation

Risk group definition. Based on EM measures, patients were stratified into three risk groups, using quartile distribution values: patients with EM lower than the 1th quartile and greater than the 3rd quartile are respectively at low- and high-risk of converting to SPMS, while the remaining patients belong to the medium-risk group **(Fig.1C2).**

Discretization and weighting. The EM and the MD parameters were combined in order to design the SP-RiSc tool, which included only variables exerting the highest predictive effect (MD lower than 4.21) (**Fig.2A**). The score design procedure handles differently discrete (age, EDSS, CLs and WM lesion) and continuous (global CTh and CCV) variables. Continuous variables had to be transformed into discrete counterparts. The discretization was performed using the lower and the upper limits of the bootstrap confidence interval for each variable within each risk group. Here we reported the lower and upper boundary values, in the low, medium and high-risk group, respectively, for the global CTh changes after two years: [0.97% - 1.01 %], [1.2% - 1.4%] and [1.7% - 1.9%], and of the CCV change in the first two years: [1.2% - 1.4%], [2.1% - 3%] and [4.3% - 5.5%]. If we consider all the possible values for a variable, the three non-overlapping intervals generate seven different classes (considering values lower than the lower limit of low-risk group, higher than the higher limit of high-risk group, and values in the middle of the disjoint intervals). A Numerical weight value ranging from 0.5 to 3.5 (step by 0.5) was assigned to each class: a higher numerical values weight indicates a higher magnitude of the variable considered. Then, the value of each category was divided by the variable MD. For the discrete variables the value was divided by its own MD value (**Fig.2B**). The final SP-RiSc resulted from the sum of the risk factors weighted by the predictive ability. The formal definition is reported as follows.

Let D_j with $j = 1, \dots, d$ and C_j with $j = 1, \dots, c$ (with c + d = 7) be the predictive discrete and continuous variables selected respectively from RSF, $r\ with\ r = 1, .., i$ $(i = 3)$ the risk groups derived by EM distribution, m_j the minimal depth estimated by RSF and l the patient index.

Then, discrete variables D_j , $let\ K_{l,dj}$ the ratio between the value of the variable, d_{lj}, and the MD measure, we define the sum of these quantities discrete sum:

$$DS_l = \sum_{j=1}^{d} K_{l,dj}$$

For continuous variables C_j, a discretization step is needed for. Respecting the ordering of the risk severity group, for each $c_{lj} \in r_i$ the bootstrap confidence interval (BCI) of the variable was estimated. Unknown data distribution was assumed. If $c_1, c, \dots, c_n$ is a random sample of variable C which has an unknown distribution; let θ be a parameter of interest associated with this distribution and let $\hat{\theta} = T(C_1, C_2, \dots, C_n)$ be the estimate of θ.

Then, θ^*=T ($C_1^*, C_2^*, \dots, C_n^*$) obtained from bootstrap sample $C_1^*, C_2^*, \dots, C_n^*$.

Let be $[2\hat{\theta} - \theta *_{(1-\alpha/2)};\ 2\hat{\theta} - \theta *_{(\alpha/2)}]_r$ the BCI of the risk group where $\theta *_{(1-\alpha/2)}$ represents 1-$\alpha/2$ percentile of the bootstrap coefficient of $\theta *$. Call the upper and lower limits of the confidence interval UL ($2\hat{\theta} - \theta *_{(\alpha/2)}$) and LL ($2\hat{\theta} - \theta *_{(1-\alpha/2)}$), respectively.

Then,

$$\begin{cases} c_{lj} < LL_{r=1} & then\ K_{l,cj} = \dfrac{0.5}{MD_{cj}} \\ LL_{r=1} \le c_{lj} \le UL_{r=1} & then\ K_{l,cj} = \dfrac{1}{MD_{cj}} \\ UL_{r=1} < c_{lj} < LL_{r=2} & then\ K_{l,cj} = \dfrac{1.5}{MD_{cj}} \\ LL_{r=2} \le c_{lj} \le UL_{r=2} & then\ K_{l,cj} = \dfrac{2}{MD_{cj}} \\ UL_{r=2} < c_{lj} < LL_{r=3} & then\ K_{l,cj} = \dfrac{2.5}{MD_{cj}} \\ LL_{r=3} \le c_{lj} \le UL_{r=3} & then\ K_{l,cj} = \dfrac{3}{MD_{cj}} \\ c_{lj} > UL_{r=3} & then\ K_{l,cj} = \dfrac{3.5}{MD_{cj}} \end{cases}$$

We introduce the sum of these quantities called *continuous sum*: $CS_l = \sum_{j=1}^{c} K_{l,cj}$. Finally, SP-RiSc was generated by summing both discrete and continuous variables previously discretized and weighted by MD.

$$\boldsymbol{SP\text{-}RiSc(l)} = \sum_{j=1}^{7} (DS_{l,j} + CS_{l,j})$$

Evaluation by ROC approach. The receiver operating characteristic (ROC) analysis (Youden index method) was used to identify on the training set the SP-RiSc cut-off that maximizes specificity and sensitivity of identifying patients at risk of entering the SP phase (**Fig.1C3**). Finally, this threshold was tested on the validation set (**Fig.1D2**).

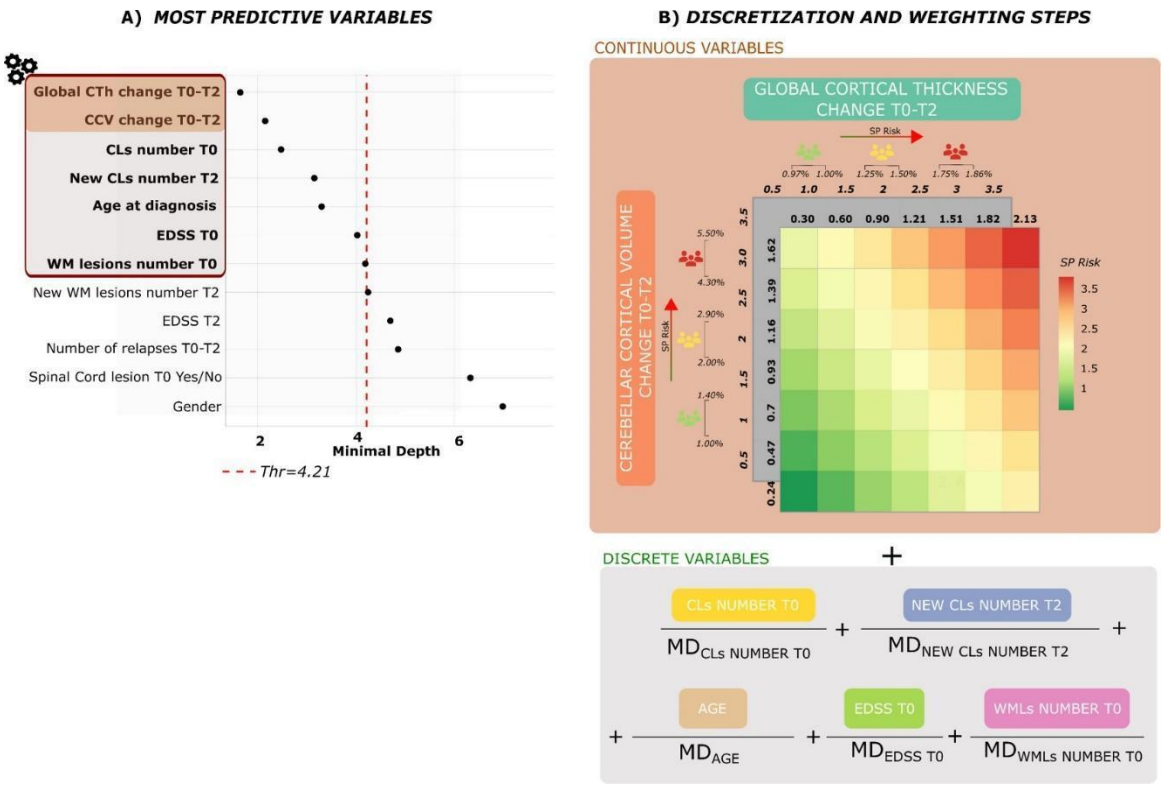

Figure 2. SP-RiSc design. **A)** ***Variables are listed based on their Minimal Depth values; lower value indicated higher predictive accuracy*****.** Predictive variables with Minimal Depth lower than the estimated Thr (4.21) are highlighted. **B)** ***Discretization steps.*** Continuous and discrete variables were discretized and weighed for Minimal Depth measure to be combined to build the SP-RiSc tool.

RSF model and score including only WM parameters

The RSF model was also performed on the training set using demographic, clinical and WM parameters collected during the two first years, therefore without considering information on GM damage. Then, the most predictive variables were combined to develop a different version of the SP-RiSc.

Results

Demographic, clinical and MRI data of the 262 RRMS patients, at diagnosis and after two years, are shown in **Table 2**. During the ten years follow-up period, 69 (26%) patients converted to SPMS; this subgroup, in comparison to those who remained in the RR phase, was distinguished at diagnosis by older age (P<0.001)

and higher number of CLs and WM lesions (P<0.001) and global CTh at T0 (P<0.01), and during the first two years by a larger number of relapses (P<0.001), by a more significant accumulation of grey matter (new CLs, and CCV change; P<0.001) and white matter (new T2 lesions; P<0.01) damage.

In the whole group, during the follow up period 114 (43.5%) patients were switched to second-line DMTs (fingolimod and natalizumab), based on the occurrence of clinical and radiological disease breakthroughs.

Features	Whole group of RRMS at T0 n= 262	RRMS at the end of f-up n= 193	SPMS at the end of f-up n=69	*p* value
Age at diagnosis, mean (SD), y	33.5(9.5)	31.6(9.6)	38.9(6.6)	<.001
Duration of follow-up, median (range)	9.55 (6.79-13.13)	9.26 (6.79-12.05)	10.16 (7.37-13.12)	<.001
Gender, Female, No. (%)	153(58.4)	73(37.8)	33(47.82)	0.05
Number of relapses T0-T2, median (range)	1 (1-3)	1(1-3)	2(1-3)	<.001
EDSS T0, median (range)	1.5(0-3.5)	1.5(0-3)	1.5(0-3.5)	<.01
EDSS T2, median (range)	2(0-2.5)	2(0-2)	2(0-2.5)	<0.05
CLs number T0, median (range)	2(0-19)	1(0-14)	6(0-19)	<.001
New CLs T2, median (range)	0(0-8)	0(0-3)	2(0-8)	<.001
WM lesion number T0, median (range)	8 (2-22)	7(2-22)	10(2-22)	<.001
New WM lesion number T2, median (range)	1(0-4)	1(0-4)	1(0-4)	<.01

CCV T0, mean (SD), cm^3	106.3 (2.2)	103.1 (2.0)	97.9 (2.4)	<.001
CCV change T0-T2, mean (SD), %	2.5(1.99)	1.8(1.3)	4.5(2.07)	<.001
Global CTh T0 mean (SD), mm	2.46 (0.21)	2.39 (0.14)	2.27 (0.25)	<.01
Global CTh change T0-T2, mean (SD), %	1.3(0.5)	1.16(0.4)	1.8(0.5)	<.001
Spinal cord lesion T0, yes, No.(%)	58(22)	34(17.60)	24(34.78)	<.01

Table 2. Demographical, clinical and radiological features collected during the two first years of disease

Selection of the most predictive variables. By applying the RSF, we have identified seven variables with MD lower than the estimated Thr (4.21) and therefore highly predictive of the risk of converting to SPMS. The strongest predictive effect was exerted by the cortical thinning (MD=1.65) and by the cerebellar cortical volume loss (MD=2.15) during the two first two years of disease, and by the CLs load at diagnosis (MD=2.47) and its increase (MD=3.15) after two years; age (MD=3.30), EDSS (MD=4.10) and the WM lesions total number at RRMS diagnosis (MD=4.17) had a moderate impact on the probability of converting to SP (**Fig.2A**). The number of WM lesions at T2 (MD=4.23), the EDSS at T2 (MD=4.66), the number of relapses during the two first years of disease (MD=4.84), the presence of the spinal cord at T0 (MD=6.25) and gender (MD=6.87) were found to have an MD higher than the Thr (=4.21) and were consequently excluded from the SP-RiSc tool design.

RSF performance assessment. Both the BS and C-Index measures confirmed the goodness of fit and the predictive accuracy of the statistical model at different follow-up time quartiles: the BS parameter decreased over time reaching value close to 0 as well the C-Index increased close to 100%. At 7 years: BS = 7.7%, Confidence Interval (CI) (6.4-10) and C-Index = 92.0%; at 8.5 years BS = 8.9% CI

(7.6,10.8) and C-Index = 91.0%; at 9.5 years BS = 8% CI(5.9,11) and C-Index = 91.4%; at 10.5 years BS = 4.6% CI(2.9,5.6) and C-Index = 90%; at 13.5 years BS = 2.0% CI(0.61,3.4) and C-Index = 90.0%. Therefore, the model resulted to be suitable both in terms of predictive accuracy and SP event discrimination, and its predictive accuracy increases proportionally with the disease duration. In contrast, when we applied the same predictive accuracy measures to the Cox PHM and AIC-Cox we found a poor performance in predicting the occurrence of SP, as the BS scores of both Cox models reached very high values close to 60% at all different follow-up time quartiles. In addition, in the Cox regressions models the C-index measures remained close to 80% and therefore lower than the RSF model (**Table 3, Table 4, Table 5**).

Significant Variables	**HR [95% CI]**	***p*-value**
Age at diagnosis	1.12 [1.06-1.16]	<0.001
Number of relapses T0-T2	1.84 [1.14-2.96]	<0.001
New CLs at T2	1.44 [1.12-1.84]	<0.001
CLs at T0	1.85 [1.42-2.42]	<0.001
EDSS T0	1.95 [1.04-3.67]	.03
Global Cortical thickness T0-T2	2.01 [1.35-3.01]	<0.001

Table 3. Cox PHM results

Significant Variables	**HR [95% CI]**	***p*-value**
Age at diagnosis	1.11[1.06-1.16]	<0.001
EDSS T0	1.93[1.04-3.57]	.03
New WM lesions at T2	1.30[1.02-1.66]	.03
CLs at T0	1.83[1.4-2.39]	<0.001
New CLs at T2	1.38[1.10-1.72]	<0.01
Global Cortical thickness T0-T2	1.98[1.34-2.93]	<0.001
Number of relapses T0-T2	1.81[1.19-2.75]	<0.01

Table 4. AIC Cox Results

Times (years)	C-index (%)		Brier Score (%) CI 95%	
	Cox PHM	AIC Cox	Cox PHM	AIC Cox
7	87	87	39 [14-57]	26[13-45]
8.5	87	87	41 [19-56]	30[16-47]
9.5	88	89	50 [31-67]	45[25-61]
10.5	88	90	57 [13-67]	56[14-90]
13.5	88	90	58 [20-65]	55[12-86]

Table 5. Cox PHM and AIC Cox performance

Secondary Progressive Risk Score (SP-RiSc) design and evaluation

Risk groups. According to the EM distribution, three groups of patients characterized by high (n=55), medium (n=54) and low (n=110) risk to enter the SP phase were identified. Patients in the high-risk group had an EM higher than 16.35 (3^{rd} quartile) while the low-risk group patients had an EM lower than 0.32 (1^{st} quartile). In the high-risk group 46 (85.5%) entered the SP phase during the follow-up period (median [IQR] time to reach the SP phase=7 years [2.35]), while in the medium group only 9 (17.7%) became SP (median [IQR] time to reach the SP phase= 8.5years [1.9]). All the patients in the low-risk group remained in the RRMS phase during the entire study period. Clinical and MRI features of each group are reported in **Table 6.**

ROC curve analysis. By combining the 7 most predictive variables (**Fig.2A**) we developed the SP-RiSc tool, which considers the different size of the predictive effect exerted by each variable (**Fig.3A**). In the training set, the optimal SP-RiSc cut-off value, estimated by the ROC curve analysis, was 17.7 and had a sensitivity of 0.91 (95%CI, 0.82-1) and specificity of 0.83 (95%CI, 0.73-0.95). (Fig 3B). Therefore, patients with a SP- RiSc ≥ of 17.7 have a 91% probability to convert to SPMS within 10 years from the disease diagnosis. In contrast, patients with SP-RiSc < 17.7 had 83% probability of remaining in the relapsing-remitting phase. The SP-RiSc predicted the individual risk of SPMS with an overall accuracy of 85% (95%CI: 80%-92%); in the training set, the score was able to discriminate 50 out of 56 SPMS patients (True Positive, TP) and 136 out of 163 patients as RRMS patients

(True Negative, TN), while 5 SPMS patients were incorrectly classified as RR (False Negative, FN) and 27 RRMS patients were misclassified as SPMS (False Positive, FP). Consequently, the Positive Predictive Value (PPV), which indicates the probability of patients being classified as truly SP, was 65% (95%CI: 55%-87%). On the contrary, the Negative Predicted Value (NPV), which is the probability of patients being classified as truly RRMS, was 97% (95%CI: 93%-100%). Finally, to evaluate the generalization property of the SP-RiSc, the threshold of 17.7 was applied on the testing set: the cut-off discriminated 12 out of 13 as patients with SP condition (TP) and 26 out of 30 as RR status (TN). The PPV was 75% (95%CI: 48%-93%) and the NPV was 96% (95%CI: 81%-100%). Therefore, results from the independent test analyses confirmed the great accuracy (88%, 95%CI: 75%-96%), high sensitivity (92%, 95%CI: 70%-100%) and specificity (87%, 95%CI: 70%-96%) of the SP-RiSc performance in identifying patients at higher risk of conversion to SPMS.

Significant predictive variables	High-risk group N=55 46(85.5%)SP patients	Medium-risk group N=54 46(17.7%)SP patients	Low-risk group N=110 0(0%)SP patients	*p*-value
Global CTh change T0-T2, mean (SD), %	1.8 (0.3)	1.3 (0.4)	0.99 (0.1)	<.001
CCV change T0-T2, mean (SD), %	4.9 (2.2)	2.5 (1.6)	1.3 (0.5)	<.001
CLs number T0, median (range)	6(1-18)	3(1-8)	1(0-5)	<.001
New CLs T2, median (range)	2(1-8)	0(0-4)	0(0-8)	<.001
Age at diagnosis, mean (SD), y	37.7 (6.9)	33.51 (11.1)	31. (10.2)	<.001
EDSS T0, median (range)	1.5(0-3)	1.5(0-3.5)	1.5(0-3.5)	<.001
WM lesion number T0, median (range)	10(2-22)	7(2-16)	7(2-21)	<.001

Table 6. Descriptive statistics of the top 7 predictive variables selected by RSF for each of the three risk groups.

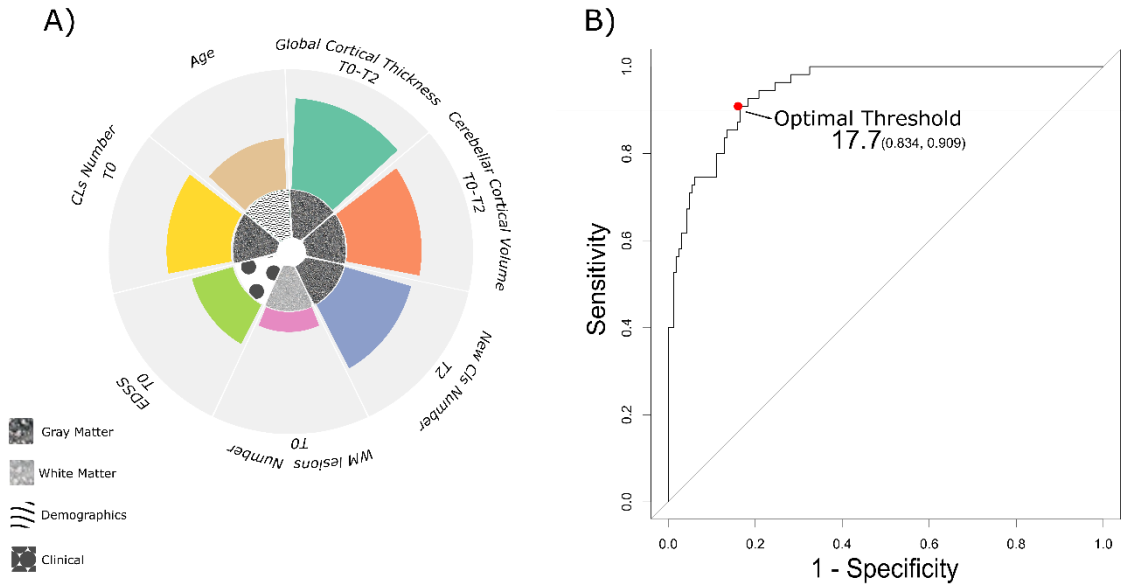

Figure 3. SP-RiSc Visualization and ROC analysis. A) **SP-RiSc tool Visualization**: The seven selected predictors are shown with different colours; the size of the predictive power on SP conversion is reflected by the size of the corresponding shape. Different white and black patterns for each significant variable were reported in the deepest circle B) **ROC curve analysis**. Detection of the optimal SP-RiSc cut-off on the training set.

Evaluation of WM parameters effect on the SP conversion.

In addition, we evaluated a different version of the SP-RiSc, without including GM damage variables, using only the age and the EDSS score at diagnosis and the number of T2 lesions and relapses during the first two years (**Table 7**). The exclusion of GM damage parameters resulted in the model with lower performance to predict the SP transition (STable3). On the training set, the ROC curve analysis was performed in order to detect the optimal cut-off of this WM version score. Therefore, score ≥23.85 indicates that the patient has higher risk to convert to SPMS in the next 10 years. The accuracy, the specificity and sensitivity were 67% (CI 95%, 60%-75%), 58% (CI 95%, 46%-73%), and 91% (CI 95%,81%-100%), respectively. Finally, the score was validated in the testing set by an accuracy of 74% (CI 95%, 59%-87%), a specificity of 67% (CI 95%, 47%-83%) and a sensitivity of 92% (CI 95%, 64%-100%). The Predictive Predicted value (PPV)

and the Negative Predicted Value (NPV) were 55% (CI 95%, 32%-76%) and 75% (CI 95%, 48%-93%), respectively. Therefore, the exclusion of GM damage parameters resulted in developing both the model and the score with lower performance, compared to the standard SP-RiSc, as shown by the C-Index and BS (**Table 8**), and by the ROC curve analyses comparison (**Fig.4**).

Variables included in the RSF model	Significant Predictive variables	MD*
Age at diagnosis	X	1.71
Number of relapses T0-T2	X	2.16
New WM lesions at T2	X	2.25
EDSS T2	X	2.95
WM lesions at T0	X	2.96
EDSS T0	X	3.07
Presence of Spinal lesion (Yes/No) at T0		4.86

Table 7. Variables sorted by Minimal Depth in RSF excluding GM parameters. *MD lower than the estimated Thr (3.19).

Times (years)	C-index (%)	Brier Score (%) CI 95%
7	75	20 [12-69]
8.5	87.6	23 [15-65]
9.5	87.4	22 [19-28]
10.5	86	25 [21-38]
13.5	86.1	13 [1-28]

Table 8. White matter model performance using by C-index and Brier Score

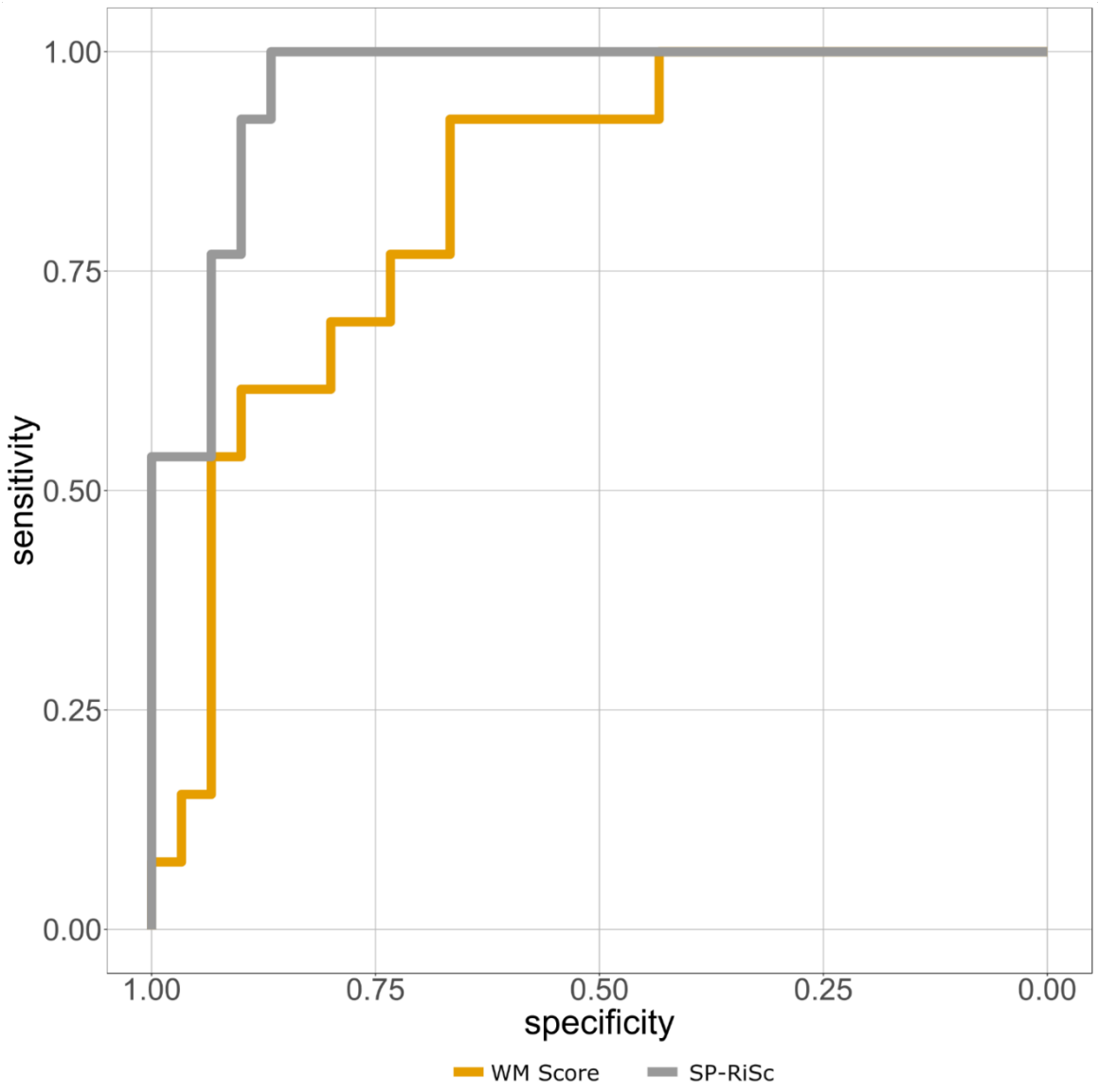

Figure 4. ROC curve plot of white matter score and SP-RiSc

Discussion

Despite extensive efforts collecting information on the natural history of MS and identifying features associated with poor prognosis, the long-term outcome of the disease remains extremely unpredictable, especially at the individual level. The conversion to the SP phase is considered the key adverse event, leading to the accumulation of severe disability, but its prevention is still an unmet therapeutic

target. The early and accurate identification of patients destined to experience a severe disease course is paramount to optimize their management by implementing an aggressive therapeutic approach timely, before irreversible damage takes place. In this study, we propose the Secondary Progressive-Risk Score (SP-RiSc), as a reliable tool to estimate the risk of SP conversion, based on demographic, clinical and MRI measures (conventional and non-conventional) collected during the first two years of the disease.

We retrospectively assessed a cohort of 262 RRMS patients followed up for a mean of 10 years. As we previously reported[44], patients who entered the SP phase were distinguished by older age at diagnosis, by a more significant accumulation of focal inflammatory WM and GM damage during the early phase of the disease, and by a larger number of early relapses. This is in line with previous predictive models, but unfortunately this information has limited prognostic use when applied to a single individual. We addressed and overcame these limitations by using the Random Survival Forest, which is a machine learning approach, allowing to develop a non-parametric model. In comparison to the more traditional Cox regression approach, the RFS model relaxes the restrictive assumptions, such as the proportional hazard or the normal distribution. We considered more suitable the use of machine learning approach firstly for the flexibility to model the data without any transformations (sometimes nonlinear effects of variables have been modelled by transformation or standardization) and secondly for the ability to manage the complex relationships between variables took in account (multicollinearity). Indeed, the machine learning approach applied in this study has been already widely used in the clinical field to improve prediction accuracy in cardiovascular events[84], to stage the esophageal cancer[83], to identify, with high performance, the disease-associated variables in metabolic genomic data[112] or to predict the mortality in rheumatoid arthritis[85].

We demonstrated that the RSF provides higher prediction performance, compared to both the Cox PHM and AIC-Cox model and to the "conventional" Cox regression model. Importantly, the RSF allowed to select and to combine only those variables more accurately distinguishing patients at higher risk of converting to SPMS. Our model highlighted the early accumulation of focal and diffuse GM damage as the most important determinants of the conversion to the progressive phase, supporting

the crucial role played by the GM pathology in the development of late severe disability[52,66,100,101]. In addition, older age at diagnosis was confirmed to independently predict a higher probability of becoming progressive[45,47,113]. Interestingly, we also confirmed that male sex, high frequency of early relapses and larger accumulation of T2 inflammatory lesions in the brain and in the cervical spine early in the disease course, are predictors of poor prognosis[12,94,98,99,113,114], but their MD was found to be higher than the threshold (i.e, 4.21). This indicated a lower prediction ability, compared to other variables, which prevented their inclusion in the SP-RiSc. In line with recent findings from the UCSF cohort[48], this is explained by the strong predictive effect exerted by measures of cortical pathology, which plausibly overshadows the effect of WM damage variables on the outcome. Indeed, our alternative model, not including parameters of GM damage, confirmed the predictive value of early relapses and T2 lesions accumulation. However, by excluding GM variables, the model performed with much lower accuracy and specificity (**Table 8 and Fig.4**). Overall, the two models with and without using measures of cortical pathology, showed similar sensitivity, which, at least partially, is related to the intrinsic relationship between the brain WM and GM damage load, with reciprocal influence from both pathological perspective and imaging-analysis methods. The predictive model, including only variables of WM pathology, is suitable for being implemented and used in MS tertiary centres, where the GM damage is not routinely radiologically assessed. However, our results demonstrated that the measurement of the cortical pathology significantly improves the prediction of the long-term outcome at individual level, and emphasizes the importance of evaluating the cortical damage, in addition to the focal inflammatory WM activity, in order to optimise the patients' management. The early accumulation of GM damage stands out as an essential therapeutic target for maximising the chances of achieving a good control of the disease activity. Previous efforts led to the development of prognostic tools based on demographic and clinical features [48,88]. The SP-RiSc provides an individual accurate estimate of the risk of conversion into the progressive phase and it has been innovatively designed by including measures of cortical pathology to improve the prognostic tool's performance. This was confirmed both by the BS and C-index, showing good

predictive accuracy of the RSF at different time points, and by the high sensitivity and specificity of the SP-RiSc in both the training and testing sets. At individual level, a SP- RiSc ≥ of 17.7 indicates a 92% probability to convert to SPMS within 10 years from the disease diagnosis. In contrast, patients with SP-RiSc < 17.7 had 87% probability of remaining in the relapsing-remitting phase.

We acknowledge some potential limitations. We did not include in our model the information on the type of symptoms at disease onset. However, the predictive role of the clinical features at presentation has been widely debated, with some studies showing worse prognosis among patients presenting with brainstem symptoms[115], but others indicating no clear effect on the clinical outcome[94]. In addition, our analyses results are based on the definition of the clinical onset of the progressive phase, which has an inevitable degree of subjectivity. However, the long follow up allowed to confirm retrospectively after one year the occurrence of the progressive course unrelated to any relapsing activity in all patients, providing high reliability to our findings. We deliberately opted not to use any minimal level of disability for capturing progression, as this approach would allow to uncover more comprehensively an element of progressive disease even in the early stage. The occurrence of progression independent of relapsing activity (PIRA) has been recently highlighted as an important component of the disability accumulation since the early phase of the disease[116]. We are aware of the potential overlapping between PIRA events and the SP course, which nevertheless plausibly share the same underlying pathological mechanisms. Finally, the relatively small sample size might represent an additional limitation of our study. However, the RSF is advantaged by providing a good performance even when applied to small size dimensional datasets[117,118]. Our results have been validated in two independent homogeneous datasets, although we acknowledge that an additional validation, especially on a larger independent cohort with neuroimaging data from different field strength MRI scanners, is important to confirm the score predictive properties and its application in the clinical setting.

Our tool could be implemented in the clinical context (**Fig.5**), especially in tertiary/academic centres where the use of non-routine GM damage MRI measures is widespread, mainly in the clinical trials scenarios. This will put the basis to

develop in future an SP-RiSc online platform with a simple interface available for the neurologist. The score can be updated with other biological baseline parameters, such as the CSF profile[74],[119] in order to further improve the predictive tool's accuracy.

In conclusion, we propose the SP-RiSc as an implemented tool to reliably estimate early in the disease course the individual prognosis, which can be potentially helpful for optimising the therapeutic strategies.

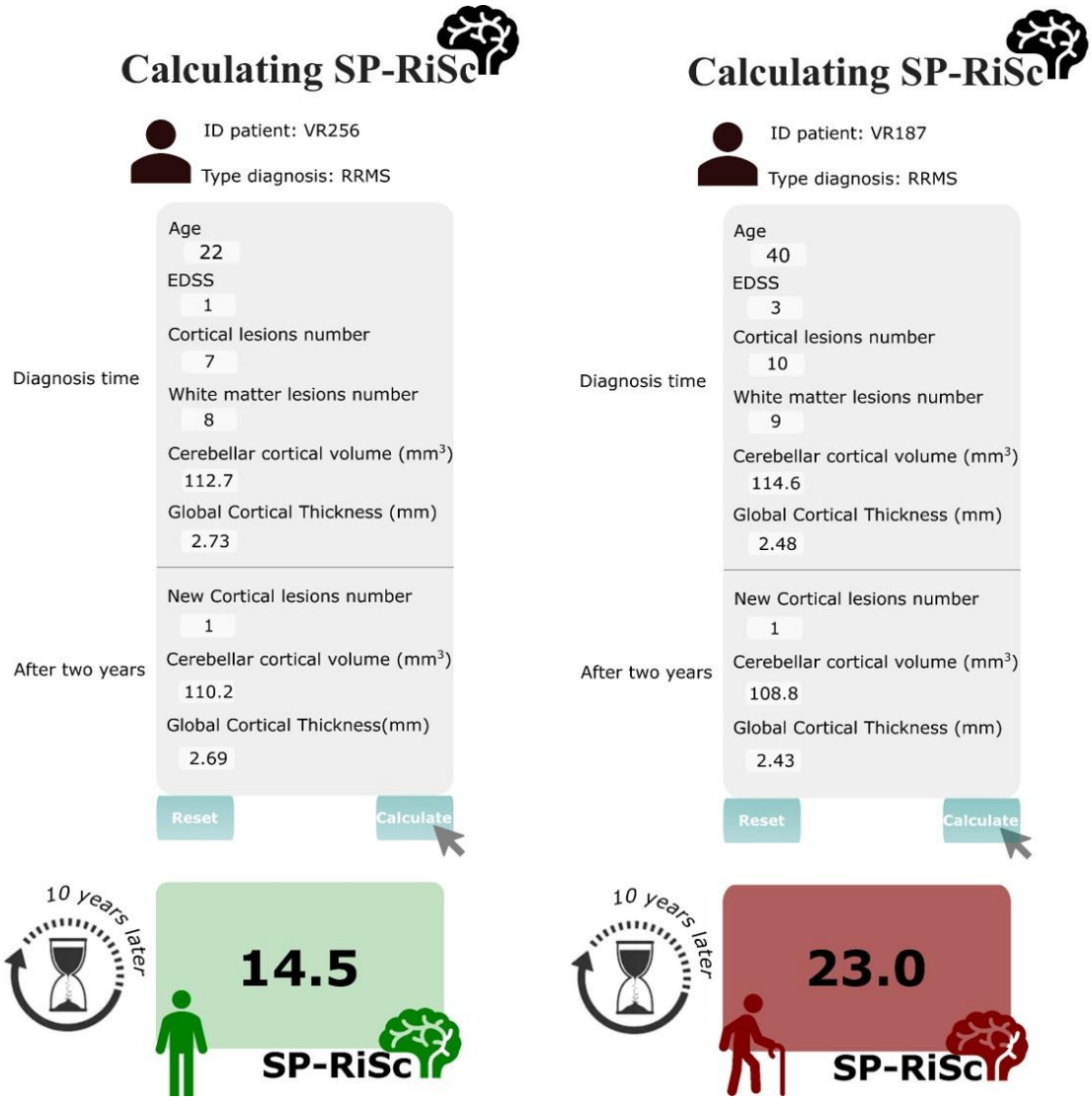

Figure 5. Draft of SP-RiSc web platform

7. Study 2: The Cerebrospinal fluid Profile Linked to Cortical Damage Predicts Multiple Sclerosis Activity

Introduction

Thanks to the recent revision of the McDonald criteria, the diagnosis of MS can be acquired early in the disease course allowing the early treatment of the disease. On the contrary, predicting disease activity and disability progression and more in general the disease evolution is more complicated, and the results are often imprecise.

Neuroimaging data have confirmed that GM damage (both focal and diffuse) can be a good predictor of long term disability progressions[58,66,120]; but the non-conventional MRI analysis required to detect cortical lesions (especially subpial lesions) and cortical atrophy are not straightforward[121,122] despite several improvements including the introduction of GM specific pulse sequences[58,121,123–125] at high field 3T and ultra-high field 7T MRI[126,127] and difficult to be applied in clinical practice.

Therefore, there is a need for additional surrogate biomarkers of GM demyelination and neurodegeneration and compartmentalised meningeal inflammation in order to identify early in the disease course those individuals at risk of a more severe disease course.

Recent neuropathological data suggested that leptomeningeal immune cell infiltration and compartmentalized inflammation within the subarachnoid space may play a key role in the pathogenesis of this cortical pathology[4,55]. Increased meningeal inflammation is associated with a gradient of neuronal, astrocyte and oligodendrocyte damage and with microglial activation, which was higher in the superficial cortical layers (I-III)[128].

Several CSF biomarkers studies have revealed their potential clinical application: the presence of high levels of the Nf-L protein is associated with a higher risk of conversion to clinically definite MS and/or increased brain and spinal cord atrophy[129]. Increased levels of pro-inflammatory cytokines and chemokines, such as CXCL13[130], CXCL12[130], TNF[131,132], and IFN-gamma[133] are detected in the CSF of MS patients.

Previous studies using post-mortem analysis of paired CSF and meningeal samples, obtained from MS cases with or without meningeal lymphoid like tissues[134], has suggested that increased TNF and IFN-gamma expression is associated with more severe cortical pathology.

In recent systematic and comprehensive analysis of inflammatory and cytotoxic molecules expressed in the meninges and CSF derived from 27 post-mortem secondary progressive MS (SPMS), and in 73 living RRMS patients, resulted a set of 18 inflammatory mediators in patient CSF captured at diagnosis, which reflects the state of meningeal inflammation and the extent of cortical damage[74]. These mediators were associated with a more severe focal and diffuse grey matter damage in living patients and with a more severe disease course of those patients evaluated post-mortem. Although these previous results might suggest that these mediators could be useful as biomarkers of disease severity, no data are today available about the real prognostic relevance of these inflammatory mediators.
Aim of the present study was the evaluation of predictive value of these biomarkers in a large population of MS patients at diagnosis.

Methods

Study population

Ninety-nine treatment naïve Relapsing Remitting MS patients (F/M=66/33, mean age=40.4±12.0 years, range 18-55, **Table 1** and **Table 2**) from the MS Centre of Verona University Hospital and from the MS Centre of Montichiari were enrolled at the time of clinical onset (T0). MS patients had confirmed MS diagnosis according to the most recent diagnostic criteria[135]. Patients included in the study had to be free of any other inflammatory disease and had to have at least 1 ml of CSF obtained in the last month. Following MS diagnosis, each patient started on first line disease modifying treatment (Interferon Beta 1a, Glatiramer Acetate, Teriflunomide and Dimethyl Fumarate) and underwent a 3T brain MRI. Patients enrolled have been monitored with clinical and radiological evaluation for at least four years after diagnosis. Expert neurologists chose properly the treatment, blinded to the results of the CSF profile. Because of disease activity and clinical worsening therapy switching was considered. Therefore, patients experiencing, during the

observational period, new relapses, EDSS progression and/or new MRI lesions dropped out of the study and were and were switched to a different therapy. At baseline and at the end of the study (T1), a subgroup of patients also underwent a comprehensive neuropsychological assessment. The Informed consent was obtained from all the patients and the local Ethics Committee approved the study.

	Whole group n = 99	*EDA n=41*	*NEDA n=58*
Age (years)	40.4±12.0 (18-55)	34.7±12.5	39.5±11.3*
Gender (F:M)	66:33	28:13	38:20
Disease duration (years)	1.8±2.2	1.4±2.1	2.1±2.3*
EDSS median (range)	2.0 (0-0-6.0)	2.0 (0.0-4.0)	1.5 (0.0-6.0)
OCBs (yes/no)	87/12	38/3	49/9
CLs number	4.3 ±5.3	7.8±6.0	1.8±3.0***
CL volume (mm3)	230 ± 154	376±76	127±85***
CTh T0 (mm)	2.4 ±0.4	2.3±0.4	2.5±0.3**
T2wMLL T0 (mm3)	960±352	1000±358	933±350
Number of Gad+ lesions	0.2±0.6	0.3±0.5	0.2±0.6
Number of relapses	1.0±0.3	1.0±0.4	1.0±0.2
Dimethyl fumarate **Teriflunomide** **Glatiramer Acetate** **Interferone Beta1a**	51 21 16 11	20 9 7 5	31 12 9 6

Table1. Characteristics of patients at study entry in the whole population, and in the two groups with and without evidence of disease activity. Data are reported as mean and standard deviation if not differently reported; P value < *0.05; ** 0.01; *** 0.001

Features	EDSS change		Relapses		New WM lesions		New Gad+ lesions	
	Yes ***n = 36***	***No*** ***n = 63***	***Yes*** ***n = 29***	***No*** ***n= 70***	***Yes*** ***n = 43***	***No*** ***n = 56***	***Yes*** ***n = 26***	***No*** ***n = 73***
Age(years)	36.9 ± 14	37.9 ± 10.7	31.9 ± 10.1*	40.0 ± 12.0	34.0 ± 11.3*	40.2 ± 12.0	32.5 ± 9.2*	39.3 ± 12.5
Gender (F:M)	24:12	42:21	21:8	45:25	30:13	36:20	20:6	46:27
Disease duration (years)	1.7±2.3	1.9±2.2	1.4±2.1	2.0±2.3	1.7±2.2	1.9±2.3	1.7±2.5	1.8±2.2
EDSS median (range)	2.0 (0.0 4.0)*	1.5 (0.0-6.0)	2.0 (0.0-4.0)	1.5 (0.0-6.0)	2.0 (0.0-4.0)	1.5 (0.0-6.0)	2.0 (0.0-4.0)	1.5 (0.0-6.0)
OCBs (yes/no)	33/3	54/9	25/4	62/8	38/5	49/7	23/3	64/9
CLs N°	8.0±6.2***	2.2±3.2	8.7 ±6.4***	2.5±3.5	7.2±3.2***	2.1±6.8	8.0±6.8	3.0±4.0
CTh T0 (mm)	2.3±0.4**	2.5±0.3	2.2±0.3**	2.5±0.3	2.3±0.3**	2.5±0.3	2.3±0.3*	2.5±0.3
T2wM VL T0 (mm^3)	995.1 ± 337.6	941.0 ± 362.2	1046.0 ± 337.4	925.4 ± 355.1	1022.5 ± 341.4	913.2 ± 356.8	1039.3 ± 374.4	932.71 ± 349.9
Gad+ lesions$	0.4±0.6*	0.2±0.5	0.3±0.6	0.2±0.6	0.3±0.6	0.2±0.5	0.3±0.6	0.2±0.5
Relapses	1.0±0.4	1.0±0.2	1.1±0.4	1.0±0.3	1.0±0.4	1.0±0.3	1.2±0.4*	0.9±0.3

Table 2. Characteristics of patients at study entry and after having divided them on the base of their clinical evolution at T1. *Data are reported as mean and standard deviation if not differently reported; P value < *0.05; ** 0.01; *** 0.001; $ = in the year before lumbar puncture.*

CSF protein analysis

CSF samples were obtained at the time of diagnosis, at least 2 months after the last relapse and within one week of the MRI, according to Consensus Guidelines for CSF and Blood Biobanking[136]. After centrifugation, the supernatant and the cell pellet were stored separately at -80°C until use. The CSF analysis was optimized and performed by two independent investigators, blinded with respect to the clinical and MRI features. The concentrations (ng/ml/mgProt) of the 18 inflammatory mediators identified in our previous cross-sectional study[74] (**Table 3 and Table 4**) were assessed using immune-assay multiplex techniques based on the Luminex technology (Bio-Plex-X200 System equipped with a magnetic workstation, BioRad, Hercules, CA, USA) according to procedures previously optimized[74]. All samples were run in duplicated in the same experiment and in 2 consecutive experiments to verify the results' reproducibility and consistency. The CSF level of each protein detected during the analysis was normalized to the total protein concentration of each CSF sample (measured by Bradford protocol).

CSF proteins	New CLs		Disease Activity	
	Yes (n= 46)	*No (n=53)*	*NEDA (n=58)*	*EDA (n=41)*
CXCL13	27.1±37.7 [0-213] ***	4.0±4.8 [0-17]	5.4±6.7 [0-25]	27.9±39.8 [0-213]***
CXCL12 (x10³)	2.9±2.2 [0.1-17.9]	2.1±2.6 [0.1-12.8]	1.6±1.0 [0.1-5.3]	3.8±3.2 [0.5-17.9]***
CCL25 (x10²)	1.1±0.7 [0-3.0]	1.1±0.8 [0-4.0]	0.9±0.6 [0-3.1]	1.4±0.9 [0-4.0]
TNF-alpha	42.8±41.4 [2-223]	30.0±32.5 [0-133]	19.1±15.7 [0-60]	59.8±45.4 [6-223]***
sTNFR1 (x10³)	5.7±4.5 [1.0-24.0]	4.3±2.6 [0.3-12.1]	3.6±1.7 [0.8-9.9]	6.9±4.6 [0.3-24.0]***
TWEAK (x10³)	2.2±2.3 [0.01-10.7]	1.6±1.6 [0.06-8.2]	1.6±1.5 [0.1-8.2]	2.3±2.5 [0.06-10.7]
APRIL (x10³)	34.1±32.1 [0.9-125.2]	27.7±27.9 [2.6-145.8]	26.3±27.6 [0.9-125.2]	36.9±32.4 [7.9-145.8] **
BAFF (x10³)	9.3±6.6 [2.4-45.0]	9.5±7.0 [1.5-36.6]	7.5±4.3 [1.5-21.6]	12.1±8.6 [2.4-45.0] ***
LIGHT (x10³)	0.6±1.0 [0-6]	0.3±0.3 [0-2]	0.2±0.3 [0-1]	0.7±1.0 [0-6] ***
IFN-gamma	18.3±20.6 [0-78]	18.2±31.1 [0-144]	7.3±8.8 [0-38]	33.8±34.7 [2-144] ***
IFN-alpha2	18.4±17.4 [0-59]	18.4±22.8 [0.0-99.0]	10.8±10.7 [0.0-32.5]	29.1±25.5 [0.0-99.0] ***
IFNlambda2 (x10³)	0.4±0.9 [0-5]	0.4±0.8 [0-4]	0.4±0.8 [0-4]	0.4±0.9 [0-5]
IL-6	33.9±62.6 [1-286]	19.6±35.6 [1-229]	8.9±8.4 [1-38]	50.7±70.9 [2-286]***
IL-8 (x10²)	0.7±0.9 [0.02-4.5]	0.5±0.7 [0.02-3.1]	0.3±0.2 [0.02-1.1]	1.0±1.0 [0.1-4.5]***
IL-10	19.2±16.9 [1-73]	23.1±24.2 [0-93]	18.6±19.3 [0-79]	25.0±23.3 [3-93]
MMP2 (x10³)	2.0±6.0 [0.09-36.5]	2.0±5.0 [0.07-27.9]	2.3±5.4 [0.07-27.9]	1.5±5.6 [0.09-36.5]
Pentraxin3 (x10³)	0.5±0.7 [0-3]	0.3±0.4 [0-3]	0.3±0.4 [0-3]	0.5±0.8 [0-4]
sCD163 (x10³)	50.5±18.8 [10-86]	44.7±25.4 [0-126]	42.4±22.0 [1-126]	54.5±21.8 [0-109]**

Table 3. Mann-Whitney test. Comparison of the mean values of CSF cytokines between MS patients' subgroups; with and without new CLs, with and without disease activity at T1.

	Relapses		New WM lesions		EDSS change	
	Yes (n = 29)	*No (n = 70)*	*Yes (n =43)*	*No (n = 56)*	*Yes (n = 36)*	*No (n = 63)*
CXCL13	34.8±45.3 [0-213]***	6.4±7.7 [0-33]	26.6±39.3 [0-213]***	5.6±6.6 [0-25]	30.1±42.0 [0-213]***	6.0±7.1 [0-33]
CXCL12 (x10^3)	3.8±3.7 [0.4-17.9]**	1.9±1.3 [0.08-6.0]	3.5±3.2 [0.3-17.9]***	1.7±1.0 [0.1-5.3]	3.9±3.3 [0.7-17.9]***	1.7±1.1 [0.1-5.3]
CCL25 (x10^2)	1.3±1.0 [0-4.0]	1.1±0.7 [0-3.1]	1.3±0.9 [0-4.0]	1.0±0.7 [0-3.1]	1.3±1.0 [0-4.0]	1.0±0.6 [0-3.1]
TNF-alpha	62.3±49.1 [6-223]***	25.0±24.1 [0-133]	54.7±44.1 [6-223]***	21.5±22.4 [0-133]	60.9±47.7 [5-223]***	21.7±18.5 [0-76]
sTNFR1 (x10^3)	7.5±5.3 [0.3-24]**	3.9±1.9 [0.8-10.9]	6.6±4.6 [0.3-24.0]***	3.6±1.8 [0.8 -9.9]	7.1±4.8 [0.3-24.0]***	3.7±1.9 [0.8-9.9]
TWEAK (x10^3)	2.5±2.7 [0.06-10.7]	1.6±1.6 [0.1-8.2]	2.0±2.4 [0.06-10.7]	1.7±1.6 [0.1-8.2]	2.4±2.6 [0.06-10.7]	1.6±1.5 [0.1-8.2]
APRIL (x10^3)	36.4±32.5 [7.2-145.8]*	28.4±28.8 [0.9-125.2]	33.2±30.5 [7.0-145.8]	28.8±29.7 [0.9-125.2]	34.0±32.2 [6.8-145.8]	28.9±28.8 [0.9-125.2]
BAFF (x10^3)	12.6±10.0 [3.4-45]*	8.1±4.3 [1.5-21.6]	11.5±8.6 [2.4-45.0]*	7.8±4.4 [1.5-21.6]	11.1±8.3 [3.8-45.0]	8.5±5.7 [1.5-36.6]
LIGHT (x10^3)	0.9±1.1 [0-6]***	0.2±0.3 [0-1]	0.7±1.0 [0-6]**	0.2±0.3 [0-1]	0.8±1.0 [0-6]***	0.2±0.3 [0-1]
IFN-gamma	35.3±39.2 [2-144]***	11.2±14.4 [0-64]	33.6±34.0 [2-144]***	6.5±7.5 [0-38]	32.8±36.5 [0-144]***	10.0±13.2 [0-66]
IFN-alpha2	31.2±28.2 [0-99]**	13.1±13.0 [0-49]	30.2±24.2 [0-99]***	9.4±9.9 [0-30]	28.2±26.1 [0-99]**	12.8±13.6 [0-58]
IFNlambda2 (x10^3)	0.5±1.0 [0-5]*	0.3±0.7 [0-4]	0.4±0.9 [0-5]	0.4±0.8 [0-4]	0.5±1.0 [0-5]**	0.3±0.8 [0-4]
IL-6	46.2±68.3 [2-286]**	18.0±38.1 [1-249]	50.0±69.2 [2-286]***	8.0±7.8 [1-38]	49.6±73.3 [3-286]***	12.9±21.3 [1-140]
IL-8 (x10^2)	1.1±1.1 [0.1-4.5]**	0.4±0.5 [0.02-2.8]	1.05±1.0 [0.1-4.5]***	0.3±0.2 [0.02-1.0]	1.0±1.1 [0.1-4.5]**	0.4±0.4 [0.02-2.1]
IL-10	25.7±25.7 [3-93]	19.4±18.8 [0-79]	24.9±22.8 [3-93]	18.5±19.5 [0-79]	22.9±23.8 [3-93]	20.3±19.6 [0-79]
MMP2 (x10^3)	1.9±6.7 [0.09-36.5]	2.0±4.9 [0.07-27.9]	1.4±5.5 [0.09-36.5]	2.4±5.4 [0.07-27.9]	0.6±0.5 [0.07-3.0]	2.8±6.7 [0.09-36.5]
Pentraxin3 (x10^3)	0.7±0.9 [0-4] ***	0.3±0.4 [0-3]	0.5±0.8 [0-3]	0.3±0.5 [0-3]	0.5±0.8 [0-3]	0.3±0.5 [0-3]
sCD163 (x10^3)	58.0±22.9 [0-109]**	43.0±21.1 [1-126]	51.4±21.8 [0-109]	44.4±23.0 [1-126]	52.7±21.9 [0-109]	44.4±22.6 [0-126]

Table 4. Mann-Whitney test. Comparison of the mean values of CSF cytokines between MS patients' subgroups; with and without relapses, with and without new WM lesions, with and without EDSS change at T1.

MRI Acquisition Protocol

3 Tesla MRI was performed on each patient at the time of diagnosis (within 1 week from the CSF examination) and then yearly for at least 4 years. All the scans were acquired at the NeuroRadiology Unit of the University Hospital of Verona, at least

2 months after the last relapse. MRI sequences were acquired using a Philips Achieva 3T MR Scanner. The following image sets were acquired:

a) 3D-T1 weighted Turbo Field Echo (TFE) (Repetition Time (TR) / Echo Time (TE)= 8.4/3.7ms, voxel size of 1x1x1mm), the acquisition time of 5:51 min;

b)3D-Double Inversion Recovery (DIR) (TR/TE=5500/275ms, Inversion Times (TI) TI1/TI2=450ms/2550ms voxel size of 1x1x1mm), Turbo Spin Echo (TSE) readout with an optimal variable flip angle scheme, number of excitations 3, acquisition time of 10:49 min;

c) 3D-Fluid Attenuated Inversion Recovery (FLAIR) (TR/TE=8000/288ms, TI=2356ms voxel size of 1x1x1mm), same TSE readout as the DIR sequence, number of excitations 1, acquisition time of 4:48 min;

d) 3D-T1 weighted TFE post contrast with the same parameters of the pre-contrast sequence (TR/TE= 8.4/3.7ms, voxel size of 1x1x1 mm, the acquisition time of 5:51 min).

MRI Analysis

A. Lesion detection

The number of WM lesions at baseline and the number of Gad positive, new and enlarging WM lesions at the end of the study were assessed on FLAIR images by a neuroradiologist with extensive experience of MS. The number of total and new cortical lesions were assessed on DIR images following the recent recommendations[135]. Owing to the suboptimal performance of the MRI in visualizing subpial lesions, the present analysis has considered mainly the intracortical and leukocortical lesions. These can be considered as a surrogate marker for the total GM demyelination as well as demonstrated by several neuropathological/MRI studies.

B. Cortical thickness evaluation.

The annualized cortical thinning was calculated using the longitudinal stream of Freesurfer image analysis suite (http://surfer.nmr.mgh.harvard.edu/). Topological defects in cortical surfaces due to WM and leukocortical lesions were corrected using a semi-automated procedure, which includes WM lesion segmentation and lesion filling. The software was applied to the 3D-T1 weighted Turbo Field Echo sequences. Five-time points, approximately equally spaced, were used for each subject. Compared with cross-sectional studies, this longitudinal design significantly reduces the confounding effect of inter-individual morphological variability by using each subject as his/her own control.

Clinical evaluation

Every six months, neurological evaluation was performed. The EDSS score, the number of relapses and the treatments assigned were also recorded. During the follow-up patients with (EDA) or without (NEDA) evidence of disease activity were identified. EDA/NEDA paradigm was defined as a composite score obtained from three related measures of disease activity: (i) evidence of relapses; (ii) confirmed disability progression as assessed by an increase of the EDSS score by at least 1 point sustained over 6 months; and (iii) evidence of new or newly enlarging WM T2 lesions[137].

Neuropsychological assessment

The Brief Repeatable Battery of Neuropsychological Tests (BRB-NT) and the Stroop Test were administered on a subgroup of 52 MS patients both at baseline and the end of the study. According to the conservative approach[138], MS patients were classified as "cognitively normal" (CN) or "cognitively impaired" if patients performed above the cut-off in all neuropsychological tests or below the cut-off in 1 or more, respectively.

Statistical analysis

The Mann-Whitney test was used to compare patients with different clinical and MRI characteristics both at baseline and the end of follow-up. Pairwise univariate Spearman rank correlation index was used to evaluate correlations between CSF proteins levels at diagnosis and both clinical and MRI variables at the end of follow-up. A false discovery rate (FDR) correction was applied.

The logistic regression model was used to estimate the relative contributions of CSF protein levels to the clinical and radiological changes at the end of the study. All the previously identified 18 CSF cytokines were treated as independent variables and their effect, which was expressed by odds ratios (ORs), on the following outcome variables was assessed: EDSS progression (binary: wors- ened/stable), relapse occurrence (binary: yes/no), new/ enlarging WM lesions (binary: yes/no), new Gad+ lesions (binary: yes/no), new CLs (binary: yes/no), and cognitive status (binary: impaired/preserved), all at the end of the study.

Before performing the logistic regression models, the multicollinearity problem among independent variables was checked using the Variance Inflation Factor (VIF). Because this phenomenon was observed, we decided to apply a features selection using a statistical learning approach called least absolute shrinkage and selection operator (LASSO) approach. The receiver operating characteristic (ROC) curve analysis (applying the Youden approach) was performed to assess the specificity and the sensitivity of each CSF protein to discriminate between EDA and NEDA patients after 4 years from the diagnosis. The whole sample was randomly split 70 to 30% into training and testing set datasets, respectively. A stratified 5-fold cross-validation was applied on the training set in order to detect

the optimal cut-off that represents the minimal threshold for the CSF biomarker (mean for each molecules' thresholds over the 5-fold test) to classify EDA patients and their effectiveness was then checked on the test data. To estimate the relative predictive effect of CSF protein levels on the time to disease activity, a non-proportional hazard Cox regression analysis was used. Hazard ratios (HRs) were obtained through comparison versus NEDA. Again, the multicollinearity issue among independent variables was checked using the VIF and a regularised approach using an elastic net penalty was applied in order to select a small significant number of predictors. A separate Cox regression analysis was performed based only on clinical and MRI parameters, including disease duration, the number of relapses in the year before diagnosis, the EDSS, the WM lesion number, the T2WM lesion volume, and the number of Gad lesions at the time of diagnosis. The predictive power of the two models, with and without CSF variables, was measured and compared using the concordance probability (C-index) at 1,2,3,and 4 years, which was estimated by a cross-validation strategy based on bootstrap resampling (with 10 bootstrap samples). Both in the logistic and in the Cox regression analyses, CSF levels were log-transformed to approximate a normal distribution as well as to obtain reliable OR and HR estimates. The log base 2 allowed a more intuitive interpretation of ORs and HRs, as each unit in log base 2 (protein level) corresponds to a doubling in protein level. All the multivariate models were adjusted for the initial treatment choice (one categorical covariate for each first-line drug) and for the age at lumbar puncture. Moreover, we decided to consider the propensity score matching approach (nearest method) to account for bias in initial treatment assignment to validate logistic regression results. The propensity score was estimated using a logistic model with treatment (handled as a dummy; y=0 if patients were treated by Interferon beta 1a/Glatiramer Acetate/ Teriflunomide and y=1 whether patients were treated by Dimethyl Fumarate), the baseline characteristics (age at lumbar puncture (LP), EDSS at T0, WM lesions number, disease duration until LP time) and the18 protein levels as covariates. Although no head to head study has been published to confirm a significant difference in term of efficacy between these first line drug, the choice to split the population in patients treated with Dimethyl Fumarate and patients treated with Interferon beta

1a/Glatiramer Acetate/ Teriflunomide has been based on the results of the phase 3 clinical trials suggesting a slightly more efficacy in favour of Tecfidera compared to other drugs, while no differences were found between Interferon beta-1a/Glatiramer Acetate/ Teriflunomide. As expected, the results of the model using the matched dataset were very similar to the previous ones. The QQ-plot (**Fig.1**) showed clearly that the two cohorts of patients (treated by Interferon beta 1a/Glatiramer Acetate/ Teriflunomide vs those treated by Dimethyl Fumarate) are very similar for all the considered variables before and after matching. In fact, the points in the Q-Q plots would lie on the 45-degree diagonal line if the variable distributions are identical in two groups: as we can see, approximately the same deviations from the diagonal line were observed before and after matching. Thus, given that the matching procedure indicates a high similarity of the two cohorts regarding all the clinical/molecular variables, we can confirm that our findings are not influenced by the first line therapy.

To estimate the relative contributions of CSF protein levels to the annualized cortical thinning, stepwise regression analysis was performed and were adjusted for age at lumbar puncture. Five-fold cross-validation was performed to estimate the goodness of fit of the models in order to increase the generalization: for the first fold, four-fifths of data were used as the training set while the remaining data were used as the testing set to measure performance. The average over the 5-fold of accuracy, specificity and sensitivity were used as performance measures.

The receiver operating characteristic (ROC) curve analysis (applying the Youden approach) was performed to assess specificity and sensitivity of each CSF protein to discriminate between EDA and NEDA patients. The whole sample was randomly split 70%-30% into training and test set datasets, respectively. A stratified 5-fold-cross-validation was applied on the training set in order to detect the optimal cut-off that represents the minimal threshold for the CSF biomarker to classify EDA patients (mean for each molecules' thresholds over the 5-test fold) and their effectiveness were checked on the test data.

In order to further evaluate the association between CSF cytokines and the disease activity, we performed a separate backward stepwise logistic regression analysis, assessing the risk of EDA/NEDA based on the disease duration, the

number of relapses in the year before diagnosis, the EDSS, the WM lesion number, the T2WM lesion volume and the number of Gad+ lesions at the time of diagnosis. The performance of this model was then compared to the performance of the model including only CSF protein levels. To estimate the relative contributions of CSF protein levels to the annualized cortical thinning, stepwise regression analysis was performed.

Finally, to differentiate the specific contribution of CSF protein levels in patients with and without evidence of disease activity, two separate stepwise regression analyses were performed in both NEDA and EDA patients. All the above-mentioned models were adjusted for age at lumbar puncture.

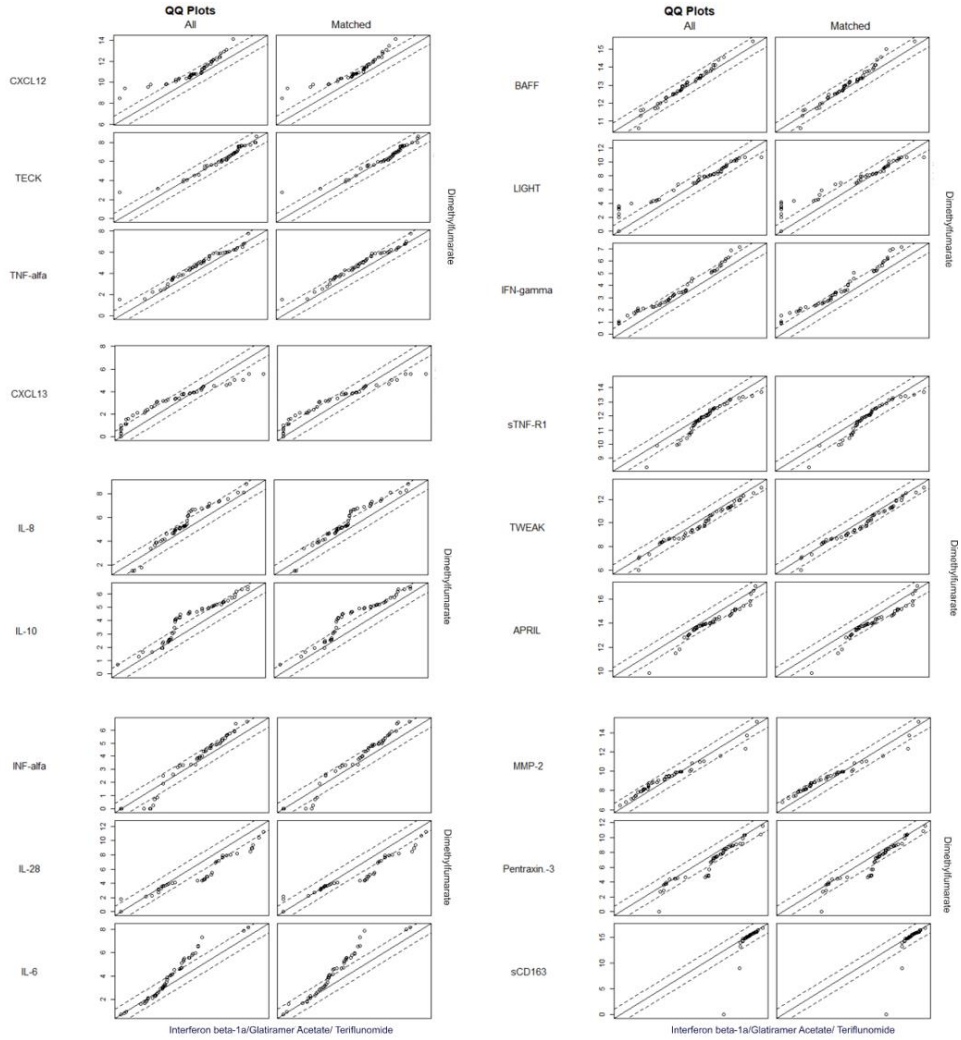

Figure 1 Q-Q plot: The two patient groups (treated with Interferon beta-1a/Glatiramer Acetate/ Teriflunomide vs those treated by Dimethyl fumarate) presented high similarity taking in account the molecular variables.

Results

Clinical and Radiological Data at the End of the Study

All nineteen patients completed the 4-years clinical and radiological follow up (median= 4.3 years, range=4-5 years). Demographic and clinical characteristics of the study's population are reported in **Table 1** and **Table 2.** Following the diagnosis, patients were started on disease modifying treatments: Dimethyl Fumarate (n=51), Teriflunomide (n=21), Glatiramer acetate (n=16) and Interferon beta-1a (n=11). By the end of the study, 58 patients (58.6%) did not show any evidence of disease activity (NEDA), while 41 (41.4%) patients experienced some disease activity: 29 patients had one or more clinical relapses (mean n° of relapse per patient=1.4±0.6, range=1-3), 43 patients showed one or more new or enlarged WM lesions (3.9±2.1, range=1-9), which in 22 patients were active (new Gad lesions=1.7±0.7, range=1-3). In addition, 36 patients experienced EDSS increase (mean increase 1.0±0.6, range=0.5-3.0). After the occurrence of disease activity, twenty-three (23.2%) patients were switched from the first line to a second one treatment (Natalizumab, Ocrelizumab or Fingolimod). No significant first line treatments difference were found among patients with or without disease activity (see **Table 1**).

CSF Profiles Identified Patients with Disease Activity During the Follow-Up Period

At diagnosis, patients who experienced disease activity during the follow-up period had higher CSF levels of CXCL13 (27.9±39.8 in EDA vs 5.4±6.7 in NEDA), CXCL12 (3760± 3187 in EDA vs 1564±0954 in NEDA), IFNγ (33.8±34.7 in EDA vs 7.3±8.8 in NEDA), TNF (59.8±45.4 in EDA vs 19.1±15.7 in NEDA) and CD163 (54460±21801 in EDA vs 42419±22012 in NEDA) (adjusted $p < 0.001$ for all tests; see **Table 3**) with respect to the NEDA patients.

An example of the CSF profile of a patient with severe clinical and radiological activity, despite being on treatment, is described in **Figure 2**.

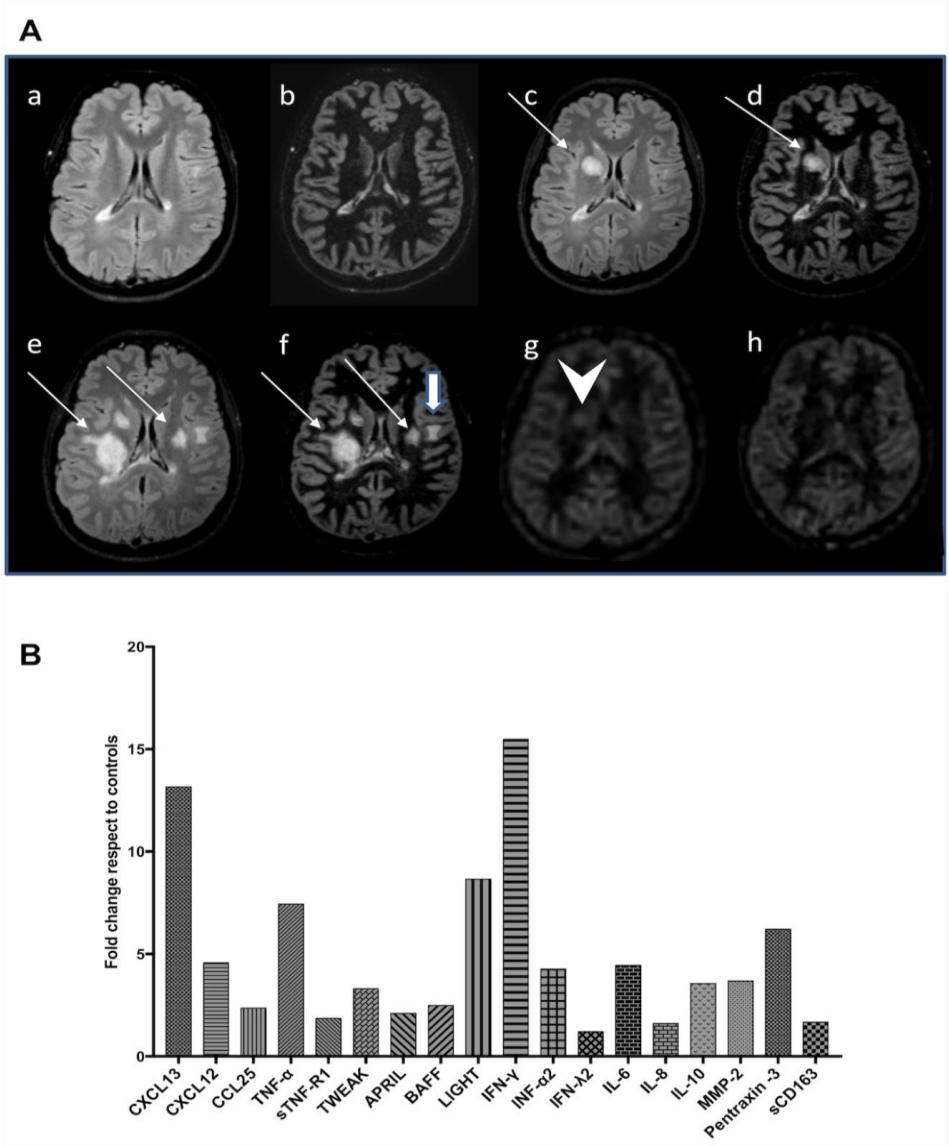

Figure 2 (**A**) Male patient 25 years old. Disease onset in February 2016. FLAIR and DIR sequence obtained at diagnosis (a and b), in 2018 (c and d), and in 2019 (e and f). The significant increase of the lesion load in the white matter (thin arrows) and in the grey matter (thick arrow) was accompanied by several severe clinical relapses, causing severe left hemiparesis. Perfusion sequence obtained in 2018 showed increased perfusion in one of the lesions, adjacent to the head of the R caudate nucleus (arrowhead); this hyperperfused lesion disappeared at the following MRI control (h). (**B**) Combined CSF inflammatory profile of the above patient with MS shown in A. The diagram shows fold changes of the 18 examined molecules concerning the group of controls (other neurological diseases). CSF = cerebrospinal fluid; DIR = Double Inversion Recovery; MRI = magnetic resonance imaging; MS = multiple sclerosis.

Several significant correlations between cytokine level and clinical and radiological parameters were found. Only the strong univariate correlations were reported below (**Fig.3**). CXCL13 levels was found to be positive correlated with EDSS worsening

(rho=0.52, (adjusted p<0.001), with the occurrence of new WM lesions (rho=0.46, adjusted p<0.001) and with the number of new relapses (rho=0.45, adjusted p<0.001). Also, TNF correlated with EDSS change (rho=0.47, adjusted p<0.001), with the number of new relapses (rho=0.42, adjusted p<0.001) and with the occurrence of new WM lesions (rho=0.50, adjusted p<0.001). IFN-gamma correlated with the occurrence of new WM lesions (rho=0.57, adjusted p<0.001), EDSS change (rho=0.38, adjusted p<0.001) and with the number of new relapses (rho=0.38, adjusted p<0.001) (**Fig.4**). Multivariable logistic regression analyses (**Table 4**) have confirmed the same independent association between cytokines and the disease activity; results were adjusted for age and type of first line treatment.

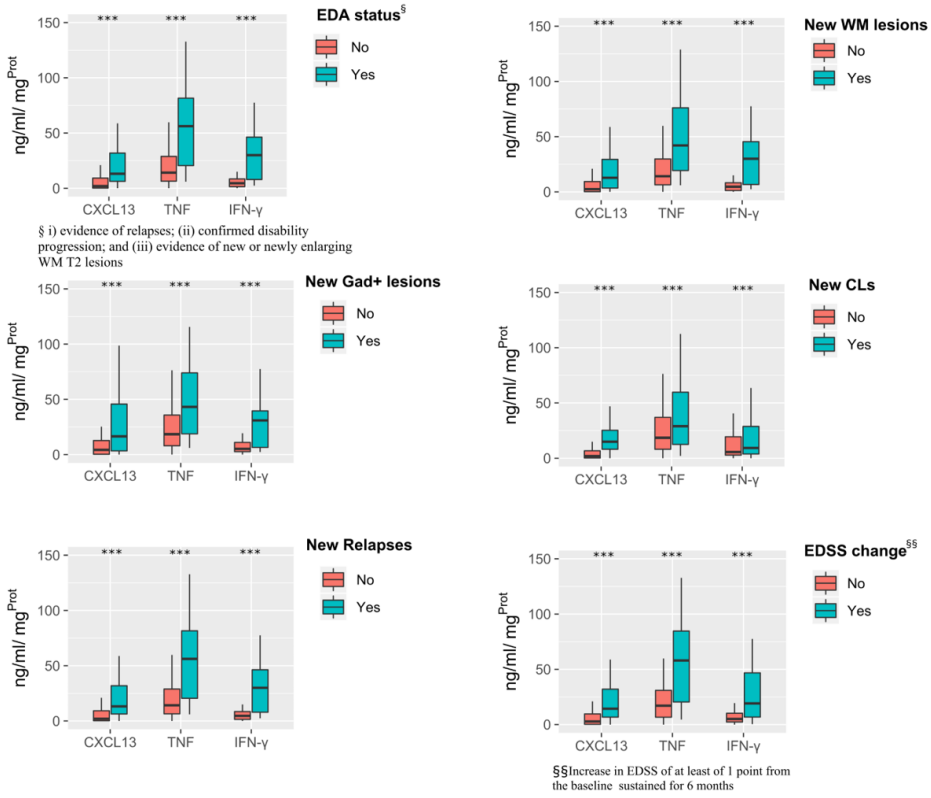

Figure 3. Boxplots of the CSF proteins level in correlation with clinical and MRI features at the end of study. Concentrations (ng/mL/mgProt) of CXCL13, TNF, and IFN-gamma are shown, among groups distinguished by the occurrence of disease activity, new WM lesions, new Gad lesions, new CLs, relapses, and EDSS change. Boxplots show the medians and the two hinges.

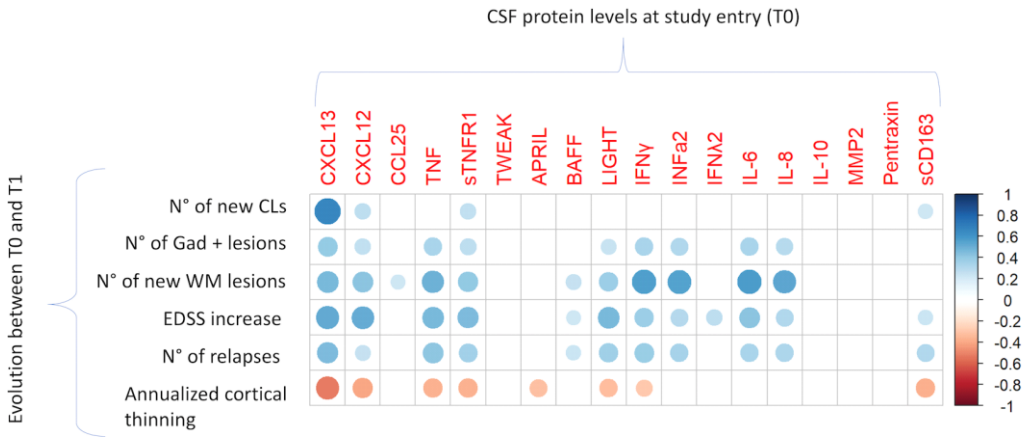

Figure 4. Correlation matrix showing Pairwise Univariate Spearman rank correlation index between CSF protein levels at diagnosis and both clinical and MRI variables at the end of follow-up. FDR correction was applied. The Spearman rank is proportional to the dimension/intensity of the bubbles

Variables selected by the model	OR	95% CI	*p-value*
N° of Relapses T0-T1			
CXCL13	3.10	1.26-4.48	0.004
Pentraxin3	1.65	1.11-2.46	0.01
IFN-gamma	2.15	0.97-4.75	0.05
IFN-alpha2	1.60	0.95-2.69	0.07
CCL25	0.52	0.24-1.44	0.10
TNF-alpha	1.78	0.84-3.76	0.12
BAFF	1.73	0.63-4.74	0.28
New Gad lesions T0-T1			
CXCL13	1.73	1.14-2.61	0.009
IFN-gamma	1.49	0.90-2.18	0.11
IFN-alpha2	1.29	0.86-1.92	0.21
TNF-alpha	1.17	0.70-1.99	0.54
sTNFR1	1.13	0.61-2.08	0.69
EDSS change T0-T1			
CXCL13	1.63	1.04-2.55	0.03
IFNgamma2	1.25	0.94-1.69	0.13
TNF-alpha	1.55	0.79-3.02	0.45
CXCL12	1.41	0.50-2.49	0.45
IFN-alpha2	1.14	0.68-1.93	0.60
sTNFR1	1.17	0.56-2.61	0.69
IL-6	1.10	0.6-2.02	0.76
LIGHT	1.03	0.75-1.39	0.86
New WM lesions T0-T1			
IFN-alpha2	1.80	1.12-2.87	0.01

CXCL13	2.47	1.38-4.42	0.02
IFN-gamma	2.07	1.03-4.1	0.04
IL-6	1.52	0.70-3.4	0.29
sTNFR1	1.23	0.54-2.80	0.62
New CLs T0-T1			
CXCL13	2.27	1.64-3.14	<0.001

Table 4. Multivariable Logistic Regression analysis.
Logistic Regression analysis association between CSF profile at study entry (T0) and clinical/MRI variables at the end of the study (T1). Odds ratio (OR), Confidence Interval (95% CI) and p-value were reported. Significant variables are reported in bold and highlighted in grey.

ROC curve analysis was performed to assess the sensitivity, and specificity for each CSF cytokine to distinguish EDA and NEDA patients (**Table 5**). The 8 CSF proteins, which showed >70% accuracy in predicting the occurrence of disease activity (CXCL13, IFN-gamma, TNF, sTNFR, sCD163, LIGHT, CXCL12, IFN-lambda2), can be considered good biomarkers for the identification of patients at higher risk of experiencing clinical or radiological breakthrough despite being on treatment.

The results of no-proportional hazard Cox regression validate the results from logistic regression and the ROC analysis (**Table 5**) in fact, higher level of CXCL13 (HR=1.35, p-value<0.01), of LIGHT (HR=1.22, p-value<0.01) and of APRIL (HR=1.78, p-value<0.01) independently predicted a higher probability of EDA. The Cox regression model, including CSF variables, was more accurate in predicting the occurrence of disease activity (C-index at 1 year = 65%; 2 years = 74%; 3 years = 73.5%; and 4 years = 71%) than the model with only clinical and conventional MRI parameters (C-index at 1 year = 49%; 2 years = 49%; 3 years = 41%; and 4 years = 44%).

	Optimal Cut-off	AUC [95% CI]	Accuracy (%)	Specificity (%)	Sensitivity (%)
LIGHT (x10³)	0.16	0.78 [0.62-0.95]	80	84	72
sTNFR1 (x10³)	5.69	0.77 [0.60-0.93]	80	89	63
CXCL13	7.85	0.80 [0.62-0.93]	77	73	81
TNF-alpha	37.73	0.76 [0.59-0.93]	77	79	73
CXCL12 (x10³)	1.91	0.80 [0.62-0.93]	77	74	82
IFN-gamma	10.54	0.67 [0.49-0.85]	70	79	55
sCD163 (x10³)	46.07	0.67 [0.49-0.85]	70	79	55
IFNlambda2	37.78	0.67 [0.49-0.85]	70	79	55
INF-alpha2	27.61	0.58 [0.43-0.74]	67	89	27
IL-6	11.07	0.67 [0.50-0.86]	67	63	72
BAFF (x10³)	7.94	0.68 [0.50-0.87]	67	63	73
APRIL (x10³)	18.786	0.61 [0.43-0.80]	63	68	54
IL-8	44.34	0.52 [0.34-0.71]	57	68	36
MMP2	449.80	0.56 [0.37-0.75]	57	57	55
CCL25	114.40	0.54 [0.35-0.73]	57	63	45
TWEAK (x10³)	1.01	0.55 [0.37-0.74]	47	53	36
IL-10	17.18	0.56 [0.37-0.75]	43	42	45
Pentraxin3 (x10³)	0.23	0.49 [0.31-0.68]	33	15	63

Table 5. The results of ROC curve analysis in the testing set was shown. For each protein CSF was reported the optimal threshold, AUC, Accuracy, Specificity and Sensitivity, in discriminating between EDA and NEDA patients.

CSF profile and GM damage at 4 years

During the observational period, forty-six patients developed one or more new CLs (mean number of CLs=3.6±2.7, range=1-8, **Table 3**). The CSF levels of CXCL13 (27.1±37.7 vs 4.0±4.8, adjusted $p<0.001$) was fivefold higher than the patients without CLs.

Both the univariate correlation and the logistic regression analysis resulted a strong association between the number of new CLs and CXCL13 CSF levels (rho=0.67,

adjusted p<0.001) (**Fig.5**), (OR=2.27, CI=1.64-3.14). see Table 4.

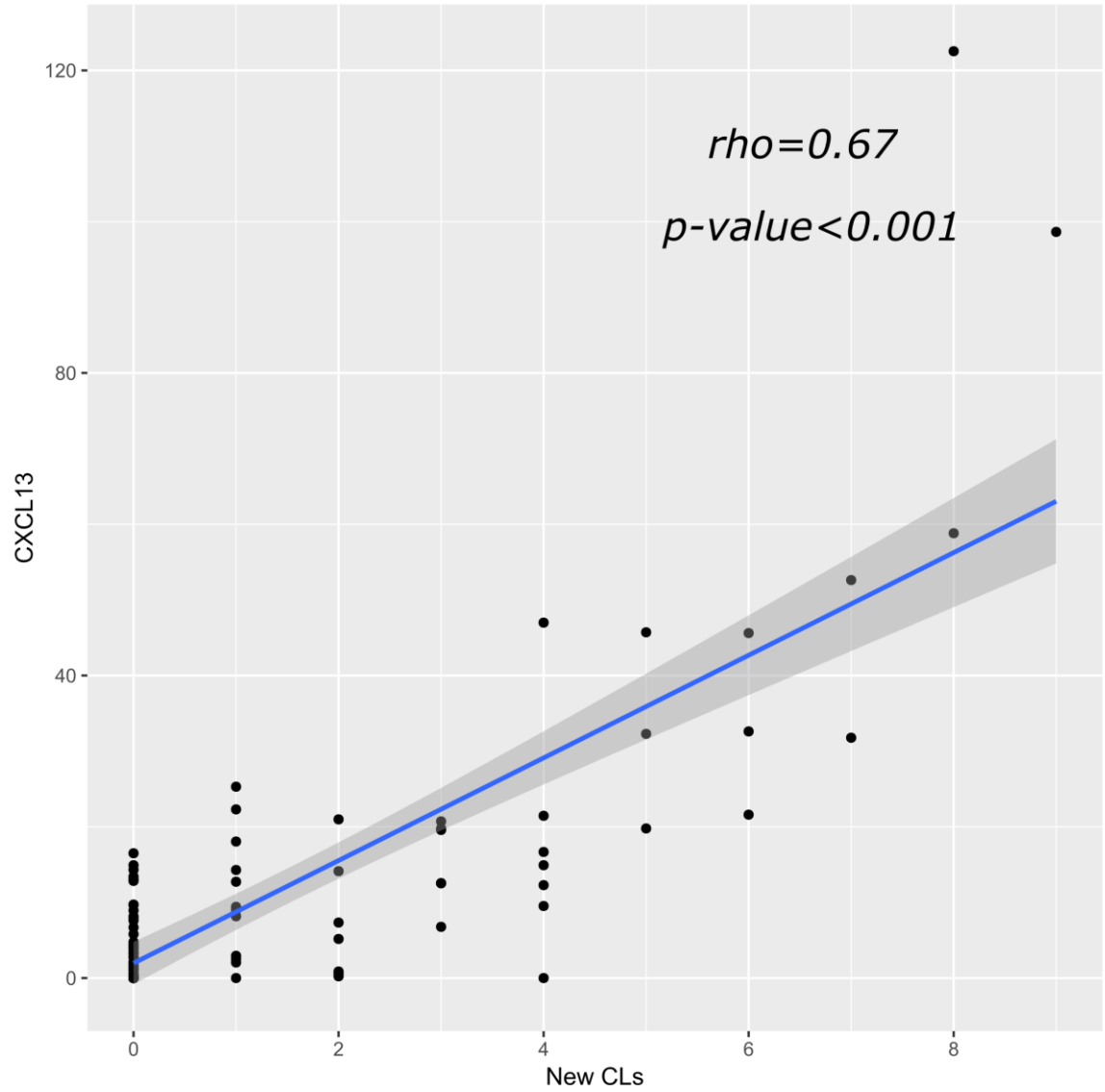

Figure 5. Scatter plot of relationship between the CXCL13 and the new CLs at T1.

Overall, the mean annualized cortical thinning in the four years of follow-up was -0.69% (standard deviation=0.27%, range=-0.19%/-1.6%). The stepwise regression analysis revealed that CXCL13 (β=4.7*10-4, p<0.001), TNF (β =3.1*10-3, p=0.004), LIGHT (β =2.6*10-4, p=0.003), sCD163 (β=4.3*10-3, p=0.009) and TWEAK (β=3.4*10-3, p=0.024) were independent predictors of the annualized cortical thinning.

Negative correlations between the rate of cortical atrophy and CSF levels of CXCL13 (rho=-0.58), CXCL12 (rho=-0.45), and sCD163 (rho=-0.47)

(adjusted $p<0.001$) were found. Moreover, at the end of follow-up, the EDA patients group presented a significant higher rate of cortical atrophy (-0.88%±0.23%) compared to the NEDA ones (-0.56%±0.20%).

The multiple regression analysis demonstrated that, among patients with EDA, CXCL13 ($\beta=6.1*10-4$, $p<0.001$), TNF ($\beta=5.1*10-3$, $p<0.001$), LIGHT ($\beta=4.6*10-4$, $p<0.001$) and sCD163 ($\beta=3.3*10-4$, $p<0.001$) CSF levels were independently associated with annualized cortical thinning. Interestingly, in the NEDA group, CXCL13 was the only CSF cytokine found to be associated with the rate of global cortical tissue loss ($\beta=3.0*$ 10-3, $p=0.009$).

CSF profile was not associated with cognitive dysfunction at 4 years

At baseline, 28 patients presented no cognitive abnormalities while 24 ones were cognitively impaired. At the end of follow-up, only 1 defined as cognitive normal patient converted as cognitive impaired. Moreover, both at T0 and T1 no significant differences of CSF levels were found between cognitive normal and impaired patients both at study entry and at the end of the study.

Discussion

In this 4-year longitudinal study, we demonstrated that among the 18 CSF inflammatory mediators, previously found to be associated with higher risk of meningeal and GM damage, multiple inflammatory cytokines were related with worsening cortical pathology. Among RRMS patients, specific CSF profiles may accurately discriminate patients destined to have higher risk of experiencing disease activity since the early stage of disease. In fact, both the multivariate model and the ROC curve analysis highlighted that, among, the studied cytokines, CXCL13, APRIL, and LIGHT are those more significantly associated with the disease activity, reflected by the occurrence of new relapses, new or enlarging WM lesions, and of disability accumulation. In this light, our data indicate that, an appropriate CSF analysis of a comprehensive inflammatory panel of biomarkers, in addition and combined with clinical and advanced MRI assessment, could represent an specific, sensitive and accurate tool to early identify patients at high risk of disease activity, including disability progression, since the earliest phase of the disease.

Although previous studies had demonstrated an association between individual CSF molecules, such as LIGHT, CXCL13 and Nf-L with severity of disease evolution[139,140], no a complex CSF inflammatory profile was associated with disease activity and no-conventional MRI parameters.

Our results showed that the characterization of the CSF inflammatory profile better predicted the disease severity compared to the early clinical and radiological parameters which had a limited prognostic value. In fact, the model including only clinical and radiological variables resulted much less accurately into the identification of patients at risk of disease activity. In general, NEDA concept mainly takes in account the inflammatory clinical and subclinical WM activity and mostly overlooks GM damage[141] involved into disease progression. In order to address this imbalance, the accumulation of cortical pathology (new CLs and cortical thickness change) and cognitive outcome were evaluated in association with the CSD cytokines. High levels of specific CSF chemokines, mainly related to lymphoid neogenesis and B-cells, such as CXCL13, TNF, TWEAK and LIGHT, not only positively correlated with more severe GM damage at diagnosis[74] but also with the cortical damage accumulation over the 4 years observational period. These results underline the key role of B-cell immunity in the biological mechanisms affecting the cortical pathology[55]. Numerous studies have provided evidence that soluble demyelinating and cytotoxic factors produced by B cells, both in the perivascular and meningeal spaces, are likely to play a major role in the development of GM damage, including cortical demyelination and synapse, and neuronal loss[134,142]. In vivo, such molecules could originate both from cells resident in the meninges or from cells within the central nervous system (CNS) parenchyma[143–145], but little is known about the occurrence of this expression in the MS brain. Interestingly, both CXCL13 and CXCL12 are indispensable chemokines for the initial recruitment and organization of B cells in the CNS. Therefore, together with the increased presence of TNF and lymphotoxin-α/β in the subarachnoid space, raised CXCL13 is likely to contribute to the formation of tertiary lymphoid tissues in the meninges[146]. Noteworthy is also the observation that the CSF levels of sCD163, a marker of the myeloid lineage cells and expressed by activated monocyte/macrophage in MS lesions and infiltrates[147] was found to be

predictive of the rate of cortical thinning. Activated monocytes/macrophages in the meningeal infiltrates and circulating in the CSF could, there- fore, mediate phagocytosis, inflammatory cell recruitment/ activation, and antigen presentation, via CD163 and CXCL13 related mechanisms[146]. This agrees with the notion that innate immunity may significantly contribute to the cortical pathology since the onset of the disease.

With the large number of currently available DMTs, characterized by different efficacy and safety profiles, efforts are being made to implement a personalized therapeutic approach early in the disease course, which can maximize the chances of achieving disease control in the long term. However, early clinical and radiological features have limited prognostic value and optimizing the treatment selection, based on the patient's expected clinical outcome, remains a significant challenge[148].

What's interestingly is that some molecules are related to and predict the occurrence of WM damage, such as new T2 WM lesions and GAD lesions, other CSF biomarkers correlated with non-conventional MRI parameters (such as cortical thinning) which are not strictly linked to acute blood-brain-barrier (BBB) damage and WM lesion activity, but are likely to be linked to intrathecal inflammation (such as CXCL13) and microglial activity (such as sCD163) that persists in the progressive stages[74,147].

All the pro-inflammatory molecules, produced by both lymphocytes and/or macrophages compartmentalized within CSF and meningeal/perivascular infiltrates, may play a direct role in determining demyelination and pathological cell alterations, but may also induce tissue damage indirectly by mediating glial (microglia and astrocytes) activation, as suggested by the relationship between sCD163 and both GM and WM pathology. Indeed, the interaction of complex inflammatory mechanisms, leading to perivascular infiltration by both T- and B-lymphocytes and monocytes, is likely to result in blood brain barrier leakage and the formation of active WM plaques[32].

This study is not without limitations. The low number of patients enrolled from only two MS centres and the lack of an independent validation cohort might limit the general applicability of our model. Nevertheless, the characteristics of our

cohort, enrolled at the time of diagnosis, when treatment had yet to begin, the comprehensive CSF evaluation and the 4-year clinical and radiological follow up using high field 3T-MRI make our results robust. Patients with or without cognitive dysfunction at the beginning or at the end of the study did not show any significant difference in the CSF profile: this could be due to the low number of patients who underwent the neuropsychological evaluation, to the short disease duration and consequently to the low level of accumulated neuronal/axonal degeneration balanced by the high brain cognitive reserves, which accounted for the small number of cognitively impaired patients.

Moreover, treatments might affect our models results. Nevertheless, all the patients were started on first-line DMTs with an almost similar effect on the disease activity[3,149] and, the choice of treatment was blinded with respect to the CSF cytokines profile. Indeed, the model including treatments, as covariate, showed very similar results, indicating that the choice of therapy did not exert any bias.

Finally, we acknowledge that the assessment of further MS-specific biomarkers of inflammation and neurodegeneration are required in order to obtain a more comprehensive CSF pattern predicting the MS outcome and/or reflecting different MS endophenotypes.

8. Study 3: The identification of Cerebrospinal fluid profile prognostic of secondary progression at diagnosis of relapsing-remitting multiple sclerosis

Introduction

As demonstrated in the recent years and confirmed in the above sections, the cerebrospinal fluid analysis, reflecting both the inflammatory nature of disease and the cell mechanisms of neuronal and glia alterations, may employ not only for supporting MS diagnosis but also evaluating and monitoring disease activity, including accumulation of GM (cortical and deep) pathology and disease progression[119]. Seeking new biomarkers could better evaluate the evolution of disease and contribute to the appropriate therapeutic decision making. To date, many studies have suggested an association between individual CSF parameters,

such as IgM index, kappa light chains, chemokine CXCL13, Nf-L and glial fibrillary acid protein with the severity of disease evaluation[139,148]. However, most of these previous studies examined only one or few molecules in correlation with limited clinical or imagining parameters, and very few studies have examined whether and how a complex CSF inflammatory profile associates with disease activity and progression[139,148]. Moreover, most of the previous studies had a cross-sectional design and only few studies have been specifically arranged to associate the transition from RRMS to SPMS or disability progression with CSF profile.

Our recent published data confirmed the value of the CSF analysis in the identification, already at the time of diagnosis, of those patients at high risk of developing a severe course, in particular with early accumulation of GM damage[119]. This is in line with several in vivo and/or ex-vivo[4,34,55,150] studies that confirmed the association of both GM damage and meningeal inflammation with a more rapid and severe disease progression and the feasible prognostic role of such data.

Considering our promising findings and the key role of focal and global GM damage, in the early stage of disease, determining the onset of SPMS progression we have proposed to investigate the prognostic value of CSF inflammatory mediators in RR patients with higher risk of experiencing the SP phase.

In order to achieve this purpose, in a subset of newly-diagnosed MS patients, which had a detailed CSF protein analysis after its collection[119], the SP-RiSc was calculated and based on individual SP-RiSC value, each patient was classified as RR or SP.

An exploratory analysis was performed to identify and compare the two different inflammatory patterns in the two sets of predicted patients and subsequently, a machine learning approach was used to identify CSF proteins mostly associated with the risk of converting into SP. To date, our group mainly focused on only 18 cytokines resulting associated both with the evolution of cortical pathology and the white matter disease activity. To investigate whether other cytokines could be linked to the rapid and severe worst outcome we have assessed an extended pool of CSF biomarkers including both neurodegenerative and protein levels. Once most predictive CSF proteins of risk of experiencing SP were

identified, they were combined into a comprehensive measure (CSFscore) which was validated on an independent SP post-mortem sample.

Methods

MS patient cohort

Thirty-seven patients treatment newly-diagnosed RR patients (24/13, F/M, mean age=34.5±11.32 years) were recruited from the MS Centre of Verona University Hospital and from MS Centre of Montechiari (**Table 1**). Inclusion criteria were: age between 18 and 55 years, the availability of a complete CSF analysis including 71 cytokines and chemokines and at least 2 years of clinical and radiological follow up performed by neurological examinations and by a 3 Tesla MRI scan acquired by the same MRI scanner. The concentrations (ng/mL/mgProt) of the 71 inflammatory mediators (**Appendix 1**) at diagnosis (T0) and demographic, clinical, conventional/non-conventional MRI data (measures of both focal and diffuse GM damage) at T0 and after two years from diagnosis (T2) were included in the analysis. The SP-RiSc (Pisani et al. 2021 European Journal of Neurology undereview, see chapter 6) was calculated for each patient, and based on the SP-RiSc value patients were classified as RR or SP (**Table 1**).

	Whole sample n=37	RR predicted patients n=25	SP predicted patients n=12
Age at diagnosis, mean (SD), years	34.50(11.32)	30.81(8.9)	42.3(13.31)*
Gender, Female, No. (%)	24(65)	17(68)	7(58)
EDSS T0, median (range)	2(0-4)	2(0-3)	3(1.4)*
CLs number T0, median (range)	2.5(0-23)	0(0-15)	9(0-23)***
WM lesion number T0, median (range)	9(3-18)	8(3-11)	13(4-15)*
New CLs T2, median (range)	0(0-9)	0(0-8)	3(0-9)***
CCV change T0-T2, mean (SD), %	2.1(2.21)	2.2(2.0)	2.1(2.7)
Global CTh change T0-T2, mean (SD), %	1.42(1.41)	1.2(1.1)	1.6(1.5)

Table 1. Characteristics of patients at study entry in the whole population, and in the two groups of predicted RR and SP patients. Data are reported as mean and standard deviation if not differently reported. P value < *0.05; ** 0.01; *** 0.001

CSF analysis

CSF sample collection and preparation were performed more than 2 months after the last relapse according to in-house guidelines (used since 1994 by the bio-bank at the MS Centre of Verona), which were in line with the Consensus Guidelines for

CSF and Blood Biobanking. The CSF, obtained at the disease diagnosis, was centrifuged soon after collection, and both the supernatant fraction and the cell pellet were separately stored at −80 °C until use. The presence of OCBs was performed by using iso-electric focusing method and blindly assessed by two independent examiners. Analysis of CSF levels of 71 inflammatory mediators was performed using a combination of immune-assay multiplex techniques based on the Luminex technology (40- and 37-Plex, Bio-Plex X200 System equipped with a magnetic workstation; BioRad, Hercules, CA) as previously[74]. All samples were run in duplicate in the same experiment (blinded respect to the pathological conditions) and in 2 consecutive experiments to verify the results; reproducibility and consistency. The CSF level of each protein detected during the analysis was normalized to the total protein concentration of each CSF sample (measured by Bradford protocol). The levels of neurofilament light chain (NF-L) in CSF were measured using the Human NF-light ELISA kit (MyBioSource, San Diego, CA, USA) according to the manufacturer's instructions.

Ex-vivo CSF sample

The CSF was collected from 29 post-mortem MS cases at time of death (mean age at death 56.8 years ±11.3, mean disease duration 25 years, F/M= 18/11) from the cisterna magna and preserved at -80 °C until use. All the CSF were obtained from the UK MS Tissue Bank at Imperial College London, under ethical approval (08/MRE09/31).

MRI analysis

Each participant underwent two MRI examinations (T0 and T2) using a Philips Achieva 3T MR System (Philips Achieva, Best, Netherlands). The MRI acquisition was performed with a sense 8 channels head coil and comprehended a 3D T1 weighted Turbo Field Echo (TFE) with Repetition Time (TR) of 8.4ms, Echo Time (TE) of 3.7ms, voxel size of 1x1x1 mm3) and acquisition time of 5:51 min; a 3D Double Inversion Recovery (DIR) with Turbo Spin Echo (TSE) readout and TR/TE=5500/292ms, Inversion Times (TI) TI1/TI2=525ms/2530ms, voxel size of 1x1x1mm3, number of excitations=3 and total acquisition time of 10:49 min; and a 3D Fluid Attenuated Inversion Recovery (FLAIR) with the following parameters

: TR/TE=5500/292ms, TI=1650ms voxel size of 1x1x1mm3, number of excitations 1, and total acquisition time of 5:44 min.

The number of cortical lesions was assessed on DIR images while white matter lesions (WML) were segmented from the FLAIR images to estimate WML number and volume. T1w images were processed using the longitudinal stream of the FreeSurfer Software suit (Fischl, 2012) (version 7.1.0) available at http://surfer.nmr.mgh.harvard.edu/ to estimate both global cortical thickness (CTh) and cerebellar volume for each subject. To minimize the effect of WML, all the T1w images were subjected to a preparatory lesion filling step prior to Freesurfer processing.

Statistical analysis

The design of the study is summarised in **Figure.1**.

Firstly, an exploratory analysis, based on a network approach, was applied in order to define the correlation structure of protein patterns among patients (**Fig1.A**). Secondly, a pathway analysis was performed to investigate the enriched functional and biological processes of protein modules detected by the network method (**Fig1.B, Fig1.C**). Finally, a tree-based ensemble machine learning regression method was applied in order to investigate the predictiveness of CSF protein to the risk of becoming SP in the next 10 years (**Fig.1, panel 2**). Once significant predictive inflammatory CSF molecules were identified **(Fig.1, panel 2.A)**, a comprehensive CSF score was defined (**Fig.1, panel 3.B**) and validated on SP post-mortem sample (**Fig.1, panel 3.C**). More details about the statistical approaches were reported below.

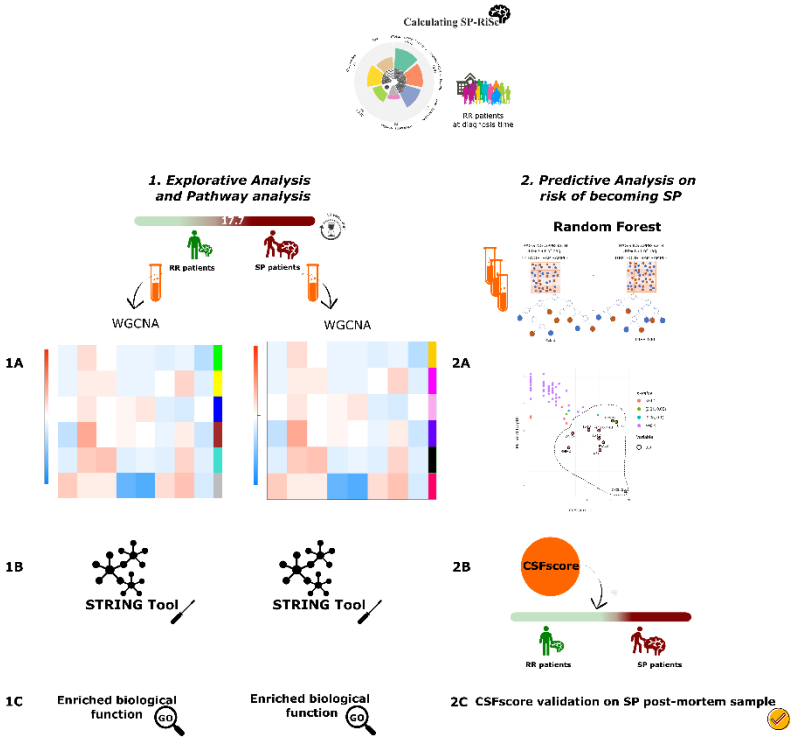

Figure 1. The overall study design: The SP-RiSc was calculated for each patient resulting in 25 RR predicted patients and 12 SP predicted patients. **1)** ***Explorative and Pathway analysis***: **1.A)** WCGNA was applied to RR and SP predicted patients separately; **1.B)** Pathway analysis **1.C)** Identification of biological processes of protein modules ***2) Predictive analysis on risk of becoming SP using CSF proteins levels: 2.A)*** Identification of significant predictive inflammatory CSF molecules; **2.B)** CSFscore design **2.C)** CSFscore validation on post-mortem SP sample

Explorative analysis

Weighted correlation network analysis

In the present study, Weighted gene co-expression network analysis[151] (WGCNA), was used. Although the WGCNA model was developed for gene data input, it has been successfully applied in various biological contexts[152,153].

The main idea behind WGCNA is to apply the network language to define the pairwise relationships (correlations) between quantitative measurements that can be defined by an $n\ x\ m$ matrix $X = [x_{il}]$ where the rows correspond to network nodes $i = (1, \dots, n)$ and the columns $(l = 1, \dots, m)$ to sample measure:

$$X = [x_{ij}] = (x_1\ x_2\ \dots\ x_n)$$

Here $i-th$ row x_i corresponds to the $i-th$ node vector across m samples. Let the vector $T=(T_t,\ldots,T_m)$ be a sample trait (i.e disease status) then the absolute value of the correlation between the the $i-th$ node profile x_i and the sample trait T:

$$GS_i = cor|(x_i, T)|$$

identifies the trait-based node significance.

WGCNA, was used to i) construct a network, ii) identify clusters (modules) of interconnected nodes (set of rows of X) which are highly connected, iii) summarize the node profiles of a given module using PC and iv) and relate the modules identified to a sample trait.

Network construction

In the first step WGCNA defines a protein co-expression similarity between protein levels m and n, denoted by $S_m = |\,cor(m,n)|$. Using a thresholding approach, the co-expression similarity was converted into the adjacency matrix $a_{ij}$with $[0,1]$ defined by hard thresholding S_m measure:

$$a_{ij} = \{1\ if\ S_{ij} \geq \tau\ \ 0\ otherwise$$

This means that whether the absolute correlation measure between the two-protein expression is above the threshold τ, the two proteins are connected in the network. In weighted network the adjacency matrix has continuous values between 0 and 1, by using a power transformation of the co-expression similarity[154,155]:

$$a_{ij_\tau} = S_{ij}^{\beta}$$

If $\beta\ \geq 1$ then a_{ij_τ}between two proteins is proportional to their similarity levels on a logarithmic scale: $log\ \left(a_{ij_\tau}\right) = \beta\ \times log\ (\ S_{ij})$.

As suggested by B. Zhang et al. 2005 the *soft* appropriate power threshold was selected to approximate scale-free topology.

Module detection

The next step was the detection of modules which are defined as highly interconnected proteins[155–158]. Proteins modules were identified by a hierarchical clustering with average linkage. Finally, each module was summarised through the eigengene (ME) of the first principle component (PC1).

Module association to trait sample

In this section, clinically significant modules were selected evaluating the strength of relationship between MEs and clinical traits.

In order to identify proteins with high module membership, the contribution of each variable (C_{var}) to the first PC was calculated as:

$$\% \, C_{var} = \frac{((L \times sd)^2 \times 100)}{\sum (L \times sd)^2}$$

Where L and sd are the loadings and standard deviation of PC1, respectively. Higher the %Cvar higher the impact of the protein on the module.

WCGNA was applied to RR and SP predicted patients separately. Finally, biological, and clinical implications of each significant model were investigated.

Pathway analysis

In order to characterise the protein modules significantly associated with the sample traits in the previous analysis we used STRING[159] to i) quantify module connectivity and ii) enriched biological function. Module connectivity was evaluated by the Protein-Protein Interaction (PPI) enrichment p-value. Low PPI p-value indicates that the nodes (proteins) are not random and that the observed number of edges (the interaction between proteins) is significant. While, strength and False Discovery Rate (FDR) measures were used to evaluate, respectively, how large and significant the enrichment effect is for each biological process detected by the pathway analysis. The p-values are adjusted by multiple testing using the Benjamini-Hochberg approach.

Random Forest Regression (RF)

Similarly, to Pisani et al. 2021 (see the sixth chapter, method section), Random Forest (RF) approach was used to investigate the predictiveness of CSF chemokines and cytokines on the risk of becoming SP in the next 10 years of disease. Array of 71 CSF proteins and the SP-RiSc measure were used as independent and outcome variables, respectively. Let p the number of variables included in the model, $p/3$ were used as the number of variables randomly sampled as candidates at each split and 500 trees as the number of trees grown to develop the RF model[160].

Minimal Depth (MD), total number of trees (times a root), and p-value measures were used to evaluate the predictiveness of features included in the model. Minimal depth variable in a tree equals the depth of the node which splits on that variable and is the closest to the root of the tree. Lower MD higher the variable predictive accuracy. Times a root measure corresponds to the total number of trees in which x_j is used for splitting the root node. Higher times a root measure higher the prediction power of the CSF protein.

While, p-value less than 0.05 means that the number of nodes in which x_j was used for splitting exceeds the theoretical number of nodes if they were random. Distribution of p-value for the one-sided binomial test used was

$$Bin\,(num\ of\ nodes, P(node\ splits\ on\ x_j\ ))$$

where the probability of split on x_j as if x_j was uniformly drawn from the r candidate variables:

$$P(node\ splits\ on\ \ x_j) = P(\ x_j\ is\ a\ candidate) \times P(\ x_j\ is\ selected)$$

According to the combination of the above measures the top 10 CSF proteins were selected as higher predictive on SP-RiSc.

The mean of squared residuals (MSR) parameter was used to estimate the overall accuracy of the RF model.

$$MSR = \sum \frac{y-\hat{y}^2}{n-p}$$

Where p is the number of the variables included in the model, y is the observed value and $\hat{y}$ is the predicted value. The natural interpretation is that lower the MSR higher was the accuracy of the RF model.

CSF score design

From the results of the random forest approach, the most 10 predictive CSF proteins were divided into six categories: 1) *proinflammatory immune response*, 2) *innate immune system (monocytes, dendritic cells, glia)*, 3) *B cell pathway*, 4) *T cell pathway*, 5) *Neurodegeneration path* and 6) *Acute immune response (antiviral and antibacterial)* identified according to known neuro-immunological processes. The MD measure was used to weigh each factor which takes part into the CSF score similarly to the SP-RiSc. The protein levels included in the appropriate cellular pathway were weighted with the average of the minimal depth of the proteins which belong to the specific path. Finally, the CSF score was calculated based on the sum of the proteins weighted by the average MD measure of the proteins belonging to the specific category. The formal definition is reported as follows.

Let P_j with $j = 1, \dots, p$ $(j = 10)$ be the predictive CSF proteins selected from RF, $c \ with \ c = 1, .., i$ $(i = 6)$ the cellular pathway, *a priori* selected, m_{jp} the minimal depth estimated by RF for each protein and l the patient index. Let m_{jc} be the average of the P_j belongs to the cellular pathway and Pw_{jc} be the P_j weighted by m_{jc}:

$$CSFscore(l) = \sum_{j=1}^{10}(Pw_{c,l})$$

Evaluation by ROC approach.

The receiver operating characteristic (ROC) analysis (Youden index method) was used to identify, on the cohort composed of 37 patients (with the complete CSF information), the CSFscore cut-off that maximizes specificity and sensitivity of identifying patients at risk of entering the SP phase. Finally, this threshold was tested on the validation post-mortem set as previous studies provided evidence that the CSF generally is stable over time in SPMS[161].

Results

The SP-RiSc was calculated for each patient resulting in 25 RR predicted patients and 12 SP predicted patients.

Weighted correlation network analysis

Both for the RR and SP set co-expression similarity between 71 protein levels was calculated. The *soft* thresholding power was estimated by the approximate scale-free topology criteria. In both RR and SP predicted patients' set the highest scale-free fit index as a function of the soft-thresholding power was considered. We choose the power 18 and 22 respectively for RR and SP patients' sample (**Fig.2**).

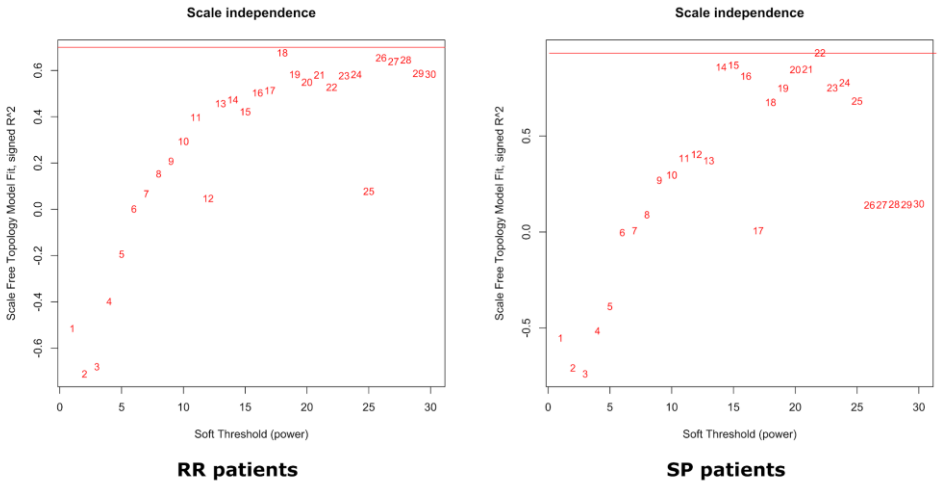

Figure 2. Analysis of network topology for various *soft*-thresholding powers. The left panel shows the scale-free fit index (y-axis) as a function of the *soft*-thresholding power (x-axis) in RR predicted patients. The left panel shows the scale-free fit index (y-axis) as a function of the *soft*-thresholding power (x-axis) in SP predicted patients.

Module detection, correlation with sample traits and pathway analysis

By using a hierarchical clustering analysis six different modules (represented by different colours) were identified in RR patients and in SP patients. Different CSF patterns were detected in the two MS predicted stages. Once the modules were identified, the ME was summarized by the first principle component (PC1) of

module expression levels which was then correlated with the sample traits (Cortical Cerebellum Volume and Global cortical thickness Change T0-T2, CLs number at T0 and new ones at T2, Age, EDSS T0, WM lesions at T0 and the SP-RiSc).

As shown in **Figure 3, panel 1.A**, in RR samples, the ME grey correlated with the number of CLs at T0 (*p*-value <0.001) and of new CLs at T2 (*p*-value <0.001) while the ME brown correlated with the EDSS T0 (*p*-value=0.04). In SP samples the MEblack correlated with CLs at T0 (*p*-value=0.04), the change of volume of cerebellum in the two first years of disease (*p*-value=0.02) and the SP-RiSc (with a moderate significance level) and MEgold was associated with the change of global cortical thickness T0-T2 (*p*-value=0.03) (**Fig.3, panel 2A**).

Then, for each significant module the proteins that contributed mostly to the association with the sample traits were identified (**Fig.3**, **panel 1.B and panel 2.B**).

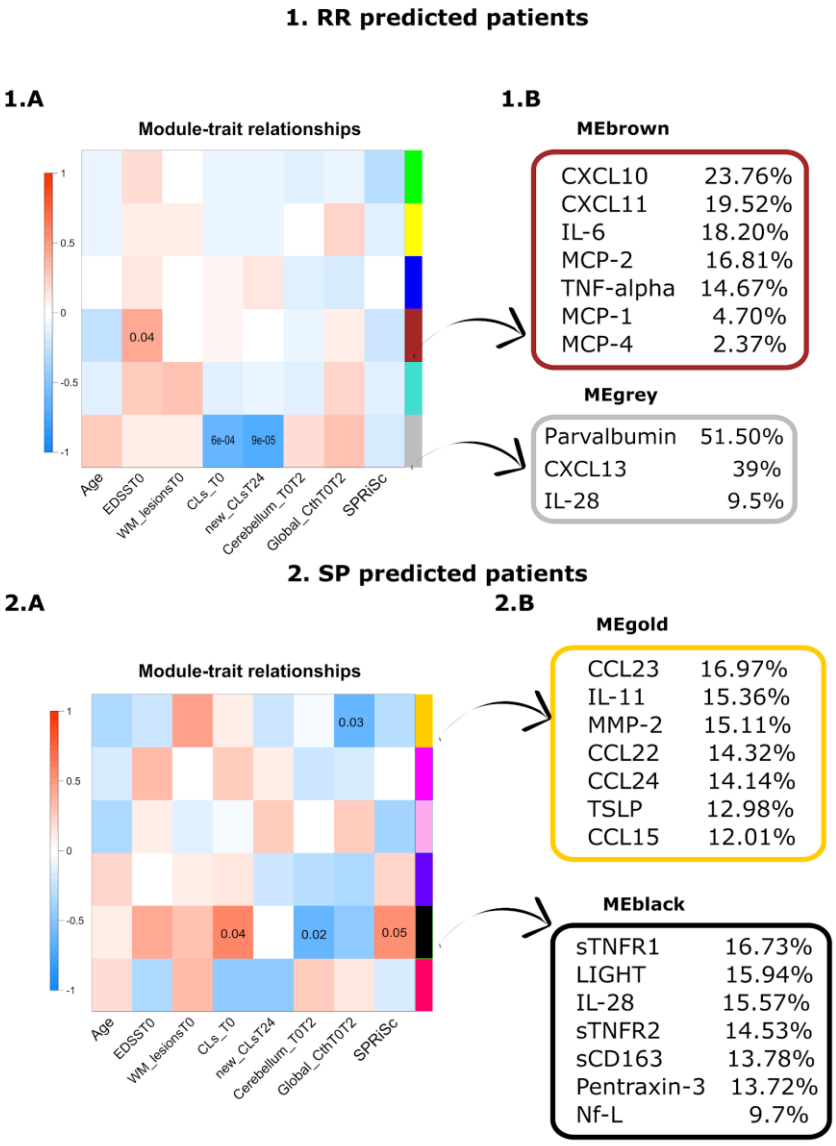

Figure 3. WGCNA results **1)** WGCNA output for RR patients: **1.A)** Correlation matrix between sample traits and ME detected. **1.B)** List of the proteins (sorted by the $\% C_{var}$) belonging to the significant MEs **2)** WGCNA output for SP patients, **2.A)** Correlation matrix between sample traits and ME detected. **2.B)** List of the proteins (sorted by the $\% C_{var}$) belonging to the significant MEs

In RR sample, the MEgrey module was composed by CXCL13, Parvalbumin and IL-28 while MCP-2(CCL8), MCP-1(CCL2), TNF-alpha, CXCL10, CXCL11, MCP-4 (CCL13) and IL-6 were found to be included in the MEbrown. The PPI

enrichment p-value of the MEbrown was less than 0.001 (**Fig.4, panel 1.A**). Pathway analysis showed that RR patients were characterized mainly by biological processes related to leukocytes migration and chemotaxis (CXCL10, CXCL11 and CCL2) (**Fig.4, panel 2.A**). Moreover, among the top 10 enriched networks, the acute inflammatory response, positively regulated by IL-6 and TNF, was detected (**Fig.4, panel 2.A**). On the contrary, the MEgrey results were not significant. The complete list of the top biological processes (Gene Ontology) sorted by the strength identified by the pathway analysis was reported in **Figure 4, panel 2.A**.

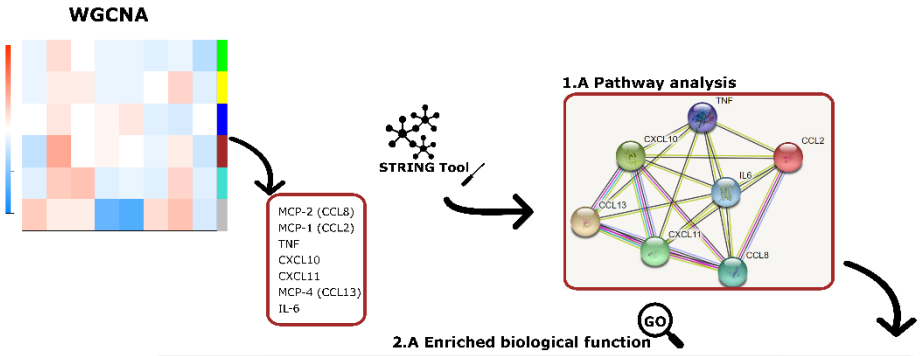

Biological Process (Gene Ontology)

GO-term	description	count in network	strength	false discovery rate
GO:0045073	regulation of chemokine biosynthetic process	2 of 11	2.71	8.32e-05
GO:0010818	T cell chemotaxis	2 of 15	2.57	0.00013
GO:0051023	regulation of immunoglobulin secretion	2 of 17	2.52	0.00016
GO:0010888	negative regulation of lipid storage	2 of 17	2.52	0.00016
GO:0072678	T cell migration	3 of 26	2.51	2.17e-06
GO:0002548	monocyte chemotaxis	4 of 41	2.44	4.74e-08
GO:1901623	regulation of lymphocyte chemotaxis	2 of 21	2.43	0.00022
GO:0048247	lymphocyte chemotaxis	4 of 45	2.4	6.01e-08
GO:0072676	lymphocyte migration	5 of 61	2.36	1.18e-09
GO:0071677	positive regulation of mononuclear cell migration	2 of 25	2.35	0.00030
GO:0002675	positive regulation of acute inflammatory response	2 of 26	2.33	0.00031

Figure 4. 1.A) Pathway analysis performed by STRING in RR patients and **2.A)** Enriched biological function identified on the MEbrown in RR patients

The SP predicted patients' set was characterized by the MEblack which included, sTNFR1, LIGHT, IL-28A, sTNFR2, sCD163, Pentraxin-3 and Nf-L and the MEgold composed by CCL23, IL-11, MMP-2, CCL22, CCL24, TSLP and CCL15. The PPI enrichment p-values of the MEblack was less than 0.001 (**Fig.5, panel 1.A**). The biological functional analysis showed that proteins included in the MEblack cluster are involved mainly in apoptosis mechanism and oxidative (**Fig.5, panel 2.A**). Moreover, Tumor Necrosis Factor (TNF) signalling (TNFR1, TNFR2 and LIGHT) resulted among the significant networks detected by the functional enrichment analysis (**Fig.5, panel 2.A**). It has been demonstrated that the binding of TNF to TNFR1 resulted in the production of pro-inflamatory cytokines and

increased pathology, involving in particular necroptosis and activation of oxidative stress pathways[162]. The presence of Nf-L proteins provided an indication of axonal damage and neuronal death. The observation of sCD163, a marker of myeloid lineage cells, among the proteins suggested the chronic persistence of inflammatory innate immune cell activation in the secondary progressive phase. The complete list of biological processes (Gene Ontology Fig), sorted by the strength, identified by the pathway analysis was reported in **Figure 5, panel 2.A**. In addition, the pathway analysis revealed that the proteins belonging to the MEgold detected by the WGCNA methods were involved in pro-inflammatory cytokine release (PPI enrichment p-value <0.001) (**Fig.6, panel 1.A**). For instance, CCL23 is produced by neutrophils and can actively increase inflammation by increasing inflammatory cell trafficking and up-regulating pro-inflammatory molecules. MMP-2 is a metalloprotease that could possibly directly induce destruction of brain extracellular matrix. The complete list of biological processes (Gene Ontology Fig), sorted by the strength, identified by the pathway analysis was reported in **Figure 6, panel 2.A**.

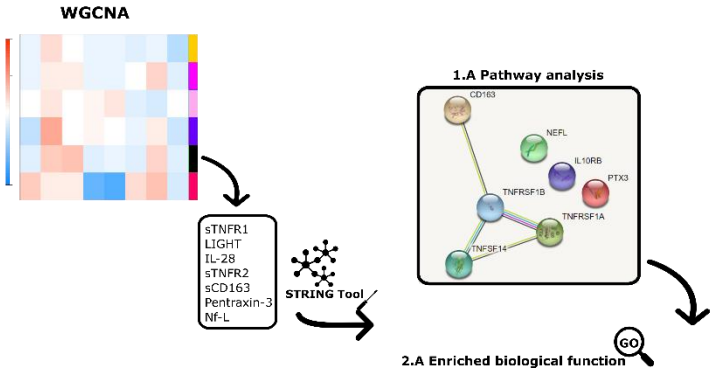

Biological Process (Gene Ontology)				
GO-term	description	count in network	strength	false discovery rate
GO:0003332	negative regulation of extracellular matrix constituent secreti...	2 of 3	3.27	0.00032
GO:1902339	positive regulation of apoptotic process involved in morphog...	2 of 7	2.9	0.00051
GO:0010614	negative regulation of cardiac muscle hypertrophy	2 of 23	2.39	0.0015
GO:0033209	tumor necrosis factor-mediated signaling pathway	3 of 81	2.02	0.00051
GO:0008630	intrinsic apoptotic signaling pathway in response to DNA da...	2 of 71	1.9	0.0058
GO:0071260	cellular response to mechanical stimulus	2 of 78	1.86	0.0066
GO:0043154	negative regulation of cysteine-type endopeptidase activity i...	2 of 91	1.79	0.0070
GO:0097191	extrinsic apoptotic signaling pathway	2 of 93	1.78	0.0071
GO:0050728	negative regulation of inflammatory response	2 of 117	1.68	0.0103
GO:0006954	inflammatory response	5 of 482	1.46	0.00011
GO:0051346	negative regulation of hydrolase activity	3 of 438	1.28	0.0068
GO:0032496	response to lipopolysaccharide	2 of 298	1.27	0.0359
GO:0019221	cytokine-mediated signaling pathway	4 of 655	1.23	0.0015
GO:0022603	regulation of anatomical structure morphogenesis	4 of 961	1.07	0.0042

Figure 5. Pathway analysis performed in SP patients on the MEblack. **1.A)** Pathway Analysis by STRING and **2.A)** Enriched biological function identified

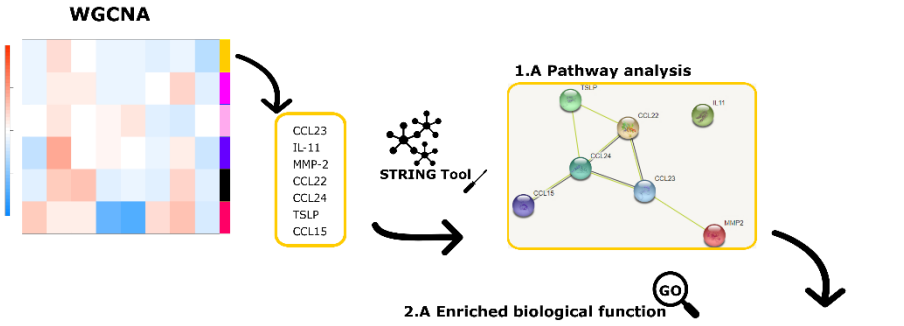

Biological Process (Gene Ontology)

GO-term	description	count in network	strength	false discovery rate
GO:0002548	monocyte chemotaxis	4 of 41	2.44	1.44e-07
GO:0048247	lymphocyte chemotaxis	4 of 45	2.4	1.44e-07
GO:0030593	neutrophil chemotaxis	4 of 59	2.28	2.08e-07
GO:0070098	chemokine-mediated signaling pathway	4 of 75	2.17	3.05e-07
GO:0071347	cellular response to interleukin-1	4 of 124	1.96	1.52e-06
GO:0071346	cellular response to interferon-gamma	4 of 155	1.86	2.66e-06
GO:0070374	positive regulation of ERK1 and ERK2 cascade	4 of 196	1.76	4.71e-06
GO:0071356	cellular response to tumor necrosis factor	4 of 197	1.75	4.71e-06
GO:0061844	antimicrobial humoral immune response mediated by antim...	2 of 107	1.72	0.0028
GO:0050729	positive regulation of inflammatory response	2 of 120	1.67	0.0034
GO:0050731	positive regulation of peptidyl-tyrosine phosphorylation	2 of 180	1.49	0.0071
GO:0019221	cytokine-mediated signaling pathway	7 of 655	1.48	2.11e-08
GO:0010469	regulation of signaling receptor activity	6 of 577	1.46	2.22e-07
GO:0043410	positive regulation of MAPK cascade	5 of 512	1.44	3.64e-06
GO:0043547	positive regulation of GTPase activity	4 of 406	1.44	5.13e-05
GO:0006954	inflammatory response	4 of 482	1.37	9.52e-05
GO:0031349	positive regulation of defense response	3 of 365	1.36	0.0010

Figure 6. Pathway analysis performed in SP patients on the MEgold. **1.A)** Pathway Analysis by STRING and **2.A)** Enriched biological function identified

The complete list of modules of CSF proteins detected by the WGCNA method was reported in **Table 2 and Table 3**.

RR patients	
MEgreen	TWEAK, sCD30, IL-26, IL-32
MEyellow	sTNFR2, BAFF, gp130, sIL-6Ra, Chitinase-3 Fibrinogen
MEblue	CCL22, CXCL9, CCL15, APRIL, IL-11 MMP-2, Pentraxin-3, TSLP, sCD163, Nf-L CXCL2
MEbrown	CXCL10, CXCL11, MCP-1, MCP-2 MCP-4, TNF-alfa, IL-6
MEturquoise	CCL21, MIP-1alfa, CXCL5, CCL20 CCL11, CCL19, CCL24, CXCL16, CCL26, CXCL12, CX3CL1, TECK, GM-CSF, sTNFR1 LIGHT, CXCL1, INF-gamma, MCP-3, INF2-alpha, MIF; INF-beta, IL-1beta; IL-29, IL-4, IL-8, IL-12p70, IL-10, IL-19; IL-16, IL-20, IL-12
MEgrey	Parvalbimin, CXCL13, IL-28A

Table 2. Complete list of Modules of CSF proteins detected in RR patients by the WGCNA method

SP patients	
MEgold	CCL22, CCL15, CCL23, IL-11, MMP-2, TSLP
MEdarkpink	CCL21, CX3CL1, GM-CSF,CXCL1,CCL1, CXCL10,MIF,CXCL9,MIP-1alpha, CXCL12, TNF, INF2-alpha, INF-beta, IL-4, IL-19, IL-22, IL-27, IL-35, Osteopontin
MEpink	CCL19, CXCL13, TECK,CXCL5, IFN-gamma, CCL11, IL-29, CCL26, IL-1beta, CXCL2, IL-6, CXCL11, IL-8, MCP-2, IL-10, MCP-3, IL-16, CCL20, IL-12; IL-20, MMP-1
MEviolet	MCP-1, CXCL16, TWEAK, BAFF, sCD30 gp130, sIL-6Ra, IL-26, IL-32, Chitinase-3,Fibrinogen
MEblack	sTNFR1, sTNFR2, LIGHT, IL-28A, Pentraxin-3, sCD163, Nf-L
MEmagenta	MCP-4, APRIL, IL-12p70, Osteocalcin, Parvalbumin

Table 3. Complete list of Modules of CSF proteins detected in SP patients by the WGCNA method

Random Forest Regression (RF)

To identify the CSF profile at diagnosis of those patients with higher risk of experiencing the secondary progressive phase, Random Forest Regression approach was applied on 37 patients who had the whole CSF information (71 proteins). The following results were related to the OOB samples evaluated by the model. The 10 most predictive CSF proteins were reported taking in account the combination of three different measures (Minimal Depth (MD), Times a root and the p-value) (**Fig.6**). CXCL13, Nf-L, Parvalbumin, MMP-2, IL-12, CCL24, IL-10, Pentraxin-3, TECK and sTNFR1 resulted the most predictive of the SP risk with a low error rate (MSR=22%). Notably, these results were in line with the explorative analysis. Indeed, among the most predictive proteins related to the transition from RR to SP phase, we found that molecules with highest contribution on the association between the ME and the clinical/MRI features.

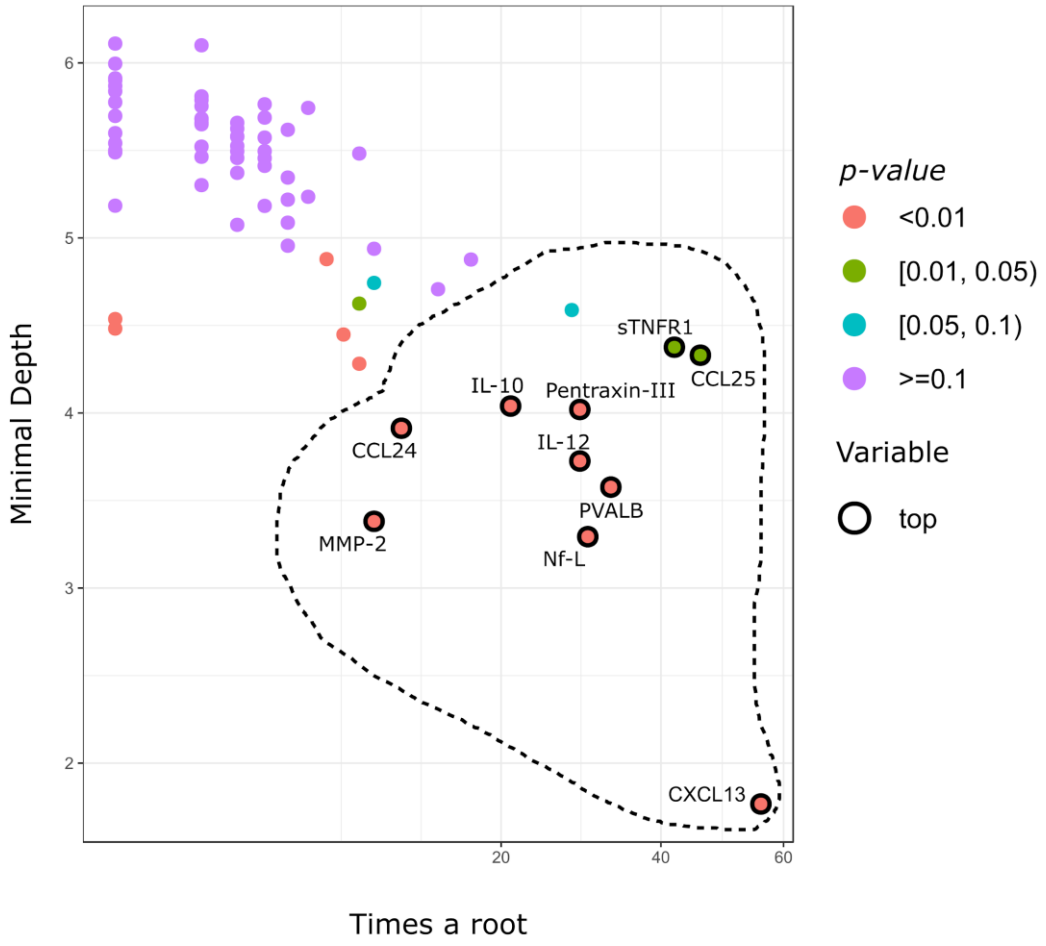

Figure 6. Multi-way importance plot with times a root parameter as function of mean minimal depth measure. The plot shows the 10 most predictive variables on the risk of experiencing SP phase. Each dot was filled according to the p-value.

The best predictive CSF proteins were combined into a comprehensive measure (CSFscore) (**Fig.7**) and ROC curve analysis was used to define the optimal-cut off defined as the threshold maximizing both sensitivity and specificity. As mentioned in the method section, each CSF protein was associated to *a priori* cell pathway as follows:

Proinflammatory immune response: sTNFR1

B cells pathway: CXCL13, IL-10

T cells pathway: IL-12

Innate immune system: MMP-2, CCL25

Neurodegeneration: Nf-L and Parvalbumin

Acute immune response pathway: CCL24 and Pentraxin-III.

The optimal CSFscore cut-off was 1292 with a specificity of 60% (95%CI, 40-80%) and a sensitivity of 58% (95%CI, 33-83%), and with an overall accuracy of 60% (95%CI, 43-75%). Therefore, patients with CSFscore ≥ 1292 have a probability of 58% to convert to SPMS in the next 10 years from the diagnosis time. In contrast, patients with SP-RiSc < 1292 have a probability of 60% of remaining in the relapsing-remitting phase. The CSFscore was able to discriminate 7 out of 12 SPMS patients (True Positive, TP) and 15 out of 25 as RRMS patients (True Negative, TN), while 5 SPMS were incorrectly classified as RR (False Negative, FN) and 10 RRMS patients were misclassified as SPMS (False Positive, FP). Indeed, the Positive Predictive Value (PPV), which indicates the probability of patients being classified as truly SP, was 41% (95%CI, 25-60%) while the Negative Predicted Value (NPV), which is the probability of patients being classified as truly RRMS was 75% (95%, 61-89%). Finally, for the CSF score validation, the threshold of 1292 was applied on the independent SP ex-vivo patients' set: the cut-off distinguished 25 out of 29 patients with SP condition reaching high sensitivity.

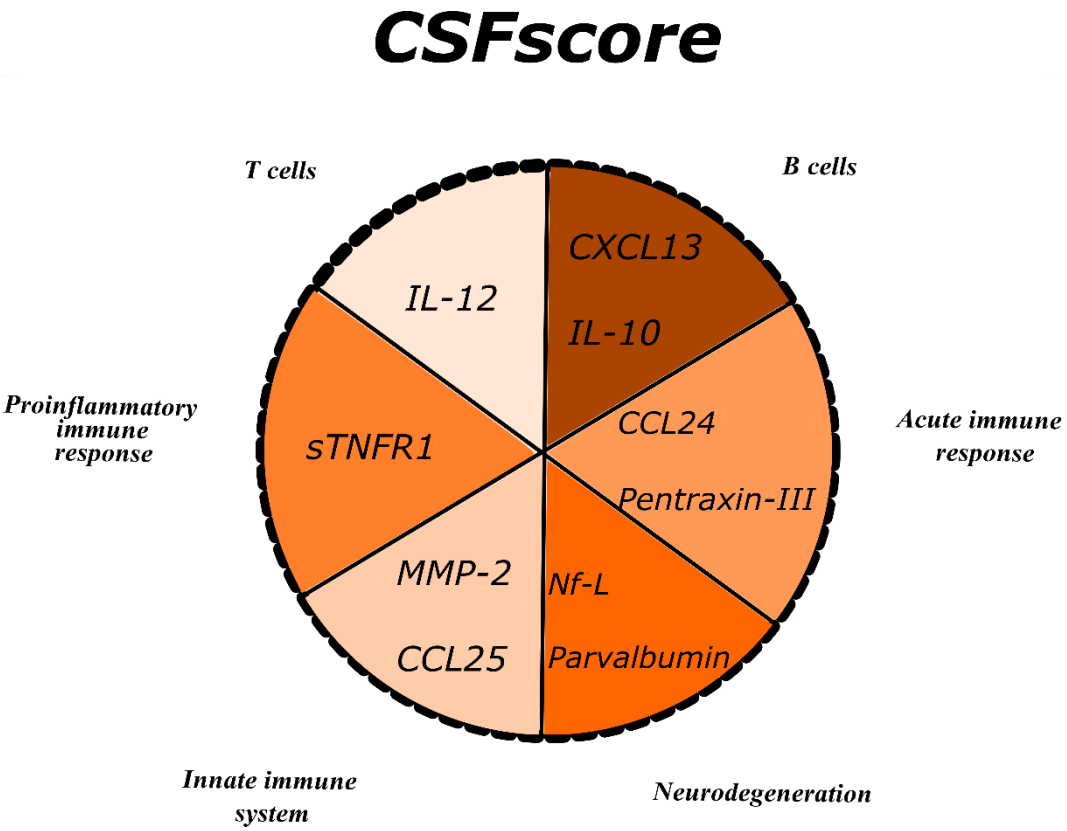

Figure 7. The best predictive CSF proteins, selected by RF, were combined into the CSFscore. Each CSF protein was associated to a known neuroimmunological process.

Discussion

MRI techniques have been widely established as the primary surrogate biomarker to highlight the mechanisms underlying the disease progression. In fact, the inclusion of both conventional and no-conventional MRI measures in the SP-RiSc tool supplied the highest accuracy on the identification of patients with higher risk of converting into SP phase, confirming the potentiality of MRI assessment especially in cortical pathology detection. Nevertheless, additionally inspections are required to make the MRI techniques more standardized and reliable[163]. Therefore, there is an unmet need to identify biomarkers which reflect the disease processes in progressive MS. Although recent studies have investigated the relationship between inflammation and ongoing tissue damage by using the CSF, the pathogenesis of disease progression in MS is still not exactly clear[53,128].

In the light of this, we examined the feasibility of using cerebrospinal fluid (CSF) proteins, measured at diagnosis, as biomarkers in progressive Multiple Sclerosis disease. Both the explorative analysis and machine learning results (confirmed on the post-mortem SP sample) revealed that high levels of specific CSF chemokines, linked to the organization and immune activity of B-cells (CXCL13, TWEAK, LIGHT, IL-10) involved into the disease progression which is mainly characterized by elevated cortical pathology. We observed, in fact, that CXCL13 not only was associated with the GM damage al diagnosis but also with the cortical load over 2 years. Interestingly, sCD163 together with Nf-L, sTNFR1, IL-28 was found to be correlated to the change of global cortical thickness over the two first years of disease. Therefore, sCD163, which is a marker of the myeloid lineage cells, could reflect the ongoing phagocytosis and inflammatory activation of innate immune response, stimulated by monocytes in the meningeal infiltrates, CSF and choroid plexus, in line with the notion that innate immunity may play a role on the cortical pathology from the time of diagnosis. Moreover, the presence of the overexpressed TNFR1, involved in TNF signalling pathway, among the most predictive variables on the SP risk confirmed the association between the pro-inflammatory cytokines and aggressive disease pathology[164]. Interestingly, two proteins, among the 10 most predictive CSF molecules associated with the SP progression, were linked to the acute immune response path: CCL24 and Pentraxin-3. CCL24, known as eotaxin-2, is involved into recruitment of eosinophil to sites of inflammatory responses to parasitic infections, as well as in allergic and autoimmune disease[165]. Notably, several studies have also found high levels of both serum and CSF CCL24 in several neurodegenerative diseases. Pentraxin-3, exert many functions in the development and maintenance of autoimmune neuroinflammation: in particular during MS neuroinflammation it facilitates myelin phagocytosis while in the animal model EAE, it could have a key role in clearance of pathogens and apoptotic cells, and in regulating mechanisms[166] of tissue injury.

In addition, both the explorative and the machine learning analysis highlighted the involvement in the MS progression not only of the proinflammatory

cytokines/chemokines but also biomarkers of neurodegeneration, such as Parvalbumin and Nf-L.

Following axonal destruction, Nf-Ls are released into the extracellular space and drain into the CSF indicating a neural death and axonal damage. Parvalbumin, which is a calcium binding protein, it is most likely related to interneuronal loss. These results are in line with our previous study[167] which suggested that Parvalbumin may represent mainly a biomarker of specific cortical neurodegeneration that is independent of demyelination. In fact, Parvalbumin CSF levels correlated both with cortical lesion number but also with global and regional cortical thinning insinuating that it could be a more specific marker of cortical neurodegeneration related atrophy. These data suggested that Nf-L and Parvalbumin levels increased in the CSF of MS patients who convert earlier into SP phase and may represent the best biomarker of early signs of neuro-axonal degeneration. It seems that for those patients who were predicted to remain in the RR phase during 10 years from the diagnosis, the CSF pattern at diagnosis reflected the first stage of the acute inflammatory process characterized by the recruitment of lymphocytes, monocytes and neutrophils in the CNS. On the contrary, the CSF profile at diagnosis of those patients who were predicted as progressive during the course of disease was mainly defined by chronic inflammation mechanism, involving the apoptosis processes, and neurodegeneration.

By combining significant molecular levels related to proinflammatory, B and T cells pathway, neurodegeneration, acute immune response and innate immune system we have shown that CSF profile at diagnosis represent a new potential biomarker for detecting patients at higher risk of entering the SP phase. In fact, the proposed CSFscore, composed by sTNFR1, CXCL13, IL-10, IL-12, MMP-2, TECK, Nf-L, Parvalbumin, CCL24 and Pentraxin3, was associated with the SP progression and so, with focal and global cortical damage. All these data

suggest that immune infiltrates compartmentalized in the subarachnoid space, and/or possibly choroid plexus, may release inflammatory/cytotoxic mediators into the CSF, creating an intracerebral milieu prone to diffusely sustain chronic inflammation and, at the same time, may directly mediate/exacerbate cortical pathology and disease progression.

These results were confirmed at time of death in post-mortem SP patients. The CSFscore, in fact, was able to identify with high sensitivity 25 out of 29 SP post-mortem patients highlighting that a specific compromised CSF profile at diagnosis may contribute to the progression of MS. Obviously, we are aware that these are preliminary results and so further exploration is needed, increasing the sample size and validating the results in other bigger independent, eventually in-vivo, samples. However, these findings can support the idea to identify early a specific combination of both neuroprotective and immunomodulatory drugs.

Conclusions

Multiple Sclerosis is characterized by an unpredictable clinical course, which is driven by acute/inflammatory and chronic/neurodegenerative processes. Although in the last years extensive efforts have been made to collect and validate the prognostic value of demographic, early clinical and MRI parameters, to date, the detection early in the disease course of patients destined to have poor outcome remains challenging. The high inter-individual variability of the disease course and of the severity and duration of symptoms, hampers the optimisation of the therapeutic approach for minimizing the risk of accumulating disability in log-term. The progressive course is a pivotal phenomenon characterized by a steady worsening of symptoms independent of the occurrence of relapses. Its occurrence is the key determinant of the individual prognosis and its probability proportionally increases with the disease duration and with patients' age[44], mostly secondary to the failure of brain compensatory mechanisms[97]. Older age at disease onset[44,45,113] and a florid early clinical[12,47,94,114] and MRI[98,99] multifocal inflammatory activity distinguish patients more likely to develop a severe disability.

The Secondary Progressive-Risk Score (SP-RiSc) tool (Pisani et al. 2021 European of Journal, under review, chapter 6), during the PhD years, was designed and developed in order to address the unmet need to objectively estimate timely the individual risk of those MS patients destined to experience long-term accumulation of severe disability. Exploiting the flexibility of machine learning approaches, the SP-RiSc was created by integrating demographic, clinical and MRI data obtained during the first 2-years after the disease diagnosis and collected from a cohort of about three hundred RRMS patients. Results demonstrated the tool has both high sensitivity and specificity. Previous predictive model showed[44] that older age and the accumulation of focal inflammatory white and GM damage during the early stage of disease are the main risk factors for development of the SP course, but with a poor prognostic accuracy at the individual level. To address this unmet need, by using the Random Survival Forest (RSF)[168], a flexible machine learning approach,

it was possible to detect and integrate only those features which accurately discriminate patients at higher risk of converting to SMPS.

The proposed tool confirmed that early focal and global GM damage loads and older age at diagnosis are the main determinants of the probability of transitioning to the progressive phase. The tool allowed to reliably establish the size of the predictive effect exerted by each variable. GM parameters were found to be more predictive than WM damage variables supporting the notion that the cortical pathology is crucial for the development of irreversible disability.

The alternative model, which did not consider GM features, was able to predict the high sensitivity but with low specificity. Overall, the model confirmed that high early relapses and early WM lesions accumulation also influence the prognosis. This could be explained, at least in part, by the intrinsic relationship between brain WM and GM damage load, with reciprocal influence from both pathological perspective and imaging-analysis methods. However, the assessment of the cortical pathology allows a more accurate prediction of the long-term outcome, emphasising the importance of evaluating the GM damage, in combination of the focal WM activity, in clinical routine. at the individual level suggesting the crucial evaluation of GM damage, in combination to the focal inflammatory WM conditioning, in clinical routine. This can ultimately be implemented for selecting patients needing more aggressive therapies early in the disease course.

Brain imaging assessment has corroborated that grey matter (cortical and deep) pathology are firmly linked to the physical disability since the initial phase of the disease[66,100]. Pathology studies demonstrated that leptomeningeal immune cell (mainly T and B-lymphocytes) and compartmentalized inflammation in the subarachnoid space contributes to the development of the cortical pathology. Lymphocytes, monocytes and activated microglial cells are involved in demyelination and neurodegeneration in MS patients, especially in the progressive phase, due to their implication in the processes of oxidative and mitochondrial damage. Therefore, we examined the prognostic role of 18 CSF mediators which had recently been found to be associated with the meningeal inflammation and grey matter pathology[74], in predicting the risk of experiencing disease activity during the first four years of RRMS disease course[119]. A specific CSF profile at diagnosis

characterized patients destined to have a more severe disease activity and worsening cortical pathology over time. Specifically, high levels of CXCL13, TNF, TWEAK, and LIGHT, mainly related to B-cells, were strongly associated with the cortical pathology at diagnosis and after four years. Moreover, our data supported the hypothesis that the innate immunity system affects the cortical pathology from the early stage of the disease. Higher CSF levels of sCD163 were significantly associated with lower cortical thickness suggesting that activated monocytes/macrophages in the meningeal infiltrates mediate phagocytosis, inflammatory cell recruitment/activation, and antigen presentation via CD163 and CXCL13 related mechanisms. Interestingly, some CSF biomarkers correlated with the WM and Gad+ lesions, others were related to the intrathecal inflammation (CXCL13) and microglial activity (sCDS13), lately persisting in the progressive phases.

These results were also confirmed in the preliminary analysis performed during the last part of PhD research. To investigate the biological processes involved in the progressive stages and in a poor prognosis, explorative analyses were performed. To identify a comprehensive and specific inflammatory pattern distinguishing of those MS patients with higher odds of experiencing a poor prognosis within the time window of 10 years, the SP-RiSc measure was calculated for each patient for whom an extensive CSF assessment was available. Patients with high probability of remaining on the RR phase and of developing the SP course in the long term were identified based on the SP-RiSc cut-off previously evaluated (Pisani et. al. 2021, chapter 6). Explorative analysis was performed to detect different CSF protein pattern at diagnosis among the two patient subsets. The results of functional enrichment analysis confirmed that those patients with a higher probability of becoming SP in the ten years following the diagnosis were characterized by a chronic intrathecal inflammation. High CSF levels of LIGHT, sTNFR1, sCD163, besides Nf-L, were found to induce apoptosis and neurodegeneration processes, confirming that the accumulation of inflammatory infiltrates in meninges with consequent GM atrophy is a distinguishing feature of progressive MS patients. In contrast, in whom are likely remain in the RR phase, an acute inflammatory process in the early stage seemed to be defined by the

recruitment of lymphocytes, monocytes and neutrophils (MCP-2, MCP-1, TNF-alpha, CXCL10) in the CNS. Further confirmations were found when the most significant discriminating CSF inflammatory mediators were identified and combined into the CSFscore. In fact, the molecules related to proinflammatory(sTNFR1), B (CXCL13 and IL-10) and T cells (IL-12), acute immune response (CCL24 and Pentraxin-3) and innate system (MMP-2 and CCL25) and neurodegeneration (Nf-L and Parvalbumin) pathways were found to be potentially predictive of the risk of SP.

Noteworthy is also the detection of CSF Parvalbumin among the most predictive molecules on the risk of progression over time. The accumulation of Parvalbumin in the CSF is a consequence of interneuronal loss. The concomitant involvement of a biomarker of the damage of Gaba-ergic neurons (Nf-L and Parvalbumin), which we have previously identified as specific biomarker of cortical neurodegeneration[167], support the hypothesis that CSF can reflect both neuroinflammatory and neurodegenerative ongoing processes. Although the CSFscore was validated on an independent post-mortem SP sample, with high sensitivity, further analyses are mandatory. The increment of the sample sizes used in all analyses, the evaluation of additional features, such as spinal cord lesion accumulation and type of onset, and the multicentre prospective validation are strictly necessary to acquire high-level evidence for the clinical application of these findings.

However, these preliminary results lay the foundation for better understanding the underlying mechanism of the disease progression supporting the notion: *i)* that progressive phase in MS is characterized mainly by a focal and diffuse cortical pathology predominant since the early stage of disease and *ii)* that the CSF of inflammatory cytokine and chemokine mediators reflect the intrathecal inflammation and have potential predictive value.

Moreover, the application of advanced analysis in the current studies, such as machine and statistical learning methods, has highlighted its potential clinical utility in MS suggesting that an interdisciplinary approach is imperative. Indeed, using the machine learning algorithm it was possible to obtain more accurate results than the traditional models widely applied in MS data processing. However, the

conventional models are characterized by restrictive assumptions, such as proportional hazard or normal distribution and by high correlated variables with each other (multicollinearity). Multicollinearity occurs frequently in biological and clinical data; hence, it is common also among the variables collected on the MS patients. Machine learning relaxes these issues improving performance.

It was showed that machine learning can provide better, more patient-specific information, supplying neurologists with greater capacity to make the most appropriate clinical decisions.

The inclusion of such innovative statistical methods in MS care, combining different types of data, may allow the development of reliable prognostic tools based on as detailed as possible patients' profile at diagnosis.

In conclusion, the application of clinical, MRI and CSF data integration, provide to create a holistic picture of the MS patients assisting the clinician in optimizing the therapeutic approach, avoiding side effects and moving closer to personalized medicine.

References

1. Lassmann, H., Brück, W. & Lucchinetti, C. F. The immunopathology of multiple sclerosis: An overview. *Brain Pathol.* **17**, 210–218 (2007).
2. Scalfari, A. *et al.* a geographically based study 10 : relapses and long-term disability. 1914–1929 (2010). doi:10.1093/brain/awq118
3. Fox, R. J. *et al.* Placebo-controlled phase 3 study of oral BG-12 or glatiramer in multiple sclerosis. *N. Engl. J. Med.* **367**, 1087–1097 (2012).
4. Lucchinetti, C. F. *et al.* Inflammatory Cortical Demyelination in Early Multiple Sclerosis. *N. Engl. J. Med.* **365**, 2188–2197 (2011).
5. Lee, A. C., Chin, J., Birbeck, G. L., Bower, J. & Meyer, A. C. Global perspectives. *Neurology* **80**, 2151–2153 (2013).
6. Domingues, H. S., Mues, M., Lassmann, H., Wekerle, H. & Krishnamoorthy, G. Functional and pathogenic differences of Th1 and Th17 cells in experimental autoimmune encephalomyelitis. *PLoS One* **5**, (2010).
7. Brucklacher-Waldert, V., Sturner, K., Kolster, M., Wolthausen, J. & Tolosa, E. Phenotypical and functional characterization of T helper 17 cells in multiple sclerosis. *A J. Neurol.* (2021). doi:10.1093/brain/awp289
8. Olsson, T., Barcellos, L. F. & Alfredsson, L. Interactions between genetic, lifestyle and environmental risk factors for multiple sclerosis. *Nat. Rev. Neurol.* **13**, 26–36 (2016).
9. Munger, K. L. *et al.* Vitamin D Status During Pregnancy and Risk of Multiple Sclerosis in Offspring of Women in the Finnish Maternity Cohort. *JAMA Neurol.* **73**, 515–519 (2016).
10. Marrie, R. A. Environmental risk factors in multiple sclerosis aetiology. *Lancet. Neurol.* **3**, 709–718 (2004).
11. Ramanujam, R. *et al.* Effect of Smoking Cessation on Multiple Sclerosis Prognosis. *JAMA Neurol.* **72**, 1117–1123 (2015).
12. Leray, E. *et al.* Evidence for a two-stage disability progression in multiple sclerosis. *Brain* **133**, 1900–1913 (2010).
13. Baecher-Allan, C., Kaskow, B. J. & Weiner, H. L. Multiple Sclerosis:

Mechanisms and Immunotherapy. *Neuron* **97**, 742–768 (2018).

14. Criste, G., Trapp, B. & Dutta, R. Axonal loss in multiple sclerosis: causes and mechanisms. *Handb. Clin. Neurol.* **122**, 101–113 (2014).

15. Lublin, F. D. & Reingold, S. C. Defining the clinical course of multiple sclerosis: results of an international survey. National Multiple Sclerosis Society (USA) Advisory Committee on Clinical Trials of New Agents in Multiple Sclerosis. *Neurology* **46**, 907–911 (1996).

16. Kurtzke JF. Rating neurologic impairment in multiple sclerosis : an expanded disability status scale (EDSS). PubMed Commons. *Neurology* **33**, 2014 (1983).

17. Filippi, M. *et al.* Multiple sclerosis. *Nat. Rev. Dis. Prim.* **4**, 1–27 (2018).

18. Filippi, M. *et al.* MRI criteria for the diagnosis of multiple sclerosis: MAGNIMS consensus guidelines. *Lancet. Neurol.* **15**, 292–303 (2016).

19. Thompson, C. P. *et al.* A naturally protective epitope of limited variability as an influenza vaccine target. *Nat. Commun.* **9**, 1–10 (2018).

20. Solomon, A. J. *et al.* The contemporary spectrum of multiple sclerosis misdiagnosis. *Neurology* **87**, 1393–1399 (2016).

21. Miller, D. H. *et al.* Differential diagnosis of suspected multiple sclerosis: A consensus approach. *Mult. Scler.* **14**, 1157–1174 (2008).

22. Brownlee, W. J., Hardy, T. A., Fazekas, F. & Miller, D. H. Diagnosis of multiple sclerosis: progress and challenges. *Lancet (London, England)* **389**, 1336–1346 (2017).

23. Lassmann, H., van Horssen, J. & Mahad, D. Progressive multiple sclerosis: pathology and pathogenesis. *Nat. Rev. Neurol.* **8**, 647–656 (2012).

24. Kuhlmann, T. *et al.* An updated histological classification system for multiple sclerosis lesions. *Acta Neuropathol.* **133**, 13–24 (2017).

25. Frischer, J. M. *et al.* Clinical and pathological insights into the dynamic nature of the white matter multiple sclerosis plaque. *Ann. Neurol.* **78**, 710–721 (2015).

26. FOG, T. TOPOGRAPHIC DISTRIBUTION OF PLAQUES IN THE SPINAL CORD IN MULTIPLE SCLEROSIS. *Arch. Neurol. Psychiatry* **63**, 382–414 (1950).

27. BROWNELL, B. & HUGHES, J. T. The distribution of plaques in the cerebrum in multiple sclerosis. *J. Neurol. Neurosurg. Psychiatry* **25**, 315–320 (1962).

28. Kutzelnigg, A. *et al.* Widespread demyelination in the cerebellar cortex in multiple sclerosis. *Brain Pathol.* **17**, 38–44 (2007).

29. Kidd, D. *et al.* Cortical lesions in multiple sclerosis. *Brain* **122 (Pt 1**, 17–26 (1999).

30. Vercellino, M. *et al.* Demyelination, inflammation, and neurodegeneration in multiple sclerosis deep gray matter. *J. Neuropathol. Exp. Neurol.* **68**, 489–502 (2009).

31. Haider, L. *et al.* Multiple sclerosis deep grey matter: the relation between demyelination, neurodegeneration, inflammation and iron. *J. Neurol. Neurosurg. Psychiatry* **85**, 1386–1395 (2014).

32. Lassmann, H. Pathogenic mechanisms associated with different clinical courses of multiple sclerosis. *Front. Immunol.* **10**, 1–14 (2019).

33. Peterson, J. W., Bö, L., Mörk, S., Chang, A. & Trapp, B. D. Transected neurites, apoptotic neurons, and reduced inflammation in cortical multiple sclerosis lesions. *Ann. Neurol.* **50**, 389–400 (2001).

34. Howell, O. W. *et al.* Meningeal inflammation is widespread and linked to cortical pathology in multiple sclerosis. *Brain* **134**, 2755–2771 (2011).

35. Bø, L., Vedeler, C. A., Nyland, H., Trapp, B. D. & Mørk, S. J. Intracortical multiple sclerosis lesions are not associated with increased lymphocyte infiltration. *Mult. Scler.* **9**, 323–331 (2003).

36. Bø, L., Vedeler, C. A., Nyland, H. I., Trapp, B. D. & Mørk, S. J. Subpial demyelination in the cerebral cortex of multiple sclerosis patients. *J. Neuropathol. Exp. Neurol.* **62**, 723–732 (2003).

37. Haider, L. *et al.* Oxidative damage in multiple sclerosis lesions. *Brain* **134**, 1914–1924 (2011).

38. Fischer, M. T. *et al.* Disease-specific molecular events in cortical multiple sclerosis lesions. *Brain* **136**, 1799–1815 (2013).

39. Wegner, C., Esiri, M. M., Chance, S. A., Palace, J. & Matthews, P. M. Neocortical neuronal, synaptic, and glial loss in multiple sclerosis. *Neurology* **67**, 960–967 (2006).

40. Dutta, R. *et al.* Demyelination causes synaptic alterations in hippocampi from multiple sclerosis patients. *Ann. Neurol.* **69**, 445–454 (2011).

41. Lorscheider, J. *et al.* Defining secondary progressive multiple sclerosis. *Brain*

139, 2395–2405 (2016).

42. Machado-Santos, J. *et al.* The compartmentalized inflammatory response in the multiple sclerosis brain is composed of tissue-resident CD8+ T lymphocytes and B cells. *Brain* **141**, 2066–2082 (2018).

43. Michel, L. *et al.* B Cells in the Multiple Sclerosis Central Nervous System: Trafficking and Contribution to CNS-Compartmentalized Inflammation. *Front. Immunol.* **6**, 636 (2015).

44. Scalfari, A., Neuhaus, A., Daumer, M., Ebers, G. C. & Muraro, P. A. Age and disability accumulation in multiple sclerosis. *Neurology* **77**, 1246–1252 (2011).

45. Crusan, D. J. *et al.* Milestone in Multiple Sclerosis. **19**, 188–198 (2014).

46. Koch, M., Mostert, J., Heersema, D. & De Keyser, J. Progression in multiple sclerosis: Further evidence of an age dependent process. *J. Neurol. Sci.* **255**, 35–41 (2007).

47. Scalfari, A. *et al.* The natural history of multiple sclerosis, a geographically based study 10: Relapses and long-term disability. *Brain* **133**, 1914–1929 (2010).

48. Cree, B. A. C. *et al.* Silent progression in disease activity–free relapsing multiple sclerosis. *Ann. Neurol.* **85**, 653–666 (2019).

49. Calabrese, M. *et al.* Exploring the origins of grey matter damage in multiple sclerosis. *Nat. Rev. Neurosci.* **16**, 147–158 (2015).

50. Greco, V. *et al.* A low-cost and versatile system for projecting wide-field visual stimuli within fMRI scanners. *Behav. Res. Methods* **48**, 614–620 (2016).

51. Farina, G. *et al.* Increased cortical lesion load and intrathecal inflammation is associated with oligoclonal bands in multiple sclerosis patients: a combined CSF and MRI study. *J. Neuroinflammation* **14**, 40 (2017).

52. Calabrese, M. *et al.* The changing clinical course of multiple sclerosis: A matter of gray matter. *Ann. Neurol.* **74**, 76–83 (2013).

53. Kutzelnigg, A. *et al.* Cortical demyelination and diffuse white matter injury in multiple sclerosis. *Brain* **128**, 2705–2712 (2005).

54. Roosendaal, S. D. *et al.* Grey matter volume in a large cohort of MS patients: relation to MRI parameters and disability. *Mult. Scler.* **17**, 1098–1106 (2011).

55. Magliozzi, R. *et al.* Meningeal B-cell follicles in secondary progressive multiple sclerosis associate with early onset of disease and severe cortical pathology.

Brain **130**, 1089–1104 (2007).

56. Carone, D. A. *et al.* Semi-automatic brain region extraction (SABRE) reveals superior cortical and deep gray matter atrophy in MS. *Neuroimage* **29**, 505–514 (2006).

57. Pirko, I., Lucchinetti, C. F., Sriram, S. & Bakshi, R. Gray matter involvement in multiple sclerosis. *Neurology* **68**, 634–642 (2007).

58. Calabrese, M. *et al.* Cortical lesion load associates with progression of disability in multiple sclerosis. *Brain* **135**, 2952–2961 (2012).

59. Mattisi, I., Barachino, L., Morra, A., Rinaldi, L. & Contribution, O. Detection of Cortical Inflammatory Lesions by Double Inversion Recovery Magnetic Resonance Imaging in Patients With Multiple Sclerosis. **64**, 1416–1422 (2007).

60. Chard, D. T. *et al.* Brain atrophy in clinically early relapsing-remitting multiple sclerosis. *Brain* **125**, 327–337 (2002).

61. Dalton, C. M. *et al.* Early development of multiple sclerosis is associated with progressive grey matter atrophy in patients presenting with clinically isolated syndromes. *Brain* **127**, 1101–1107 (2004).

62. Filippi, M. *et al.* Evidence for widespread axonal damage at the earliest clinical stage of multiple sclerosis. *Brain* **126**, 433–437 (2003).

63. Bergsland, N. *et al.* Subcortical and cortical gray matter atrophy in a large sample of patients with clinically isolated syndrome and early relapsing-remitting multiple sclerosis. *Am. J. Neuroradiol.* **33**, 1573–1578 (2012).

64. Calabrese, M. *et al.* A 3-year magnetic resonance imaging study of cortical lesions in relapse-onset multiple sclerosis. *Ann. Neurol.* **67**, 376–383 (2010).

65. Fisher, E., Lee, J.-C., Nakamura, K. & Rudick, R. A. Gray matter atrophy in multiple sclerosis: a longitudinal study. *Ann. Neurol.* **64**, 255–265 (2008).

66. Fisniku, L. K. *et al.* Gray matter atrophy is related to long-term disability in multiple sclerosis. *Ann. Neurol.* **64**, 247–254 (2008).

67. Casserly, C. *et al.* Spinal Cord Atrophy in Multiple Sclerosis: A Systematic Review and Meta-Analysis. *J. Neuroimaging* **28**, 556–586 (2018).

68. Arrambide, G. *et al.* Spinal cord lesions: A modest contributor to diagnosis in clinically isolated syndromes but a relevant prognostic factor. *Mult. Scler. J.* **24**, 301–312 (2018).

69. Imrell, K., Greiner, E., Hillert, J. & Masterman, T. HLA-DRB115 and cerebrospinal-fluid-specific oligoclonal immunoglobulin G bands lower age at attainment of important disease milestones in multiple sclerosis. *J. Neuroimmunol.* **210**, 128–130 (2009).

70. Senel, M. *et al.* CSF Free Light Chains as a Marker of Intrathecal Immunoglobulin Synthesis in Multiple Sclerosis: A Blood-CSF Barrier Related Evaluation in a Large Cohort. *Front. Immunol.* **10**, 641 (2019).

71. Izquierdo, G. *et al.* Intrathecal IgG synthesis: marker of progression in multiple sclerosis patients. *Acta Neurol. Scand.* **105**, 158–163 (2002).

72. Villar, L. *et al.* Influence of oligoclonal IgM specificity in multiple sclerosis disease course. *Mult. Scler.* **14**, 183–187 (2008).

73. Khademi, M. *et al.* Cerebrospinal fluid CXCL13 in multiple sclerosis: a suggestive prognostic marker for the disease course. *Mult. Scler.* **17**, 335–343 (2011).

74. Magliozzi, R. *et al.* Inflammatory intrathecal profiles and cortical damage in multiple sclerosis. *Ann. Neurol.* **83**, 739–755 (2018).

75. Salzer, J., Svenningsson, A. & Sundström, P. Neurofilament light as a prognostic marker in multiple sclerosis. *Mult. Scler.* **16**, 287–292 (2010).

76. Kuhle, J. *et al.* Serum neurofilament is associated with progression of brain atrophy and disability in early MS. *Neurology* **88**, 826–831 (2017).

77. Comabella, M. *et al.* Cerebrospinal fluid chitinase 3-like 1 levels are associated with conversion to multiple sclerosis. *Brain* **133**, 1082–1093 (2010).

78. Vågberg, M. *et al.* Automated Determination of Brain Parenchymal Fraction in Multiple Sclerosis. *Am. J. Neuroradiol.* **34**, 498 LP – 504 (2013).

79. Giovannoni, G., Bermel, R., Phillips, T. & Rudick, R. A brief history of NEDA. *Multiple sclerosis and related disorders* **20**, 228–230 (2018).

80. Kappos, L. *et al.* Inclusion of brain volume loss in a revised measure of 'no evidence of disease activity' (NEDA-4) in relapsing-remitting multiple sclerosis. *Mult. Scler.* **22**, 1297–1305 (2016).

81. De Stefano, N. *et al.* Clinical relevance of brain volume measures in multiple sclerosis. *CNS Drugs* **28**, 147–156 (2014).

82. Ontaneda, D., Tallantyre, E., Kalincik, T., Planchon, S. M. & Evangelou, N. Early highly effective versus escalation treatment approaches in relapsing multiple

sclerosis. *Lancet. Neurol.* **18**, 973–980 (2019).

83. Ishwaran, H., Blackstone, E. H., Apperson-Hansen, C. & Rice, T. W. A novel approach to cancer staging: Application to esophageal cancer. *Biostatistics* **10**, 603–620 (2009).

84. Hsich, E., Gorodeski, E. Z., Blackstone, E. H., Ishwaran, H. & Lauer, M. S. Identifying important risk factors for survival in patient with systolic heart failure using random survival forests. *Circ. Cardiovasc. Qual. Outcomes* **4**, 39–45 (2011).

85. Lezcano-Valverde, J. M. *et al.* Development and validation of a multivariate predictive model for rheumatoid arthritis mortality using a machine learning approach. *Sci. Rep.* **7**, 1–10 (2017).

86. Bergamaschi, R., Berzuini, C., Romani, A. & Cosi, V. Predicting secondary progression in relapsing-remitting multiple sclerosis: A Bayesian analysis. *J. Neurol. Sci.* **189**, 13–21 (2001).

87. Bergamaschi, R. *et al.* BREMSO: a simple score to predict early the natural course of multiple sclerosis. *Eur. J. Neurol.* **22**, 981–989 (2015).

88. Manouchehrinia, A. *et al.* Predicting risk of secondary progression in multiple sclerosis: A nomogram. *Mult. Scler. J.* **25**, 1102–1112 (2019).

89. Bergamaschi, R. *et al.* Early prediction of the long term evolution of multiple sclerosis: The Bayesian Risk Estimate for Multiple Sclerosis (BREMS) score. *J. Neurol. Neurosurg. Psychiatry* **78**, 757–759 (2007).

90. Yoo, Y. *et al.* Deep learning of joint myelin and T1w MRI features in normal-appearing brain tissue to distinguish between multiple sclerosis patients and healthy controls. *NeuroImage Clin.* **17**, 169–178 (2018).

91. Salem, M. *et al.* A fully convolutional neural network for new T2-w lesion detection in multiple sclerosis. *NeuroImage Clin.* **25**, 102149 (2020).

92. Jog, A., Carass, A., Roy, S., Pham, D. L. & Prince, J. L. Random forest regression for magnetic resonance image synthesis. *Med. Image Anal.* **35**, 475–488 (2017).

93. Manouchehrinia, A. *et al.* Predicting risk of secondary progression in multiple sclerosis: A nomogram. *Mult. Scler.* **25**, 1102–1112 (2019).

94. Confavreux, C., Vukusic, S. & Adeleine, P. Early clinical predictors and progression of irreversible disability in multiple sclerosis: An amnesic process. *Brain* **126**, 770–782 (2003).

95. Scott, T. F. Understanding the impact of relapses in the overall course of MS;

refinement of the 2 stage natural history model. *J. Neuroimmunol.* **305**, 162–166 (2017).

96. Dendrou, C. A., Fugger, L. & Friese, M. A. Immunopathology of multiple sclerosis. *Nat. Rev. Immunol.* **15**, 545–558 (2015).

97. Feinstein, A., Freeman, J. & Lo, A. C. Treatment of progressive multiple sclerosis: What works, what does not, and what is needed. *Lancet Neurol.* **14**, 194–207 (2015).

98. Tintore, M. *et al.* Defining high, medium and low impact prognostic factors for developing multiple sclerosis. *Brain* **138**, 1863–1874 (2015).

99. Brownlee, W. J. *et al.* Early imaging predictors of long-term outcomes in relapse-onset multiple sclerosis. *Brain* **142**, 2276–2287 (2019).

100. Filippi, M. *et al.* Gray matter damage predicts the accumulation of disability 13 years later in MS. *Neurology* **81**, 1759 LP – 1767 (2013).

101. Scalfari, A. *et al.* The cortical damage, early relapses, and onset of the progressive phase in multiple sclerosis. *Neurology* **90**, e2107–e2118 (2018).

102. McDonald, W. I. *et al.* Recommended diagnostic criteria for multiple sclerosis: Guidelines from the International Panel on the Diagnosis of Multiple Sclerosis. *Ann. Neurol.* **50**, 121–127 (2001).

103. Association, W. M. World Medical Association Declaration of Helsinki: Ethical Principles for Medical Research Involving Human Subjects. *JAMA* **310**, 2191–2194 (2013).

104. Fox, R. J. *et al.* Placebo-Controlled Phase 3 Study of Oral BG-12 or Glatiramer in Multiple Sclerosis. *N. Engl. J. Med.* **367**, 1087–1097 (2012).

105. Geurts, J. J. G. *et al.* Consensus recommendations for MS cortical lesion scoring using double inversion recovery MRI. *Neurology* **76**, 418 LP – 424 (2011).

106. Bsteh, G. *et al.* Long term clinical prognostic factors in relapsing-remitting multiple sclerosis: Insights from a 10-Year observational study. *PLoS One* **11**, 1–14 (2016).

107. Ishwaran, H., Kogalur, U. B., Blackstone, E. H. & Lauer, M. S. Random survival forests. *Ann. Appl. Stat.* **2**, 841–860 (2008).

108. Breiman, L., Friedman, J. H., Olshen, R. A. & Stone, C. J. Classification and regression trees. *Classif. Regres. Trees* 1–358 (2017). doi:10.1201/9781315139470

109. Mogensen, U. B., Ishwaran, H. & Gerds, T. A. Evaluating Random Forests for Survival Analysis using Prediction Error Curves. *J. Stat. Softw.* **50**, 1–23 (2012).

110. Ishwaran, H., Kogalur, U. B., Gorodeski, E. Z., Minn, A. J. & Lauer, M. S. High-dimensional variable selection for survival data. *J. Am. Stat. Assoc.* **105**, 205–217 (2010).

111. Gerds, T. A. & Schumacher, M. Consistent Estimation of the Expected Brier Score in General Survival Models with Right-Censored Event Times. *Biometrical J.* **48**, 1029–1040 (2006).

112. Dietrich, S. *et al.* Random Survival Forest in practice: a method for modelling complex metabolomics data in time to event analysis. *Int. J. Epidemiol.* **45**, 1406–1420 (2016).

113. Koch, M., Mostert, J., Heersema, D. & De Keyser, J. Progression in multiple sclerosis: Further evidence of an age dependent process. *J. Neurol. Sci.* **255**, 35–41 (2007).

114. Tremlett, H., Yousefi, M., Devonshire, V., Rieckmann, P. & Zhao, Y. Impact of multiple sclerosis relapses on progression diminishes with time. *Neurology* **73**, 1616–1623 (2009).

115. Misicka, E., Sept, C. & Briggs, F. B. S. Predicting onset of secondary-progressive multiple sclerosis using genetic and non-genetic factors. *J. Neurol.* (2020). doi:10.1007/s00415-020-09850-z

116. Kappos, L. *et al.* Contribution of Relapse-Independent Progression vs Relapse-Associated Worsening to Overall Confirmed Disability Accumulation in Typical Relapsing Multiple Sclerosis in a Pooled Analysis of 2 Randomized Clinical Trials. *JAMA Neurol.* **77**, 1132–1140 (2020).

117. Biau, G. & Scornet, E. A random forest guided tour. *TEST* **25**, 197–227 (2016).

118. Schmid, M., Welchowski, T., Wright, M. N. & Berger, M. Discrete-time survival forests with Hellinger distance decision trees. *Data Min. Knowl. Discov.* **34**, 812–832 (2020).

119. Magliozzi, R. *et al.* The CSF profile linked to cortical damage predicts Multiple Sclerosis activity. *Ann. Neurol.* **n/a**, (2020).

120. Filippi, M. *et al.* Assessment of system dysfunction in the brain through MRI-based connectomics. *Lancet. Neurol.* **12**, 1189–1199 (2013).

121. Geurts, J. J. G. *et al.* Cortical lesions in multiple sclerosis: combined postmortem

MR imaging and histopathology. *AJNR. Am. J. Neuroradiol.* **26**, 572–577 (2005).

122. Seewann, A. *et al.* Imaging the tip of the iceberg: visualization of cortical lesions in multiple sclerosis. *Mult. Scler.* **17**, 1202–1210 (2011).

123. Calabrese, M. *et al.* Detection of cortical inflammatory lesions by double inversion recovery magnetic resonance imaging in patients with multiple sclerosis. *Arch. Neurol.* **64**, 1416–1422 (2007).

124. Seewann, A. *et al.* Postmortem verification of MS cortical lesion detection with 3D DIR. *Neurology* **78**, 302–308 (2012).

125. Sethi, V. *et al.* Improved detection of cortical MS lesions with phase-sensitive inversion recovery MRI. *J. Neurol. Neurosurg. Psychiatry* **83**, 877–882 (2012).

126. Kilsdonk, I. D. *et al.* Multicontrast MR Imaging at 7T in Multiple Sclerosis: Highest Lesion Detection in Cortical Gray Matter with 3D-FLAIR. *Am. J. Neuroradiol.* **34**, 791 LP – 796 (2013).

127. Filippi, M. *et al.* Ultra-high-field MR imaging in multiple sclerosis. *J. Neurol. Neurosurg. Psychiatry* **85**, 60–66 (2014).

128. Magliozzi, R. *et al.* A Gradient of neuronal loss and meningeal inflammation in multiple sclerosis. *Ann. Neurol.* **68**, 477–493 (2010).

129. Petzold, A., Steenwijk, M. D., Eikelenboom, J. M., Wattjes, M. P. & Uitdehaag, B. M. Elevated CSF neurofilament proteins predict brain atrophy: A 15-year follow-up study. *Mult. Scler.* **22**, 1154–1162 (2016).

130. Krumbholz, M. *et al.* Chemokines in multiple sclerosis: CXCL12 and CXCL13 up-regulation is differentially linked to CNS immune cell recruitment. *Brain* **129**, 200–211 (2006).

131. Sharief, M. K. & Hentges, R. Association between tumor necrosis factor-alpha and disease progression in patients with multiple sclerosis. *N. Engl. J. Med.* **325**, 467–472 (1991).

132. Baraczka, K., Nékám, K., Pozsonyi, T., Szüts, I. & Ormos, G. Investigation of cytokine (tumor necrosis factor-alpha, interleukin-6, interleukin-10) concentrations in the cerebrospinal fluid of female patients with multiple sclerosis and systemic lupus erythematosus. *Eur. J. Neurol.* **11**, 37–42 (2004).

133. Duan, H. *et al.* Soluble CD146 in cerebrospinal fluid of active multiple sclerosis. *Neuroscience* **235**, 16–26 (2013).

134. Gardner, C. *et al.* Cortical grey matter demyelination can be induced by elevated

pro-inflammatory cytokines in the subarachnoid space of MOG-immunized rats. *Brain* **136**, 3596–3608 (2013).

135. Polman, C. H. *et al.* Diagnostic criteria for multiple sclerosis: 2010 revisions to the McDonald criteria. *Ann. Neurol.* **69**, 292–302 (2011).

136. Teunissen, C. E. *et al.* A consensus protocol for the standardization of cerebrospinal fluid collection and biobanking. *Neurology* **73**, 1914–1922 (2009).

137. Havrdova, E., Galetta, S., Stefoski, D. & Comi, G. Freedom from disease activity in multiple sclerosis. *Neurology* **74 Suppl 3**, S3-7 (2010).

138. Pitteri, M., Romualdi, C., Magliozzi, R., Monaco, S. & Calabrese, M. Cognitive impairment predicts disability progression and cortical thinning in MS: An 8-year study. *Mult. Scler.* **23**, 848–854 (2017).

139. Komori, M. *et al.* Cerebrospinal fluid markers reveal intrathecal inflammation in progressive multiple sclerosis. *Ann. Neurol.* **78**, 3–20 (2015).

140. Ferraro, D. *et al.* Cerebrospinal fluid CXCL13 in clinically isolated syndrome patients: Association with oligoclonal IgM bands and prediction of Multiple Sclerosis diagnosis. *J. Neuroimmunol.* **283**, 64–69 (2015).

141. Giovannoni, G., Tomic, D., Bright, J. R. & Havrdová, E. 'No evident disease activity': The use of combined assessments in the management of patients with multiple sclerosis. *Mult. Scler.* **23**, 1179–1187 (2017).

142. Lisak, R. P. *et al.* Secretory products of multiple sclerosis B cells are cytotoxic to oligodendroglia in vitro. *J. Neuroimmunol.* **246**, 85–95 (2012).

143. Rainey-Barger, E. K. *et al.* The lymphoid chemokine, CXCL13, is dispensable for the initial recruitment of B cells to the acutely inflamed central nervous system. *Brain. Behav. Immun.* **25**, 922–931 (2011).

144. Esen, N., Rainey-Barger, E. K., Huber, A. K., Blakely, P. K. & Irani, D. N. Type-I interferons suppress microglial production of the lymphoid chemokine, CXCL13. *Glia* **62**, 1452–1462 (2014).

145. Stilund, M. *et al.* Biomarkers of inflammation and axonal degeneration/damage in patients with newly diagnosed multiple sclerosis: contributions of the soluble CD163 CSF/serum ratio to a biomarker panel. *PLoS One* **10**, e0119681 (2015).

146. Aloisi, F. & Pujol-Borrell, R. Lymphoid neogenesis in chronic inflammatory diseases. *Nat. Rev. Immunol.* **6**, 205–217 (2006).

147. Stilund, M. *et al.* Soluble CD163 as a Marker of Macrophage Activity in Newly

Diagnosed Patients with Multiple Sclerosis. *PLoS One* **9**, e98588 (2014).

148. Ruggieri, S., Pontecorvo, S., Tortorella, C. & Gasperini, C. Induction treatment strategy in multiple sclerosis: a review of past experiences and future perspectives. *Mult. Scler. Demyelinating Disord.* **3**, 5 (2018).

149. Mikol, D. D. *et al.* Comparison of subcutaneous interferon beta-1a with glatiramer acetate in patients with relapsing multiple sclerosis (the REbif vs Glatiramer Acetate in Relapsing MS Disease [REGARD] study): a multicentre, randomised, parallel, open-label trial. *Lancet. Neurol.* **7**, 903–914 (2008).

150. Haider, L. *et al.* The topograpy of demyelination and neurodegeneration in the multiple sclerosis brain. *Brain* **139**, 807–815 (2016).

151. Langfelder, P. & Horvath, S. WGCNA: an R package for weighted correlation network analysis. *BMC Bioinformatics* **9**, 559 (2008).

152. Pei, G., Chen, L. & Zhang, W. WGCNA Application to Proteomic and Metabolomic Data Analysis. *Methods Enzymol.* **585**, 135–158 (2017).

153. Vella, D., Zoppis, I., Mauri, G., Mauri, P. & Di Silvestre, D. From protein-protein interactions to protein co-expression networks: a new perspective to evaluate large-scale proteomic data. *Eurasip J. Bioinforma. Syst. Biol.* **2017**, (2017).

154. Horvath, S. & Mischel, P. Weighted Gene Co-expression Network Analysis (WGCNA) R Tutorial , Part C Breast Cancer Microarray Data . **4**, 1–12

155. Zhang, B. & Horvath, S. A general framework for weighted gene co-expression network analysis. *Stat. Appl. Genet. Mol. Biol.* **4**, Article17 (2005).

156. Li, A. & Horvath, S. Network neighborhood analysis with the multi-node topological overlap measure. *Bioinformatics* **23**, 222–231 (2007).

157. Ravasz, E., Somera, A. L., Mongru, D. A., Oltvai, Z. N. & Barabási, A. L. Hierarchical organization of modularity in metabolic networks. *Science* **297**, 1551–1555 (2002).

158. Yip, A. M. & Horvath, S. Gene network interconnectedness and the generalized topological overlap measure. *BMC Bioinformatics* **8**, 1–14 (2007).

159. Szklarczyk, D. *et al.* STRING v11: Protein-protein association networks with increased coverage, supporting functional discovery in genome-wide experimental datasets. *Nucleic Acids Res.* **47**, D607–D613 (2019).

160. Breiman, L. E. O. Random Forests. 5–32 (2001).

161. Romme Christensen, J. *et al.* CSF inflammation and axonal damage are increased and correlate in progressive multiple sclerosis. *Mult. Scler.* **19**, 877–884 (2013).

162. Kassiotis, G. *et al.* A tumor necrosis factor-induced model of human primary demyelinating diseases develops in immunodeficient mice. *Eur. J. Immunol.* **29**, 912–917 (1999).

163. Filippi, M., Preziosa, P. & Rocca, M. A. MRI in multiple sclerosis: what is changing? *Curr. Opin. Neurol.* **31**, 386–395 (2018).

164. Magliozzi, R. *et al.* Meningeal inflammation changes the balance of TNF signalling in cortical grey matter in multiple sclerosis. *J. Neuroinflammation* **16**, 259 (2019).

165. Min, J.-W. *et al.* Comparison of plasma eotaxin family level in aspirin-induced and aspirin-tolerant asthma patients. *Chest* **128**, 3127–3132 (2005).

166. Ummenthum, K. *et al.* Pentraxin-3 is upregulated in the central nervous system during MS and EAE, but does not modulate experimental neurological disease. *Eur. J. Immunol.* **46**, 701–711 (2016).

167. Magliozzi, R. *et al.* CSF parvalbumin levels reflect interneuron loss linked with cortical pathology in multiple sclerosis. *Ann. Clin. Transl. Neurol.* (2021). doi:10.1002/acn3.51298

168. Ishwaran, H., Kogalur, U. B., Blackstone, E. H. & Lauer, M. S. Random survival forests. *Ann. Appl. Stat.* **2**, 841–860 (2008).

Appendix 1

	Whole cohort	RR patients	SP patients
CCL21	**1811.55(1317.73)**	**1853.99(1502.2)**	**1769.74(1097.07)**
CXCL13	**15.12(33.4)**	**8.02(13.63)**	**32.53(55.83)**
CXCL5	**683.43(715.20)**	**787.54(819.16)**	**601.03(532.07)**
CCL11	**102.05(130.52)**	**130.7(151.18)**	**72.92(74.22)**
CCL24	**68.72(64.64)**	**70.22(58.9)**	**78.63(81.99)**
CCL26	**66.39(81.27)**	**82.59(91.2)**	**51.38(59.97)**
CX3CL1	**398.84(362.49)**	**419.37(405.69)**	**411(319.58)**
GM-CSF	**123.74(144.69)**	**150.68(163.89)**	**93.55(108.68)**
CXCL1	**135.65(140.40)**	**158.91(160.66)**	**116.02(100.59)**
CXCL2	**84.29(99.87)**	**104.3(117.72)**	**60.46(55.26)**
CCL1	**56.84(61.94)**	**65.32(66.39)**	**56.7(54.4)**
CXCL10	**561.42(647.37)**	**529.79(682.55)**	**703.59(665)**
CXCL11	**137.74(735.78)**	**207.02(938.58)**	**34.22(55.89)**

MCP-1	**647.61(834.51)**	**720.71(955.11)**	**588.61(682.54)**
MCP-2	**375.03(823.51)**	**527.69(1008.16)**	**171.81(291.84)**
MCP-3	**63.63(67.52)**	**77.67(77.02)**	**50.33(43.34)**
MCP-4	**6.54(14.71)**	**4.91(6.97)**	**11.4(25.12)**
CCL22	**61.57(105.22)**	**54.42(86.51)**	**89.57(147.77)**
MIF	**1839.15(2027.82)**	**1422.18(1028.87)**	**2770.74(3304.34)**
CXCL9	**83.11(69.58)**	**80.97(79.99)**	**87.28(57.38)**
MIP-1alpha	**7.23(6.09)**	**7.13(5.22)**	**8.53(8.23)**
CCL15	**546.63(531.90)**	**544.93(580.75)**	**617.66(508.41)**
CCL20	**1.83(2.25)**	**2.29(2.51)**	**1.41(1.69)**
CCL19	**139.67(115.59)**	**114.37(98.08)**	**166.07(135.13)**
CCL23	**18.93(26.21)**	**20.31(26.71)**	**20.9(28.7)**
CXCL16	**1751.41(1392.77)**	**1710.66(1285.31)**	**1977.97(1794.72)**
CXCL12	**3005.12(3266.93)**	**2990.97(3528.5)**	**3480.52(3203.48)**
TECK	**115.19(83.92)**	**118.27(90.86)**	**121.06(81.8)**
TNF	**39.91(42.93)**	**40.15(49.39)**	**44.68(33.77)**
sTNFR1	**4327.68(3143.71)**	**4239.06(3168.17)**	**4953.42(3515.12)**

sTNFR2	**1026.67(922.35)**	**955.47(817.69)**	**1348.17(1168.85)**
TWEAK	**1411.87(1420.84)**	**1052.92(1018.61)**	**1948.53(2000.14)**
APRIL	**24579.89(24753.31)**	**20079.35(14207.03)**	**37495.59(38531.32)**
BAFF	**10762.89(8969.34)**	**11012.86(8545.39)**	**11239.17(11215.19)**
LIGHT	**312.83(436.31)**	**322.61(404.51)**	**385.63(539.57)**
sCD30	**1180.65(1254.79)**	**968.71(968.67)**	**1497.82(1748.07)**
IFN-gamma	**27.49(34.97)**	**34.7(40.22)**	**19.6(22.74)**
INF-alpha2	**24.35(26.63)**	**30.09(29.31)**	**19.94(19.73)**
INF-beta	**41.78(36.17)**	**48.2(37.55)**	**39.04(33.65)**
IL-28A	**98.45(274.13)**	**129.27(342.4)**	**64.75(93.09)**
IL-29	**48.63(53.29)**	**61.42(59.75)**	**37.04(33.77)**
gp130	**78506.59(80736.44)**	**64148.23(44680.59)**	**110240.87(131476.67)**
IL-1beta	**4.00(5.13)**	**5.22(5.75)**	**2.6(3.53)**
IL-4	**23.58(24.70)**	**23.34(25.3)**	**29.09(25.88)**
IL-6	**36.43(59.42)**	**40.18(54.72)**	**37.01(76.54)**
IL-8	**89.85(98.40)**	**104.4(110.42)**	**79.88(78.92)**

IL-10	**29.12(23.56)**	**31.92(25.34)**	**21.87(21.58)**
IL-16	**159.22(173.65)**	**177.87(174.72)**	**163.2(186.19)**
sIL6-Ra	**3354.18(2109.68)**	**3209.69(2295.81)**	**3572.64(2032.97)**
IL-11	**3.45(13.00)**	**4.34(15.85)**	**2.65(7.37)**
IL-12	**26.53(31.79)**	**35.3(35.51)**	**15.42(20.03)**
IL-12p70	**4.67(6.66)**	**5.21(5.75)**	**5.01(8.89)**
IL-19	**59.07(57.57)**	**73.37(61.01)**	**47.53(45.21)**
IL-20	**77.11(105.06)**	**101.89(119.72)**	**49.04(65.86)**
IL-22	**41.13(37.59)**	**49.84(41.65)**	**30.03(26.82)**
IL-26	**785.74(1456.23)**	**788.87(1779.3)**	**555.28(593.38)**
IL-27	**211.53(184.02)**	**245.62(199.14)**	**189.36(153.57)**
IL-32	**162.63(201.60)**	**149.02(213.83)**	**121.79(118.7)**
IL-34	**472.93(451.80)**	**529.4(515.29)**	**360.36(322.85)**
IL-35	**314.48(199.71)**	**358.87(207.5)**	**276.46(171.5)**
MMP-1	**1199.63(1306.82)**	**1495.02(1464.85)**	**948.39(862.26)**
MMP-2	**1932.64(5722.61)**	**2276.31(6939.26)**	**1513.79(3472.36)**
Osteocalcin	**766.13(517.60)**	**829.4(590.75)**	**701.09(407.83)**

Osteopontin	**76516.77(88510.25)**	**92933.9(98583.1)**	**65793.9(66033.45)**
Pentraxin-3	**242.88(377.82)**	**239.81(447.79)**	**273.72(271.79)**
TSLP	**52.30(55.81)**	**61.42(64.97)**	**46.7(34.18)**
sCD163	**42648.12(24437.98)**	**43329.32(27691.09)**	**42445.98(19896.84)**
Chitinase-3	**45747.25(40675.47)**	**50078.68(48346.39)**	**40192.4(27023.57)**
Nf-L	**1.71(1.2)**	**1.49(0.83)**	**2.44(1.66)**
Parvalbumin	**12.96(17.38)**	**10.44(13.8)**	**20.9(23.63)**
Fibrinogen	**1330.96(1125.17)**	**1519.1(1357.21)**	**1242.22(716)**

CSF protein levels at study entry in the whole population, and in two groups of predicted RR and SP patients. Data are reported as mean and standard deviation if not differently reported.